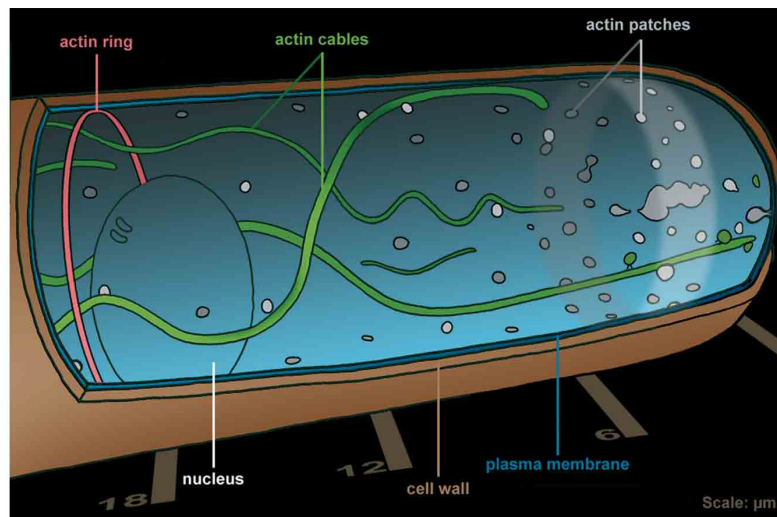


**Morphogenesis of a filamentous fungus:
Dynamics of the actin cytoskeleton
and control of hyphal integrity in *Ashbya gossypii***



Inauguraldissertation
zur
Erlangung der Würde eines Doktors der Philosophie
vorgelegt der
Philosophisch-Naturwissenschaftlichen Fakultät
der Universität Basel
von
Pierre Philippe Laissue
aus Courgenay JU
Basel, 2004

Genehmigt von der Philosophisch-Naturwissenschaftlichen Fakultät

auf Antrag von

Prof. Dr. Peter Philippsen, Prof. Dr. Ueli Aebi und Prof. Dr. Martin Spiess

Basel, den 21.09.2004

Prof. Dr. Hans-Jakob Wirz

Dekan

Cover illustration :

Schematic representation of the components of the actin cytoskeleton in *Ashbya gossypii*. Shown are the first twenty micrometers of a hypha (zero μm being the very tip). Nucleus, cell wall and plasma membrane are indicated for orientation. The main structures of the actin cytoskeleton are actin patches, concentrated in the apical region, actin cables emanating from the tip, and actin rings, auxiliary structures required for forming hyphal crosswalls, the septa.

Table of Contents

Thesis Summary	7
Part I - The dynamic actin cytoskeleton of <i>Ashbya gossypii</i>	8
Abstract	9
Introduction	10
<i>The filamentous fungus <i>Ashbya gossypii</i> is well suited for model studies</i>	11
<i>The actin cytoskeleton is a key player for the growing tip</i>	12
Materials and Methods	15
<i>Construction of AgCap1p-GFP, AgCap2p-GFP and AgAbp140p-GFP</i>	15
<i>Analysis of the Cap1p, Cap2p and Abp140p protein sequences</i>	16
<i>Staining Procedures</i>	16
<i>Microscope Setup</i>	17
<i>Image Acquisition and Processing</i>	17
Results	19
ACTIN PATCHES	19
<i>Actin patches are concentrated in the apical zone</i>	19
<i>Sequence analysis of AgCap1p and AgCap2p</i>	19
<i>AgCap1p-GFP and AgCap2p-GFP colocalize fully with actin patches in rhodamine-phalloidin stainings</i>	20
<i>Characterization of the AgCap-GFP strains</i>	21
<i>Actin patches visible with Cap-GFP move rapidly in distinct ways</i>	21
<i>A constitutively activated formin causes Cap-GFP patches to form elongated structures</i>	23
<i>Effect of Latrunculin A on actin patches</i>	23
<i>Actin patches suggest maintenance of polarization by endocytic cycling</i>	24
ACTIN CABLES	25
<i>Sequence analysis of AgAbp140p</i>	25
<i>AgAbp140p-GFP fully colocalizes with actin cables and rings in rhodamine-phalloidin stainings</i>	25
<i>Abp140p-GFP cables are often associated with actin patches</i>	25
<i>Characterization of the AgAbp140p-GFP strain</i>	26
<i>Actin cables visualized with Abp140p-GFP are highly motile and flexible</i>	26
<i>Actin patches move towards the tip on Abp140p-GFP cables</i>	26
<i>Actin cable based vesicle transport is defect in the formin deletion mutant ΔAgbni1</i>	27
ACTIN RINGS	28
Discussion	30
<i>A model for organisation of the actin cytoskeleton in <i>A. gossypii</i></i>	30
References	34
Figures and Tables	39
Supplemental Material	52

Part II – Far11p is required to prevent premature hyphal abscission

in the filamentous fungus <i>Ashbya gossypii</i>	57
Abstract	58
Introduction	58
Materials and Methods.....	59
<i>Cell wall staining</i>	59
<i>Cytoskeletal staining</i>	60
<i>Microscope setup</i>	60
<i>Image acquisition and processing</i>	60
<i>Analysis of the AgFar11p protein sequence</i>	61
Results	61
<i>Analysis of the AgFar11p protein sequence</i>	62
<i>Agfar11Δ mutants commit hyphal abscission</i>	62
<i>Hyphal abscission occurs at septa of the Agfar11Δ mutant</i>	63
<i>Hyphal abscission leads to complete separation</i>	63
<i>Hyphal abscission is often followed by displacement and lysis</i>	64
<i>Sporangium formation in wild type features hyphal abscission and lysis as well</i>	65
Discussion.....	65
References.....	67
Figures	70
Supplemental Material	73
Appendix	74
<i>Table 1: Filter spectra and specifications on microscope Meta2</i>	79
<i>Table 2: Filter spectra and specifications on microscope PicMic</i>	80
Acknowledgements	81
Curriculum vitae	82
Erklärung	85

to my parents – thank you for all the support

Thesis Summary

This thesis deals primarily with the dynamics and organisation of the actin cytoskeleton in *Ashbya gossypii*. The structures, parameters and dynamic behavior of the different aspects of the actin cytoskeleton were analyzed in detail. A model of the organisation of actin in the tip of *A. gossypii* is presented. Herefore, three proteins tagged with GFP were recorded by fluorescence microscopy. The two subunits of actin capping protein AgCap1p-GFP and AgCap2-GFP were used for analysis of actin patches. The other structures are actin cables and actin rings. They were visualized with a weak actin crosslinker, AgABP140p-GFP, which is present in both structures. Further GFP constructs were used for vesicles destined for exocytosis (AgSec4-GFP) and for an actin patch mutant (Bnr1 Δ DAD-Cap1GFP). The tip organisation model comprises of three processes: endocytosis, exocytosis and polarization through vesicle recycling. Experimental findings also support this model. FRAP experiments and a membrane fluidizer are used for apical membrane analysis, as well as an endocytosis marker and an actin inhibiting drug.

While this part of the study is being submitted for publication, part of the section regarding Sec4-GFP has recently been published in *Molecular Biology of the Cell*.

In a second approach, a protein responsible for hyphal fusion in *N. crassa* and for the cell cycle in *S. cerevisiae* was characterized in *A. gossypii*. AgFar11 is responsible for premature hyphal abscission and is a possible link to the cell cycle of *A. gossypii*. This is the result of sequential analysis of AgFar11p and microscopic study of a deletion mutant thereof. These findings will soon be submitted as well.

An appendix features details on fluorescence microscopy, which was key to this work.

I have continued to study both aspects for a year now. In this process, the work has evolved considerably, and for reasons of succinctness, image quality and newest findings, I would strongly recommend reading the corresponding scientific publications.

Part I - The dynamic actin cytoskeleton of *Ashbya gossypii*

Abstract

Polarized growth is an intriguing aspect in a continuously elongating organism like *A. gossypii*. We therefore attempted a detailed study of the live actin cytoskeleton in this model filamentous fungus. We analyse the different components of the actin cytoskeleton tagged with Green Fluorescent Protein (GFP) by means of rapid, multi-dimensional video microscopy, studying their structural and dynamic properties.

Cap1p and Cap2p are the subunits making up capping protein, a heterodimer which binds the barbed end of actin filaments. GFP-labelled variants of each were studied. Cap1-GFP and Cap2-GFP colocalize with actin patches in rhodamine-phalloidin stainings. They are highly enriched in the first six micrometers from the tip, mostly cortical, and at sites of septation and branch formation. Cap1p-GFP and Cap2p-GFP patches moved at 224 (+98) nm/s over distances of 0.8 μm (+/-0.7 μm) and generally had a lifetime of 14 seconds ((+/-6.5). Sequential recordings of the entire hypha were analysed, suggesting that these particles undergo a pattern of movement consistent with their role in endocytosis. That is, following an initial non-motile stage, actin patches undergo random movement near their site of formation, often followed by a secondary, linear retrograde movement away from the tip. Co-stainings with the endocytosis marker FM4-64 show partial colocalization, further supporting the notion that actin patches are involved in endocytosis. A second movement type is that of retrograde patches returning to the tip, resulting in a cycling pattern. This suggests maintenance of polarization by endocytic recycling, a mechanism which was corroborated by experiments concerning lateral diffusion in the apical membrane. Application of Latrunculin A results in depolarized, spherical tips. The combination of these results suggests that apart from their role in endocytosis, Cap-GFP patches are charged with the task of maintaining polarization by endocytic recycling.

Actin cables and actin rings were made visible by using a GFP tagged variant of Abp140p, an F-actin binding and crosslinking protein. Abp140p-GFP colocalizes fully with actin cables, actin patches and actin rings in rhodamine phalloidin stainings. Abp140p-GFP cables are mostly cortical, often helical, can be as long as 40 μm and are highly motile. The different fluorescent intensities indicate existence of actin bundles with different numbers of cables. Elongation of the tip of a cable is 184 (+/-62) nm/s. Fine cables in the apical zone often feature Abp140p-GFP patches moving to the tip, where they desintegrate. This is strongly reminiscent of the short, straight actin cables in *S. cerevisiae*, which have been shown to transport exocytic vesicles to the site where a new cell wall is formed. We conclude with a model of the hyphal organisation of the actin cytoskeleton in *A. gossypii*.

abbreviations: CP capping protein, Cap-GFP (= either Cap1-GFP or Cap2-GFP), A.g. *Ashbya gossypii*

Introduction

Apical growth is the primary mode of growth in filamentous fungi. Elucidation of the interactions and of the dynamics of these different components is providing unique insight into the mechanisms of polarized growth.

In the last few years, exciting discoveries about actin have been made mainly using the cytoskeleton of the unicellular budding yeast *Saccharomyces cerevisiae*. The ultrastructure of actin patches has been revealed (Young et al., 2004), their life cycle analysed (Smith et al., 2001), a factor coupling endocytosis and actin patches discovered (Kaksonen et al., 2003), and actin cables visualized (Yang et al., 2002), just to name a few. This new information expands the concept of the many different chores the actin cytoskeleton has (see Pruyne and Bretscher, 2000). Yet, most studies have been done in the budding yeast *Saccharomyces cerevisiae*, and while good knowledge regarding actin patches was also gained from the fission yeast *Schizosaccharomyces pombe* (Takagi et al., 2003; Pelham and Chang, 2001), very little is known about the actin cytoskeleton and its dynamics in filamentous fungi. *Ashbya gossypii*, a novel filamentous model fungus, is well suited to help fill this information gap.

Many observations concerning the development of filamentous fungi have been described in meanwhile standard volumes of mycology (Carlile et al., 2001; Gow and Gadd, 1995; Griffin, 1994). Under favourable environmental conditions, fungal spores germinate and form hyphae. During this process, the spore absorbs water through its wall, the cytoplasm becomes activated, nuclear division takes place, more cytoplasm is synthesized, and from the wall of the germinated spore a germ tube bulges out, enveloped by a wall of its own that is formed as the tube grows. The cell wall forms an extracellular layer that is rigid enough to withstand substantial internal turgor pressure, yet flexible enough to permit the cell to grow. This makes of the fungal hypha a continuously moving mass of protoplasm in a continuously extending tube, with occasional branching occurring further back in the hypha. This unique mode of growth – continuous tip extension - is the hallmark of fungi, and it accounts, in combination with their enzyme repertoire, for much of their environmental and economic significance. It ultimately enables a sessile cell to acquire needed nutrients by exploring the local environment - the same principle which can be found in the extension of root hairs and pollen tubes in plants. Underlying this rapid growth are turnover and synthesis of cytoskeletal elements, and exocytosis and endocytosis of membrane vesicles.

The most important part of a hypha for this kind of growth is the tip. The hyphal tip plays a vital role for navigation, elongation and maintenance of the fungus. The rate of tip extension can be extremely rapid - up to 20 μm per minute. It is supported by the continuous movement of materials into the tip from older regions of the hyphae. Factors responsible for this tubular growth are located at the very tip, polarizing the actin cytoskeleton and hereby the whole cell. So the tip is a site of heavy traffic: Material for the plasma membrane and the cell wall and

catabolic enzymes to degrade the nutrition in the surroundings need to be disposed of, while the digested food has to be transported into the cell. All this happens while the tip is growing and the factors vectorising growth are kept in place.

In a nutshell, exocytosis of vesicles at the apex provides precursor material for the continuously expanding cell wall of the growing cell, while endocytosis accounts for nutrient uptake and especially polarization by vesicle recycling - a way to keep membrane proteins at the tip. But the orchestration of these events is not yet understood. Elucidation of the ultrastructural organisation, of interactions and of the dynamics of these different components is providing an important clue into the mechanisms of polarized growth.

The filamentous fungus *Ashbya gossypii* is well suited for model studies

The filamentous fungus *Ashbya gossypii*, an *Ascomycete*, belongs to the family of *Saccharomycetaceae* (Prillinger, Schweigkoffer et al. 1997) in the order of *Saccharomycetales* and was first described in 1926 by Ashby and Nowell. It possesses the smallest known genome of a free-living eukaryote. The completion of the whole genome sequencing project in *A. gossypii* revealed the most compact known eukaryotic genome (Dietrich et al., 2004), which consists of nine million base pairs distributed on 7 haploid chromosomes, containing 4720 open reading frames with very few gene duplications. Interestingly, 95 % of all genes identified in *A. gossypii* had a homologue in the budding yeast *S. cerevisiae* and for all 200 genes implicated in cell polarity in *S. cerevisiae*, homologues could be identified in *A. gossypii*.

Figure 1 (Movie S01) shows a young mycelium of wild type. The development of *A. gossypii* starts with a phase of isotropic growth. The middle part of the needle-shaped spore (indicated by an asterisk) forms a germ bubble (g), where actin patches localize randomly at the cortex (Knechtle et al., 2003). Then, actin patches start to concentrate at one region at the cortex perpendicular to the axis of the needle, thus marking the site of germ tube emergence. This polarized actin cytoskeleton directs growth from this region causing the first germ tube to extend and form a unipolar germling. Actin localizes as cortical patches to the tip or the germ and less frequently to the hyphal cortex. Actin cables run from the tip into the hypha. The germ tube maintains polarisation and extends consistently in one direction. At the opposite side of the germ bubble a second germ tube is formed to give rise to a bipolar germling. Additional sites of polarity are established at the hyphal cortex and initiate lateral branches. Actin rings are formed at sites that will later form septa, chitin-rich ring-like structures. The first septum is preferably formed at the neck between germ bubble and first germ tube. Hyphal tip growth speed increases during maturation and apical tip branching occurs in mature mycelium (Ayad-Durieux et al., 2000; Wendland and Philippsen, 2000; Wendland and Philippsen, 2001). As no cytokinesis occurs in *A. gossypii*, hyphae consist of multinucleated compartments limited by septa, which are ring-like structures and thus do not divide off the compartments. Sporangia, usually containing eight spores, can be observed in older

mycelium. The spores, which are needle shaped with a whip-like appendix, are set free by lysis.

ARS plasmids of *S. cerevisiae* are able to freely replicate in *A. gossypii*. Moreover, *Ashbya* integrates DNA exclusively via homologous recombination (Steiner et al., 1995). It is the only known filamentous that has both of these properties, which made it possible to develop a very powerful tool for functional genome analysis including PCR-based one-step gene targeting (Wach et al., 1994; Wendland et al., 2000) and recombinant plasmid technology (Steiner and Philippsen, 1994; Steiner et al., 1995). Due to the highly efficient recombination, the background of false positive in such gene-replacement experiments is significantly reduced. For PCR-based one-step gene targeting there is no time consuming in cloning steps because the cassettes can be produced quickly by PCR. All that is needed to construct a cassette is the sequence information of the gene of interest and the DNA template of the selectable marker gene.

Ashbya was originally isolated as a cotton pathogen and causes a disease called stigmatomycosis which affects the development of the hair cells in cotton bolls. It is also a pathogen on citrus plants and tomatoes, where it causes the infected fruits to dry out and collapse (Phaff and Starmer, 1987). Insects like *Antestia* and *Dysdercus* serve as carriers for the needle shape spores as well as for parts of mycelium, thus transferring the disease from plant to plant.

The actin cytoskeleton is a key player for the growing tip

Actin filaments form a cytoskeletal and motility system in all eukaryotes. In the last three decades, eminent discoveries have been made about the many structural facets of the actin molecule and the filaments it forms (dos Remedios and Dickens, 1978; Aebi et al., 1980; Fowler and Aebi, 1983; Steinmetz et al., 1997; Kammerer et al., 1998) as well as the bundling of actin filaments (Millonig et al., 1988; Meyer et al., 1990; Guild et al., 2003). As an essential part of the cytoskeleton, networks of cross-linked actin filaments resist deformation, transmit forces, and restrict diffusion of organelles. A network of cortical actin filaments excludes organelles, reinforces the plasma membranes, and restricts the lateral motion of some integral membranes protein. The actin cytoskeleton complements and interacts physically with cytoskeletal structures composed of microtubules and intermediate filaments.

The actin filament itself is a right-handed, two-strand long-pitch helix. Actin filaments themselves are polarized, owing to the uniform orientation of the asymmetrical subunits along the polymer. One end is called the barbed end, the other the pointed end (according to the arrowhead appearance of actin filaments decorated with myosin in the electron microscope). Actin filaments grow and shrink by addition and loss of actin subunits at the two ends of the filament. The two ends, barbed and pointed, are both able to add and lose subunits. Polymerisation is favoured at the barbed end over the pointed end in terms of steady-state affinity binding.

Reorganization of the actin cytoskeleton is essential for cell-shape change, cell motility, and regulation of cell-to-cell and cell-to-matrix adhesion (Pollard and Cooper, 1986; Gumbiner, 1996; Lauffenburger and Horwitz, 1996). In the budding yeast *Saccharomyces cerevisiae*, the actin cytoskeleton is involved in the establishment and maintenance of polarized secretion and cell growth. Polarization of actin cables and actin patches, two major components of the yeast actin cytoskeleton, is critical for establishment of cell polarity in budding and mating yeast, and many recent discoveries have helped elucidate the role and orchestration of the different parts of the fungal actin cytoskeleton.

A comparison of the genetic basis of the actin cytoskeleton in *A. gossypii* and *S. cerevisiae* is made in Table 0. While components for actin cables and actin rings (neck rings) are all present - albeit often duplicated in *S. cerevisiae* - one important component of actin patches is missing. The F-actin binding domain in Sla2p has been shown to play a role in endocytosis (Baggett et al., 2003). Kaksonen et al. identified ScSla2p as a linker between endocytosis and actin patches. This is an item of the actin patch toolbox that is missing in *A. gossypii*. While this is no indication that these processes are not coupled in *A. gossypii*, it demonstrates that *A. gossypii* must have processes at least partially different from the organisation in *S. cerevisiae*.

The main components of the actin cytoskeleton of *Ashbya gossypii* are depicted in Figure 2 (Movie S02).

Actin patches:

Actin patches are cortical membrane zones invested with F-actin and a host of actin-binding and regulatory proteins including, for example, capping proteins (e.g. Cap1p, Cap2p) and actin nucleation proteins (the Arp2/3 complex). They are core components of the yeast actin cytoskeleton, undergo redistribution during establishment of cell polarity and contain at least 30 proteins (Smith et al., 2001).

Actin cables:

Actin cables are bundles of actin filaments lying at the cell cortex (Knechtle et al., 2003). Aligned along the axis of growth in hyphae, they serve as tracks for polarized particle movement. This accounts for their important role in establishing and maintaining polarity. Actin cables are randomly distributed in nondividing *S. cerevisiae* cells, but are oriented along the mother-bud axis during polarized growth from late G₁ to M phase (Yang and Pon, 2002).

Actin rings:

They are a prerequisite for septum formation, but not required for polarized growth. *A. gossypii* deletion mutants have been described which are totally devoid of actin rings and septa, but still grow in a normal polarized manner (Wendland et al., 2002).

We used CAP1 and CAP2, the two subunits which make up capping protein, and fused them with the ORF for GFP to visualize actin patches in live conditions. CAP1 and CAP2 belong to the family of actin capping proteins. While some capping proteins have been shown to sever actin filaments (Sizonenko et al., 1996), their main role is to block addition and dissociation of actin subunits to and from an actin filament by binding to its barbed or pointed end. Many of these proteins also stimulate the formation of new filaments that grow only at their free end. The capping protein of *S. cerevisiae* has been shown to be one of four components required for actin polymerization and motility in vitro (Loisel et al., 1999), although actin patches lacking capping protein seem relatively normal (Young et al., 2004).

CAP1 corresponds to the alpha subunit of CP (capping protein). CAP1 is encoded by the single gene CAP1 with a Mr of 32 kD. The association of both the a subunit CAP1 and b subunit CAP2 make up CP, a heterodimer. Conservation thereof can be seen in the fact that the alpha and beta subunits of nematode actin capping protein function in yeast (Waddle et al., 1993). The interaction of CP with actin is essential for the proper assembly of actin filaments. During the cell cycle, CP colocalizes with actin in cortical patches but not with actin cables or actin rings.

Null mutants of CAP1 and/or CAP2 are viable in *S. cerevisiae*. They grow slowly and have cell size heterogeneity, a severe deficit or complete absence of actin cables, and depolarization of the cortical actin patches. Deletion of one subunit leads to disappearance of the other. Deletion of the gene for one subunit leads to a loss of protein for the other subunit. The null mutant has a severe deficit of actin cables and an increased number of actin spots in the mother. Cells are round and relatively large. These features are heterogeneous within a population of cells and vary with genetic background. Overexpression of CAP1 and CAP2 also causes loss of actin cables and cell enlargement, as well as the additional traits of aberrant morphogenesis and cell wall thickening. Capping protein null strains and overexpression strains exhibited normal polarized secretion during bud growth

For visualization of actin cables and rings, we used ABP140 fused to GFP. Asakura et al. discovered 1998 that actin binding protein 140 (Abp140p) is an F-actin binding protein in budding yeast. Two years ago, it was used by Yang and Pon to label actin cables and record their dynamics in living yeast. Abp140p does not show homology to any known actin binding protein and is expressed in cells by fusion of two ORFs (YOR239W and YOR240W) by means of a +1 translational frameshift. The encoded protein Abp140p consists of 628 amino acids with a calculated Mr of 71,484 kD (the '140' in the name stemming from the fact that it immuno-precipitates as a dimer). Abp140p interacts directly with F-actin and binds along the sides of F-actin. Abp140p has a weak F-actin-cross-linking activity. Abp140p binds to F-actin at a molar ratio of one Abp140p molecule to about 30 actin molecules. In comparison, the stoichiometry of the binding of most cross-linking proteins to actin molecules is 1:4 - 1:6. Abp140p-GFP colocalizes with both cortical actin patches and cytoplasmic actin cables in intact cells. ABP140 is not required for cell growth and does not affect actin polymerisation,

and deletion mutants of ABP140 are viable.

Materials and Methods

Construction of AgCap1p-GFP, AgCap2p-GFP and AgAbp140p-GFP

(kindly provided by Philipp Knechtle and Hans-Peter Schmitz)

We were interested in the localisation pattern and the dynamics of AgCAP1 and AgCAP2 and decided to integrate a second copy of each of these genes that is C-terminally fused to GFP. The plasmid pGUG (Knechtle P., PhD Thesis, 2003) was amplified with oligonucleotides for the selected ORFs: AgCAP1: 5CAP1GFPpGUG x 3CAP1GFPpGUG; AgCAP2: 5'CAP2GFPpGUG x 3'CAP2GFPpGUG. The deletion set was 50 bp each for AgCAP1 and AgCAP2. For a C-terminal GFP fusion of AgCap1p and AgCap2p, the plasmids pAGCAP1 and pAGCAP2 were transformed with the respective PCR product. Verification for a correct recombination was done by PCR using oligonucleotides CAP1verfor x Green2 for the 5'-site and G3.2 x CAP1verrev for the 3'-site in pAGCAP1-GFP; pAGCAP2-GFP was verified using CAP2verfor x Green2 for the 5'-site and G3.2 x CAP2verrev for the 3'-site. The plasmid pAGCAP1-GFP was digested with BglII. Blunt ends were generated in a "fill-in" reaction using a polymerase with a 5' - 3' exonuclease activity. The 2279 bp fragment was then subcloned into the Scal site of pAIC. The new plasmid pAIC_AGCAP1-GFP carried the AgCAP1 ORF C-terminally fused to GFP without any remaining of the GEN3 module. The promoter region of AgCAP1 was 483 bp in length. pAIC_AGCAP1-GFP was amplified in *E.coli* and digested PstI/Sall to obtain the AgCAP1-GFP fusion gene with flanking homologies to the AgADE locus. 5 µg were transformed into the Agade2delta1 strain. Homokaryotic transformants were obtained and named AgCAP1-GFP. Verification was done by PCR using oligonucleotides Agade2verfor x Agade2verrev. The plasmid pAGCAP2-GFP was digested with EcoRV/HinDIII. Blunt ends were generated in a "fill-in" reaction using a polymerase with a 5' - 3' exonuclease activity. The 3014 bp fragment was then subcloned into the Scal site of pAIC. The new plasmid pAIC_AGCAP2-GFP carried the AgCAP2 ORF C-terminally fused to GFP. The promoter region of AgCAP2 was 1294 bp in length, the ScURA3 terminator from the GUG module was shortened from 286 bp to 136 bp in length. pAIC_AGCAP2-GFP was amplified in *E. coli* and digested with SpeI/HinDIII to obtain the AgCAP2-GFP fusion gene with flanking homologies to the AgADE locus. 5 µg were transformed into Agade2.1. Homokaryotic transformants were obtained and named AgCAP2-GFP. Verification was done by PCR using oligonucleotides Agade2verfor x Agade2verrev.

The C-terminus of Abp140p was tagged with GFP(S65T) by using PCR-based insertion into a plasmid bearing a copy of ABP140. The sequence of the homolog of ScABP140 was retrieved from the *A. gossypii* genome database. Primers 02.378 and 02.379 were designed

and used for PCR amplification with genomic *A. gossypii* DNA as template. Obtained PCR product was cut with *HinDIII* and *BamHI* and ligated into YCPlac111 (Gietz and Schiestl, 1991) cut with the same restriction enzymes. The resulting vector was dubbed YCPABP140. Primers 02.272 and 02.279 were used to obtain the GFP and resistance marker fragment from pGUG (Knechtle et al., PhD Thesis). Co-transformation of this fragment together with YCPABP140 was performed in *S. cerevisiae* and transformants subsequently grown under selective pressure by G418. Growing colonies were picked and the YCPABP140-GFP plasmid isolated. The plasmid was then transformed via electrophoresis into *A. gossypii* and the resulting strain grown under selective conditions. Since integration is of plasmidic nature, hyphae with strong signals were chosen directly with the microscope under weak UV illumination (10%) and then recorded.

Analysis of the Cap1p, Cap2p and Abp140p protein sequences

The sequences of ABR007C, ADL101C and ACR130W, the *A. gossypii* homologs of CAP1, CAP2 and ABP140, were retrieved from the Ashbya genome database, generated from the complete genome sequencing approach by Dietrich et al., 2004. The resulting amino acid sequences were used for analyzing similarity to the homologous genes in *S. cerevisiae* (YKL007W, YIL034C and YOR239W, respectively).

Regions of identity were defined using the Align Plus 5.03 module of the CloneManager 7.03 suite (Scientific & Educational Software, Cary, NC). "Compare multiple sequences" was used in Multi-Way mode for multiple alignment without reference. "Align two sequences" in the global alignment mode was used to determine the percentage of identity in similar regions. For all analyses, the BLOSUM 62 scoring matrix for amino acids was chosen.

Staining Procedures

The actin cytoskeleton was visualized using phalloidin coupled fluorophores (according to Amberg, 1998, modified). *A. gossypii* was cultured in AFM (selective conditions for ABP140-GFP). All subsequent steps were performed on ice and without centrifugation to assure maximum preservation of the delicate actin cytoskeleton. After letting mycelia settle to the ground, 200 μ l of the culture were mixed with 1.5 ml of 4% paraformaldehyde and fixed for 1 h. 100 μ l of settled mycelia were washed twice with phosphate-buffered saline (PBS), and resuspended in PBST (PBS containing 0.03% Triton X-100). The concentration of rhodamine-phalloidin (6.6 μ M in MeOH; Molecular Probes, Eugene, OR) was reduced to 5 μ l per 100 μ l mycelium. This way, the usually overpowering fluorescence of actin patches in the tip was reduced as to reveal the less bright structures as well. The dye was incubated with mycelia for 1 to 1.5 hours in the dark. After three washing procedures in PBST, mycelia were resuspended in 50 μ l of Vectashield mounting medium (Vector Laboratories, Burlingame, CA). Five microliter thereof were put on a slide, covered with a coverslip and sealed with

rubber cement ("Fixogum," Marabuwerke GmbH & Co., D-71732 Tamm). Images were taken during the next five hours to avoid the possibility of age-induced artifacts.

The endocytic live dye FM4-64 was added to the coverslip of time-lapse slides to an end concentration of 2 μ M. Absorption sucked in the dye and uptake could quickly thereafter be observed in the microscope. The same technique was used for administration of the membrane fluidizer Benzyl alcohol [20 μ M] and the actin-inhibiting drug Latrunculin A (in concentrations of 10, 50 and 200 μ M).

Microscope Setup

The microscopy units used (as described in Hoepfner et al., 2000, modified) consisted of two 'Axioplan 2 imaging e' microscopes (Carl Zeiss, Feldbach, Switzerland). One was equipped with the objectives Plan Neofluar 100x Ph3 N.A. 1.3, Plan Neofluar 63x Ph3 N.A. 1.3, Plan Neofluar 40x Ph3 N.A. 1.3 and the illumination sources 75 W XBO, HBO and 100 W halogen. The other, with the objectives Plan Apochromat 100x DIC N.A. 1.4, Plan Apochromat 63x DIC N.A. 1.4, Plan Neofluar 40x Ph3 N.A. 1.3 and the illumination sources 75 W XBO and 100 W halogen. The UV illumination source was controlled by a MAC2000 shutter and filter wheel system (Ludl Electronics, Hawthorne, NY, USA). The cameras were a TE/CCD-1000PB and an NTE/CCD back-illuminated cooled charge-coupled device (Princeton Instruments, Trenton, NJ). Phase contrast and DIC filters for Nomarski illumination were used for brightfield imaging, according to the manufacturer (Carl Zeiss). Following filter sets were applied for different fluorophores: DIC filter for Nomarski Illumination and #41018 for GFP with excitation spectrum at 450-490nm and a longpass emission at 500+ (Chroma Technology Corp, Rockingham, VT); for rhodamine-phalloidin double stainings with GFP, Chroma filter #41025 Piston GFP with a bandpass emission of 500-530nm (excitation at 450-490) for GFP and Zeiss Filter #15 for rhodamine (ex: 540-552, em: 590+). The FM4-64 live dye in Cap-GFP strains was recorded with the same double labelling filter set. Excitation intensity was controlled with different neutral density filters (Chroma Technology). The setup, including microscope, camera, and Ludl controller, was controlled by MetaMorph 4.1.7 software (Universal Imaging Corporation, Downingtown, PA).

For FRAP experiments, a Leica TCS-NT-SP1 and a Zeiss CLSM 510 META were used. An area with the diameter of 3 μ m was bleached by 32x zoom and subsequent recovery recorded during two to three minutes. The bleached area was plasma membrane either stained by FM4-64 or labelled with Rho1-GFP.

Image Acquisition and Processing

With a fluorescent image taken every 2 minutes, growing hyphae could be observed for 2 hours and 40 minutes without harm, although the GFP signal was bleached gradually and hyphal autofluorescence increases with exposure to UV light. Alternatively, streaming movies

of a single focal plane of a specimen provided temporal resolution of three images per second. To assure that the movement of all observed structures were integrated, we further performed rapid sequential recording in all three spatial axes. With x,y and z being combined with the dimension of time, this is also called 4D microscopy. This way, the entire fluorescent action in the apical zone of a hypha could be recorded in 2-3 seconds for a single timepoint, resulting in complete three-dimensional information over a timespan of averagely 2 minutes. When strong fluorescent signals were recorded, no other image processing than adjustment of contrast was used. This was done with the "Scale Image" of the Metamorph drop-in. With many signals in this study being of rather weak nature, though, deconvolution yielded unsatisfying results. Another method was chosen to reduce the diffuse hyphal background and thus emphasize the GFP signal. For these cases, the "Flatten Background" algorithm worked fine (object size definition of four pixels). While the whole image gets more grainy this way, the contrast is sometimes dramatically increased. To avoid processing artifacts by different methods, this was the only processing applied. Movement analysis was performed by following individual elements (i.e. actin patch or actin cable) through time and space, selecting the pixel with the highest fluorescent intensity as the center of the element. Coordinates and paths were logged directly in Excel worksheets and evaluated there. Measurement of brightness was achieved using MetaMorph's "Region measurements" drop-in. Fluorescent picture sets of two labels were combined using Meta-Morph's "Color overlay" and "Color align" drop-in. The time-lapse and 4D image series were transformed into movies (QuickTime (Apple Computer, Cupertino, CA) using MetaMorph. Adobe Photoshop 6.0 (Adobe Systems, Mountain View, CA) was used for still pictures. For time-lapse acquisition, the fungus was grown on a slide with a cavity (time-lapse slide) that was filled with agar-solidified AFM (AMM for fluorescent images). Spores were preincubated in a humid chamber without coverslip until they reached the required developmental stage. Then, a coverslip was applied.

Results

ACTIN PATCHES

Actin patches are concentrated in the apical zone

The amount and distribution of actin patches was assessed in rhodamine-phalloidin stainings of fixed wildtype mycelium (Table 1). We wanted to assure that actin patches are indeed concentrated at the tip, and not simply brighter, an effect which might mask a polarization of actin patches in numbers. For this, we divided the hyphal tip into three adjacent zones (Table 1 A). The first six micrometers at the very tip were determined by eye in different specimens as the zone where actin patches are brightest and seem most numerous. The two following zones of the same length provided a 'control' by showing the average patch number in the subapical region. An example of a hypha is given (Table 1 B). All examined hyphae were stained with the same procedure and recorded in three dimensions as not to miss any patches. Table 1 C shows the variation of actin patch density within the same hypha and between individuals. There is an average of 66 (± 20 , $n=28$ specimens) actin patches in the first 18 μm of the tip, ranging from 123 to 42. The densest accumulation is in the apical zone just beneath the tip. These dense zones are indicative of polar growth. The first, apical segment of the six micrometers at the tip has 45 (± 6) percent actin patches, while the following two segments are roughly equal (28 (± 4) percent for 6-12 μm and 27 (± 5) percent for the last 12-18 μm). We measured the hyphal diameter of the same specimens where actin patches were counted to assure that a higher number of actin patches is not due to a larger hyphal diameter. It is not the case that higher amounts of actin patches correspond to a larger diameter of the hypha, whether within the same hypha nor between individuals (Table 1 D). Thus, the zone of polarization is restricted to the first six μm after the very tip.

But rhodamine-phalloidin is used in fixed mycelium and cannot inform about the live actin cytoskeleton. So we used two actin capping proteins tagged with GFP to visualize actin patches in *A. gossypii*.

Sequence analysis of AgCap1p and AgCap2p

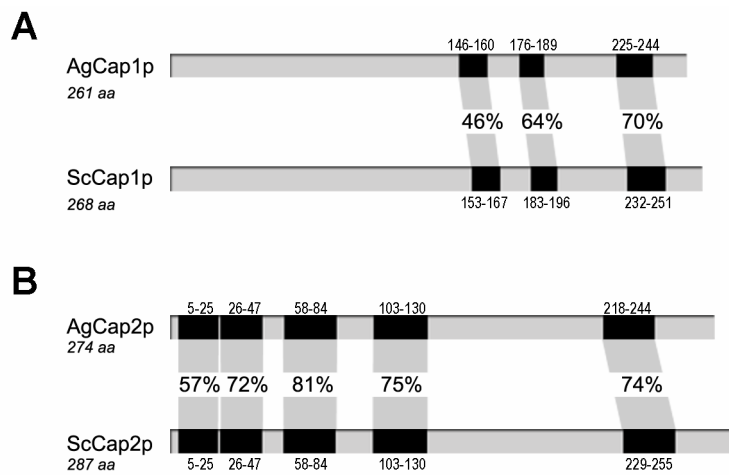
Figure 3 A shows the alignment of AgCap1p and ScCap1p. The putative protein AgCap1p has a length of 261 amino acids. It shares 45% identity with ScCap1p, which is only 7 amino acids longer. Identity increases towards the C-terminus. The protein was modeled with SWISS-PROT (Guex and Peitsch, 1997) (Figure 3 B) and shows the same 'mushroom' structure seen in the model for budding yeast. Amino acids 239R and 251W at the COOH terminus of the alpha subunit (Cap1p) were shown to be paramount to the model proposed for the alpha-beta subunit combined protein as investigated in the study of Kim and

coworkers (2004). In this model, the C-terminus of each subunit forms a 'tentacle' which binds to a groove in the actin monomer. The amino acids 239R and 251W are the pivots for the 'tentacle' of the Cap1p subunit, and substituting them results in a weak binding affinity of Cap1p to actin. These structurally important amino acids were found at the same alignment positions in *A. gossypii* (R232 and W244 in Ashbya). They are shown as green molecule structures in Figure 3 B. Figure 3 C compares AgCap2p and ScCap2p. The identity of AgCap2p and ScCap2p is more than 10% higher, though, although it increases towards the N-terminus in this case. The difference of amino acids lies at 13 (274 for *A. gossypii*, 284 for *S. cerevisiae*). Cap2p in budding yeast has been shown to be of less importance than Cap1p. While necessary for high affinity capping, it contributes over 1000 times less to actin capping than the alpha subunit Cap1p. The SWISS-PROT model features a similar structure for AgCap2p as that for AgCap1p (Figure 3 D). The two subunits form a heterodimer.

CapZ, the capping protein of the chicken sarcomer which was analyzed by the multiwavelength anomalous dispersion crystallography at 0.21nm resolution (Yamashita et al., 2003), was used as a template in both cases. The resulting homology-based model for *A. gossypii* CP is similar to that of chicken CP. Both models share important structural features of the 'tentacle' model: CapZ has a pair of mobile extensions for actin binding, probably forming flexible links to the end of the actin filament. The same amphipathic alpha-helix is found at the C-terminus in each monomer of the *A. gossypii* CP. Pivotal basic residues linking the tentacle to the mushroom-like main structure are found at conserved places in *A. gossypii* CP as well.

Addition to Figure 3:

Comparison of highly homologous regions in the Cap1 (A) and Cap2 protein (B) of *A. gossypii* and *S. cerevisiae*.



AgCap1p-GFP and AgCap2p-GFP colocalize fully with actin patches in rhodamine-phalloidin stainings

In double stainings of Rhodamine-Phalloidin in the Cap-GFP strain, Cap-GFP proteins colocalize fully with rhodamine-phalloidin stained actin patches (Figure 4 A). An accumulation of Cap-GFP actin patches in the apical zone is observed in both cases. Since growth and

structure of the mutant Cap-GFP strains are identical to wildtype, we conclude that both Cap1p-GFP and Cap2p-GFP label fully functional actin patches.

While the majority of Cap-GFP patches corresponded to the rhodamine-phalloidin staining in terms of fluorescent intensity, exceptions could be found (Figure 4 B and C). About 5% of all patches did not show a corresponding relative intensity between Cap-GFP patches and actin patches labelled by rhodamine-phalloidine. An explanation therefore is discussed later.

Live actin patches were then visualized using Cap-GFP strains.

Characterization of the AgCap-GFP strains

The first observation was long-term, to confirm the expectation that Cap-GFP patches should localize at all time to polarized tips (Figure 5 and Movie S03). In addition, sites of emerging branches can be determined by a gathering of Cap-GFP patches. The specimen shown was observed for nearly three hours. However, hyphal autofluorescence increases with age and UV illumination. With both Cap-GFP signals being of low intensity, we focused on mycelium between 12 and 20 hours old, usually recording activity over periods between one and ten minutes.

Figure 6 shows still images from such short-term recordings. Since up to three images may be taken per second, the movement of individual patches may be followed. Figure 6 A (Movie S04) has the usual concentration of actin patches at the tip, with a few running further back in the hypha. In certain conditions, hyphal tips will grow towards the coverslip, enabling a frontal view of the activity in the tip. In Figure 6 B (Movie S05), it can be seen that Cap-GFP patches localize mainly to the cortex of the hyphal tip, while the spherical segment of the very tip is patch-free. In the apical zone, though, actin patches moving in the cytosol are observed more often. Figure 6 C (Movie S06) confirms a cortical distribution of actin patches further back in the hypha, although some patches may be seen in the cytosol. The cortical localization of actin patches is similar to the findings in *S. cerevisiae* and *S. pombe*.

Cap-GFP patches can be seen in all stages of *A. gossypii*'s life cycle (Figure 7 and Movies S07 and S08). Beginning with the germ bubble (Figure 7 A and B), it is then visible in unipolar germlings (Figure 7 C), young mycelium with lateral branches (Figure 7 D) and also in old mycelium featuring tip branching (data not shown).

Actin cables and rings are not labeled by either Cap-GFP strain, and the Cap-GFP strains are devoid of filamentous structures.

Actin patches visible with Cap-GFP move rapidly in distinct ways

We analyzed movement of Cap-GFP patches in rapid sequential Z-series of hyphal tips, resulting in so-called 4D-movies. Since the human eye is adapted primarily to movement (Russ, 1996), the movies of the section Supplemental Material should be considered.

Figure 8 shows activity of Cap-GFP patches at the hyphal tip. Figure 8 A (Movie 09) is another case of a tip growing towards the objective. This way, actin patch movement can be seen frontally at the very tip. There are patches coming from the cytoplasm to the front and reversing at the tip, following the plasma membrane. It is clear that, although patches come to the tip, the very center of the tip is mostly devoid of patches. This agrees with a patch-free spherical tip segment first observed in Rhodamine-Phalloidin stainings of wildtype (Knechtle et al., 2003). Figure 8 B (Movie S10) shows thirty images of a rapid 4D recording of a hyphal tip viewed from the side. Any patch chosen in the subapical region can be seen moving away from the tip. Movement in the apical zone seems rather chaotic and is hard to define, as the directionality of single patches often appears to be random.

From multiple 4D recordings, the dynamic parameters were evaluated (Table 2). Patch speed was measured, following patches through one plane in rapid time-lapse movies (Table 2 A). It averages 224 (+98) nm/s (n=84), thus lying below patch speeds measured in *S. cerevisiae* (386.6 (+/-176.9) nm/s (Smith et al., 2001); 490 +/- 300 nm/s (Doyle and Botstein, 1996; Waddle et al., 1996)) and *S.p.* (320 (+/-140) nm/s; Pelham and Chang, 2001)). The running distances of patches were also determined. They vary depending on the zone. Cap-GFP patches in the apical zone run short distances rarely exceeding 1 μm . Especially redirecting patches disappear once they have reached the very tip. Patches further back in the hypha can cover distances over 5 μm , though. This makes for a wide spread, resulting in an average distance of 0.8 μm (+/-0.7 μm).

The lifetime of patches was measured in 4D recordings (Table 2 B). With an average of 14 seconds ((+/-6.5); n=64), they live 1.5 times longer than Abp1-GFP patches in budding yeast (10.9 +/-4.2). The spread of speed measurements is also larger in *A. gossypii*, ranging from five seconds to half a minute. This is, however, significantly lower than the lifetime of over two minutes measured in Crn1-GFP patches of *S. pombe*.

In *S. cerevisiae* and *S. pombe*, patches were described as showing directed and random movement (Waddle et al., 1996; Pelham and Chang, 2001). While random movement is also observed in *A. gossypii* Cap-GFP patches, the movement of many patches falls into three possible categories (Table 2 C). The first, most obvious movement is retrograde, i.e. away from the tip. It can be seen in rapid sequential time lapse (4D) movies of AgCap-GFP tips. Of 84 patches with an obvious directionality, 66 moved away from the tip, while only 10 moved towards it. 8 patches moved to the center of the hypha, i.e. its longitudinal (rotationally symmetrical) axis.

We attempted to resolve the seemingly chaotic movement of actin patches in the apical region. For this means, movement of individual Cap-GFP patches was traced and combined in the schematic representation of the hyphal tip (Figure 9). The most prominent movement of patches away from the tip is already evident in 4D movies. It is depicted in Figure 9 A. A different movement was discovered late due to its nature: In the apical region distal from the tip, Cap-GFP patches often return to the tip (Figure 9 B and Movie S11). This is a process of

redirection, where actin patches appearing at the plasma membrane three to six μm behind the tip move back towards the tip in the cytosol.

A constitutively activated formin causes Cap-GFP patches to form elongated structures

Formins are being thoroughly investigated in *A. gossypii*, and one formin has been shown to be involved in the formation of actin cables, mediating transport of secretory vesicles. In a deletion of the formin Bnr1 in *A. gossypii*, hyphal tips were enlarged and had more actin patches than wild type (Hans-Peter Schmitz, personal communication). We wanted to see what kind of role this formin plays in actin patches in live conditions. To this end, we integrated a constitutively activated formin, BNR1 with the regulatory domain DAD deleted, into the CAP1-GFP strain.

The dynamic properties of Bnr1 Δ DAD-Cap1p-GFP patches do not differ from those measured in the Cap-GFP strains. Directionality of movement is similar to the wild-type Cap-GFP strains, and the average patch speed was 208nm/s (+/-176), thus lying in the normal range of Cap-GFP patches. But these strains with the constitutively activated Bnr1 show an interesting feature: Their Cap1-GFP patches are often associated with fluorescent, elongated structures. This is shown in Figure 10 (Movie S12), where three images of a single-plane streaming recording are shown. The cable-like structures persisted for 40 seconds. We were surprised to find such structures, because no filamentous structures can be observed in the normal Cap-GFP strains. Hence, the filamentous structures must originate from the Cap-GFP patches themselves. While the mechanism for this is not clear, it shows that these elongated structures and actin patches are closely related.

Effect of Latrunculin A on actin patches

The actin depolymerizing drug Latrunculin A was added to study its effect on Cap-GFP patches (Figure 11). Administered in high doses (200 μM), it leads to their gradual destruction and a subsequent blurred fluorescence in the hypha (Figure 11 A). It also seems to inhibit actin patch movement in low doses (25-50 μM , data not shown). Prolonged exposure to Lata causes tips to swell, resulting in the typical 'frog fingers' (Figure 11 B). The swollen tips eventually lyse, probably due to a weakened cell wall collapsing under turgor pressure.

Actin patches have been shown to function in the endocytotic process in *S. cerevisiae* (Kaksonen et al., 2003). FM4-64, a marker for endocytosis (Vida et al., 1995; Fischer-Parton et al., 2000), was used in combination with Cap-GFP strains (Figure 12). Half a minute after addition to the microscope slide (2-20 μM), FM4-64 appeared as dots at the tip, corresponding to putative endosomes. These dots colocalize with Cap-GFP actin patches (while not every actin patch contains FM4-64). This observation is consistent with dye internalization by endocytosis. With FM4-64 also strongly staining the plasma membrane, it is

noteworthy that at the very tip fluorescence is markedly decreased. The plasma membrane is either thinner in this area, or FM4-64 uptake is obstructed there. Another possibility is that the new addition of membrane rapidly dilutes the dye.

Actin patches suggest maintenance of polarization by endocytic cycling

In *S. cerevisiae*, it has been shown that polarity can be maintained by endocytic cycling of membrane proteins responsible for polarized growth (Valdez-Taubas and Pelham, 2003). For this mechanism, slow diffusion in the plasma membrane is required. Filipin was shown to stain shmoo, the elongated and polarized yeast appearance which form in response to mating pheromone, in a highly polarized manner (Bagnat and Simons, 2002). This is probably due to the high affinity of Filipin for sterols. Filipin also brightly stains the apical region of hyphae in *A. gossypii* (Hanspeter Helfer, personal communication), indicating that the tip may be rich in sterols, resulting in slow diffusion in the apical region of the plasma membrane. We proceeded to investigate the properties of the apical membrane in *A. gossypii* in two ways to evaluate if endocytic cycling contributes to polarity in *A. gossypii*. We would predict that such a mechanism of polarity maintenance would be crucial in a permanently polarized hypha.

Benzyl alcohol is a membrane fluidizer (Mukhopadhyay et al, 2002; Sinicrope et al., 1992). It increases fluidity of the plasma membrane in *S. cerevisiae* by 12%. We applied it to young mycelium of the Cap-GFP strains with normal apical concentration of actin patches (Figure 13 A). The observed effect two minutes later is shown in Figure 13 B. Indeed, fluidization of the plasma membrane makes the polarisation of actin patches in the tip disappear. The recordings were evaluated statistically to corroborate this impression (Figure 13 C): Benzyl alcohol equalizes the polarized distribution of Cap-GFP patches.

We proceeded to perform FRAP experiments to determine the diffusion constant of the apical membrane of *A. gossypii* (Figure 14). For an area with the diameter of three micrometers, two minutes are required to recover fluorescence. A diffusion constant of $0.0086 \mu\text{m}^2/\text{s}$ (± 0.0016) was determined. Although 3-4 times more fluid than the plasma membrane in *S. cerevisiae*, it is nowhere near the rapid diffusion in mammalian COS cells. The results, obtained with FM4-64 stained membranes, was confirmed using a AgRho1-GFP strain, in which the membrane is brightly fluorescent.

While actin patches are the most prominent element of the fungal actin cytoskeleton, the two other important components, actin cables and actin rings, were not visualized with Cap-GFP constructs. For this reason, we continued the study by labeling an actin binding protein.

ACTIN CABLES

Sequence analysis of AgAbp140p

AgAbp140p was compared to its homolog in budding yeast (Figure 15). They share 49% identity, which is more prominent at the C-terminal half of the protein. ScAbp140p is 58 amino acids longer than AgAbp140p. With no crystallographical analysis of Abp140p yet, a structural comparison could not be performed.

The translational frameshift found in *S. cerevisiae* at the base pairs 829-835 was also detected in *A. gossypii*, at the position 643-650. The heptamer with the frameshift is identical in both organisms: CTT-AGG-C. Interestingly, this sequence is now used to detect hitherto unknown frameshifts in other proteins (Shah et al., 2002).

AgAbp140p-GFP fully colocalizes with actin cables and rings in rhodamine-phalloidin stainings

The appearance and localization of actin cables was assessed in Rhodamine-Phalloidin stainings of the cytoskeleton of wildtype and of the fixed Abp140p-GFP strain (Figure 16). Actin cables and rings feature complete colocalization. The general appearance of actin in Rhodamine-Phalloidin stainings is described and pictured in Knechtle et al. (2003) and is consistent with the findings in this study. Apart from staining actin cables, actin patches are also labelled with Abp140p-GFP, albeit less strongly than the cables. Abp140p-GFP patches are found predominantly at the tip. The brightest signal in Abp140p-GFP strains is found at actin rings, though. The results regarding this structure are presented later on. With growth and structure of the Abp140-GFP strain being indiscriminate to wildtype, we conclude that Abp140p-GFP is a completely functional label for actin cables, rings and patches in a fully functional strain. We proceeded to study the dynamics of actin cables, patches and rings with this strain.

Abp140p-GFP cables are often associated with actin patches

An observation in many studies of the fungal actin cytoskeleton was that actin patches are often associated with actin cables. This notion was corroborated in rhodamine-phalloidin stainings as well as in live recordings of the Abp140p-GFP strain (Figure 17 A and B, respectively). Due to the difference in fluorescent intensity of these two structures, the percentage of actin patches associated with cables could not reliably be determined, though. Interestingly, Abp140p-GFP patches observed at the end of Abp140p-GFP cables are strongly reminiscent of actin comet tails seen in bacteria like *Lysteria*, which hijack the actin cytoskeleton of the invaded host.

The possibility that these punctate structures are merely the bright diametral circle of cross-sectioned cables was eliminated by making complete three-dimensional recordings of the hypha at different time steps. With the entire hypha being covered in 0.4 μm steps at different time points, no cross-sections of Abp140-GFP cables are made.

Characterization of the *AgAbp140p-GFP* strain

As with Cap-GFP patches, Abp140p-GFP labelled structures can be seen in all developmental stages in *A. gossypii*. As presented in Figure 18 A, actin cables are seen already in germ bubbles of the Abp140p-GFP strain. In unipolar germlings (Figure 18 B and Movie S13), they align along the main germ tube axis, emanating from the tip. The tip itself often features Abp140p-GFP actin patches. In older mycelium of 12-20 hours of age, actin cables are oriented along the axis of growth in an often spiral manner (Figure 18 C and Movie S14). Three-dimensional reconstructions reveal that they are predominantly cortical. Some are as long as 40 μm .

Actin cables visualized with *Abp140p-GFP* are highly motile and flexible

The first impression of dynamic Abp140p-GFP cables is that they are surprisingly motile. Possibly, the term 'track', which is often used for actin cables, is misleading in its association with rigidity. Figure 19 shows dynamic actin cables in the Abp140p-GFP strain. In Figure 19 A (Movie S15), a cable is shown of which the end at the tip of the germ tube (marked by an arrowhead) moves toward the germ bubble. The inverse movement can be seen in Figure 19 B (also Movie S15), where a minute later, a bright segment of a cable moves towards the tip. Bright cables towards the back of the hypha show nicely how much Abp140p-GFP cables may change appearance within two minutes (Figure 19 C (Movie S16) and Figure 19 D (Movie S17)). Bright cables found back in a hypha can also be observed in rhodamine-phalloidin stainings of wild type. In both cases, though, they are not observed in young mycelial stages. They appear remote from the tip in older individuals of more than 20h age.

By following the growing ends of Abp140p-GFP cables, we were able to measure cable elongation (Table 3). The average rate of extension of the tip of an elongating actin cable is 184 (+/-62) nm/s (n=19). Although slower and spread over a smaller range, it is in the same order of magnitude observed for Abp140p-GFP cables in *S. cerevisiae* (290 +/-80 μm /s).

Actin patches move towards the tip on *Abp140p-GFP* cables

Concomitant with the observation that in Abp140-GFP strains, actin patches are often associated with actin cables, Abp140p-GFP patches are also regularly associated with cables emanating from the tip (Figure 20 A and Movies S18 and S19). They can also be seen at the tip without being linked to a cable. A most decisive observation is that Abp140p-GFP cables

emanating from the very tip feature punctate structures which are delivered to the tip, where they dissolve. Three such events are pictured in Figure 20 B (Movie S20), Figure 20 C and D. This movement was always directed towards the tip. The punctate structures in Abp140p-GFP strains colocalize with actin patches in rhodamine-phalloidin stainings, and the speed achieved by these punctate structures is similar to that of Cap-GFP patches (174nm/s (+/- 68)). Cables at the tip are often shorter-lived than brightly fluorescing cables towards the back of the hypha. Tip-associated cables exist for merely half a minute, while the bright cables back in the hyphal body may persist for well over two minutes.

In the presence of the actin polymerization inhibitor Latrunculin A, Abp140p-GFP cables are abolished, giving rise to a uniformly blurred GFP fluorescence in the hypha (data not shown). Unlike Cap-GFP patches, mobility of Abp140p-GFP cables could not be arrested. Even with low doses of LatA, they disintegrated rapidly. The cause for this may be that the actin in actin cables is more easily accessible for phalloidin than in actin patches.

Actin cable based vesicle transport is defect in the formin deletion mutant Δ Agbni1

Because Formins were reported to catalyse actin cable polymerization (Pruyne et al., 2002; Sagot et al., 2002b), we investigated the actin cytoskeleton of another formin deletion mutant, Δ Agbni1. To confirm that AgBni1p is needed for secretory vesicle transport, the *SEC4* homolog of *Ashbya* was isolated by Hans-Peter Schmitz and fused to GFP. In budding yeast, the gene product of *SEC4* fused to GFP localizes to secretory vesicles and moves in a directed manner towards the bud tip along actin cables (Schott *et al.*, 2002). We transformed *A. gossypii* with a plasmid carrying an amino-terminal fusion of GFP to AgSEC4 under its native promoter. As shown in Figure 21 A (Movie S21), the fusion product localizes mainly to the tip. Using video microscopy, movements of vesicles towards the tip can be observed. Two sets of frames of this movie, demonstrating tip-directed movements, are shown in Figure 21 B (Movie S22 and S23). Vesicles move with an average speed of $0.9 \pm 0.5 \mu\text{m}/\text{sec}$ ($n=29$) observable over distances up to 10 μm . Addition of Latrunculin A, which disrupts actin structures, abolishes vesicular movement and apical localization, giving rise to a uniform fluorescence within hyphae (Figure 21 C). In order to observe the localization of vesicles in the absence of AgBni1p we transformed heterokaryotic mycelium of Δ Agbni1 with the plasmid carrying the GFP-AgSec4p marker. Spores of these transformants were grown under conditions selective for both, the deletion and the plasmid. The GFP signal was distributed all over the cells (Figure 21 D). This verifies that continuous tip-directed transport of secretory vesicles via actin cables is essential for hyphal growth.

ACTIN RINGS

A surprising result was that in the Abp140p-GFP, actin rings are labelled strongly. This was not the case for Abp140p-GFP in *S. cerevisiae*. The strength of this signal became obvious in one experiment: We integrated ABP140-GFP in the genome. While the signal intensity for actin cables was disappointingly low, the actin rings were still well visible. However, the actin ring is a difficult structure to study, as the exact site and time of its genesis are rather hard to predict.

Actin rings are no barrier for actin cables. Figure 22 A (Movies S24 and S25) shows two examples where actin cables clearly pass through actin rings. Figure 21 B shows still images of a three-dimensional reconstruction, in which the ring is viewed frontally. At twenty seconds, two filamentous structures are clearly seen inside the ring. The original recording, in which these filaments are viewed from the side, identifies them clearly as Abp140p-GFP cables.

Actin rings are not uniform in their distribution of fluorescent label. Figure 22 C shows how fluorescent intensity of Abp140p-GFP actin rings varies in time and concentrates at different places of the ring. At timepoint 0, the top part of the ring is weakly stained, while its 'sides' are brightly labelled. Two minutes later, the bulk of signal is found to the right side of the ring, while another two minutes on, the top of the ring is brightest. The nature and reason of this shifting are unknown.

Actin rings may exist for a long while. In one case, an actin ring was observed for more than seven minutes, with its fluorescent intensity being barely diminished even by photobleaching. (Figure 22 D and Movie S26). It is unclear if septum formation requires the actin ring for a long period as a scaffold.

With the cytoplasm visible by hyphal autofluorescence in older specimens, it was observed that cytoplasmic flow is unrestricted by actin rings (data not shown).

To confirm the strong concentration of Abp140p-GFP at actin rings, the fusion construct was integrated into the genome, under control of its native promoter. The resulting GFP signal was again strongest in the actin ring (Figure 23). Bright field images assured that these actin rings were found at sites of septum formation. While actin cables are not well visible in this strain with the genomic Abp140p-GFP, it may be well used for studying development of the actin ring. Since an actin ring is the structural precursor of a septum, this is most suitable for investigating the process of septation.

Cap-GFP patches are also involved in septation (Figure 23). They were found to temporarily localize to septa. Figure 24 shows three septa in different stages of development. When a septum is barely visible in the brightfield DIC image, Cap-GFP patches are already concentrated at its site in the fluorescence image (first column, Movie S27). With increased

development, the septum gets stronger contrasted in DIC images, and the number of Cap-GFP patches localizing to it is increased (middle column, Movie S28). When the septum has fully developed, Cap-GFP patches are no longer visible at its site (right column).

Septation is a well-balanced process. Disturbed septation may lead to complete demise of the organism. This is demonstrated in the second part of this thesis, highlighting the importance of this process.

As an overview, the dynamic data are summarized and compared with the budding yeast *Saccharomyces cerevisiae* and the fission yeast *Schizosaccharomyces pombe* in the following table:

Organism	<i>Ashbya gossypii</i>	<i>Saccharomyces cerevisiae</i>	<i>Schizosaccharomyces pombe</i>
Actin patch speed [nm/s]	224 (+/-98)	386.6 (+/-76.9)	320 (+/-140)
Actin patch distances [nm]	787 (+/-675)	764.7 (+/-420)	-
Actin patch lifetime [s]	14 (+/-6.5)	10.9 (+/-4.2)	many over 120, longest 224
Direction of actin patch movement	Away from tip, redirected, and movement towards tip on actin cables	Away from sites of polarized growth	primarily undirected at cell tips, directed along actin cables away from cell tips
Diffusion constant of plasma membrane [nm ² /s]*	8.6 (+/-1.6)	2.5	-
Cable elongation rate [nm/s]	184 (+/-62)	290 (+/-80)	-
References	this study	Actin patches: Smith et al., 2001. Diffusion constant: Valdez-Taubas and Pelham, 2003. Cable elongation: Yang and Pon, 2002	Pelham and Chang, 2001

* for comparison: mammalian COS cells: 100 nm²/s
Spiny dendrites of cerebellar Purkinje neurons: 43000 nm²/s (+/-11000)

Comparison of dynamic parameters of the actin cytoskeleton of the three fungi *A. gossypii*, *S. cerevisiae* and *S. pombe*

Discussion

A model for organisation of the actin cytoskeleton in A. gossypii

The combined findings of this study give rise to a hypothetical model in which the actin cytoskeleton is responsible for endocytosis, maintenance of polarization and exocytosis and plays a major role in septation as well. This is summarized in Figure 25.

Endocytosis:

In this model, the bulk of Cap-GFP actin patches is responsible for endocytosis. This is supported by the high percentage of backward movement in Cap-GFP patches, which is necessarily a feature of endocytosis in a filamentous fungus. Partial colocalizations with the endocytic marker FM4-64 further corroborate this hypothesis. FM4-64 is a membrane-selective dye which is incorporated into endocytic vesicle membranes (Fischer-Parton et al., 2000) and thus concluded to be a marker for endocytosis. Adding to incorporation in a wide range of filamentous fungi, it is also taken up in *A. gossypii*. With the punctate structures of FM4-64 colocalizing with Cap-GFP patches, this is a strong argument for an endocytotic function of actin patches in *A. gossypii*. These endocytic Cap-GFP patches usually reach the subapical region and disintegrate 6-12 μm behind the tip. While endocytosis is not solely restricted to the tip, this is where most endocytic material seems to come from. Still, patches appearing at septa might also be formed in subapical regions. Using the upper average values for Cap-GFP patch speed and lifetime, a rather quick patch will make a maximum of 6.6 μm in his lifetime. But septa are usually constructed over 20 μm behind the tip. So endocytosis must also occur in hyphal parts remote from the tip. While endocytosis has not definitely been proven to occur in fungal hyphae, the evidence is clearly in favor of this function (Read and Kalkman, 2003).

Polarization by endocytic cycling:

The other movement, redirection of retrograde Cap-GFP patches back towards the tip, may prove to be responsible for maintenance of polarization. In the budding yeast, it has been shown that this can be achieved by endocytic cycling (Valdez-Taubas and Pelham, 2003). Indications that recycling of vesicles plays a role in polarization is also found in other fungi, for example *Ustilago maydis* (Wedlich-Soeldner et al, 2000), where impaired endocytosis results in a non-polarized distribution of cell wall components and morphological changes.

Several findings argue for this function of Cap-GFP patches. Firstly, endocytic cycling as a mode for polarization implies cycling as a motion. This was made visible by following Cap-GFP patches in the apical region. They are endocytosed behind the tip, turn around and move towards the tip again. This movement can not readily be explained by pure endo- or exocytosis. Secondly, endocytic cycling requires slow diffusion in the plasma membrane. Although lateral diffusion in the plasma membrane of *A. gossypii* is three to four times faster

than in *S. cerevisiae*, ($8.6 \text{ nm}^2/\text{s} \pm 1.6$, compared to $2.5 \text{ nm}^2/\text{s}$ in budding yeast), this is several orders of magnitudes slower than the diffusion coefficients measured in polarized neurons ($43000 \text{ nm}^2/\text{s} (\pm 11000)$; Schmidt et al., 2003) or mammalian COS cells ($100 \text{ nm}^2/\text{s}$; Valdez-Taubas and Pelham, 2003). In any case, this slow lateral diffusion is responsible for the polarization of Cap-GFP patches. This was shown by the experiment with a membrane fluidizer, which caused the loss of amassed Cap-GFP patches in the apical region. Two possible explanations exist for this result. One being that factors for triggering endocytic vesicles are at the polarized region of the tip, where sterols reduce lateral mobility in the plasma membrane. The other explanation is that polarization by endocytic cycling, which requires a low lateral mobility of the membrane, is made impossible. The different domain of the apical membrane is overmore visible in stainings with the sterol dye Filipin (Hanspeter Helfer, personal communication).

Thirdly, the fact that tips depolarize to a spherical shape by addition of the actin-depolymerizing drug Latrunculin A reveals the central role of the actin cytoskeleton in polarization. Hence, maintenance of polarization may plausibly be attributed, at least in part, to Cap-GFP patches.

Asymmetric distribution of proteins to distinct domains in the plasma membrane is crucial to the function of a polarized cell. This can be done by constructing a very physical barrier to the plasma membrane that works like a crosswall. This mechanism is found in epithelia, where distinct apical and basolateral surfaces are maintained by tight junctions. In *A. gossypii*, the only structure which could account for this is the septum. Yet, the septum appears about $40 \mu\text{m}$ behind the tip, making it a highly unlikely candidate for maintenance of polarization. Another possibility is cytoskeletal tethering, as proposed for polarized neurons (Winckler et al., 1999). Tethering means that a cytoskeletal structure keeps the membrane proteins responsible for polarization in place. This is a way to avoid having to alter the properties of the plasma membrane. A protein which links the cytoskeleton to the membrane is required for cytoskeletal tethering. In the polarized neuron, this is done by ankyrin - a role which might be occupied in *A. gossypii* by Cdc42 (Pruyne and Bretscher, 2000). But Abp140p-GFP cables to the tip are a short-timed event and not a durable scaffold, and cytoskeletal tethering has not been observed in any other fungal organism.

Actin cables might be part of the polarization maintenance machinery. Punctate structures moving along cables towards the tip were observed. If actin cables in *A. gossypii* grow the same way as in *S. cerevisiae* - from the site of polarization, that is - then they would emanate from the tip. Since myosin V, a barbed-end directed motor for vesicular transport, uses actin cables as tracks for polarized secretion, the punctate structures seen on Abp140p-GFP cables may well be vesicles destined for exocytosis. The polarization of rapid Myo2p-driven vesicles along actin cables occurs independently of the distribution of actin patches (Pruyne et al., 1998). Hence, patches do not seem to play a direct role in targeting vesicles to the cell surface. Yet, actin patches and actin cables are often associated. In a study in *S. pombe*, the actin patch component Coronin was tagged with GFP, and actin patches were subsequently

observed moving along cables also labelled by Coronin. It is thus possible that actin cables serve as tracks for Myo2p-driven vesicles as well as actin patches.

Pelham and Chang (2003) proposed that actin cables may be the tails formed by actin patches. Patches would be the nucleators for F-actin filaments in this scenario. The filaments would then immediately be bundled and stabilized to form an actin cable. While there is no evidence for this hypothesis, the association of Abp140p-GFP patches with cables bears a striking resemblance to an actin comet tail.

Exocytosis:

A last direction of patches is movement towards the tip without redirection. This calls for exocytosis. A function of actin patches in deposition of the cell wall was suggested for *S. pombe* and *S. cerevisiae* (Takagi et al., 2003; Doyle and Botstein, 1996; Kobori et al., 1989). But while Cap-GFP patches may contribute to exocytosis, they are surely not the only operators for this function. This is reflected by the rather low percentage of patches moving from back in the hypha towards the tip. If Abp140p-GFP patches are different from the Cap-GFP patches, then their movement towards the tip is indicative of exocytosis. Also, other exocytic vesicles were observed in *A. gossypii*. Sec4p is a RabGTPase that is essential for fusion of secretory vesicles with the plasma membrane. Sec4p, being bound to vesicles, also polarizes to the cap in a Myo2p-dependent manner (Walch-Solimena et al., 1997; Schott et al., 1999). Analysis of a Sec4p-GFP strain of *A. gossypii* (Schmitz et al., submitted) revealed that Sec4p-vesicles move towards the tip, where they desintegrate. This is done with remarkable speed: They average 855 (+555) nm/s (n=29). Clearly, Cap-GFP patches are not the only vesicular structure responsible for exocytosis.

It is known from several studies that actin cables can serve as tracks for different cargos such as secretory vesicles (Johnston et al., 1991), several organelles (Hoepfner et al., 2001, Rossanese et al., 2001, Hill et al., 1996 and Simon et al., 1995) as well as mRNA (Bobola et al., 1996, Sil and Herskowitz, 1996 and Takizawa et al., 2000). Using the AgSec4p fused to GFP we were able to show that secretory vesicles move along actin cables and accumulate at the hyphal tips. They no longer do so in AgBNI1 deleted hyphae even though the polarisome component AgSpa2p localizes correctly. Thus the material needed for the permanently polarized growth is distributed along the cortex leading to non-directed surface expansion which explains the misshapen structure of the giant mutant cells before they finally lyse.

The very last section of the tip often being devoid of Cap-GFP patches agrees with a patch-free spherical tip segment first observed in Rhodamine-Phalloidin stainings of wildtype (Knechtle et al., 2003). This zone is possibly filled with tip-growing factors and exocytosed Abp140p-GFP patches, while endocytosis occurs at the periphery of the very tip. A dense structure seen at the tip in electron microscope images shows that *Ashbya* possesses a Spitzenkörper, after all (Robert Roberson, personal communication).

Septation:

Apart from flocking in the tip, Cap-GFP patches also gather at septa. While Cap-GFP patches move to the septum and away from it, no net direction could be determined. The number of patches and their activity are strongly reminiscent of the apical patch action. With actin patch accumulations indicating polarization, the septum may thus be viewed as just the other end of polarity in an *A. gossypii* hyphal compartment. Of course, its nature is different, since actin patches disappear once the septum is fully constructed. Interestingly, the disappearance is not observed in Far11 deletion mutants (see 'Far11p is required to prevent premature hyphal abscission in the filamentous fungus *Ashbya gossypii*').

Actin rings are not coupled to polarization. While AgCla4p is required for proper formation of actin rings, deletion strains show cortical patches concentrated at tips, and a fully developed network of actin cables is also found (Ayad-Durieux et al., 2000). But an actin ring is the structural precursor of the septum and forms early in its development. Since the mechanism of septal formation is not well understood yet, good insight might be gained by using the genomic or plasmidic AgABP140-GFP strain in septin knockouts.

It is possible that there are different types of the same actin structure. In budding yeast, two populations of actin cables were described (Yang and Pon, 2001). The first one, cables which extend from the bud along the mother-bud axis, can, in terms of polarized orientation, be compared to the tip-associated cables in *A. gossypii*. The second population, short cables, which are randomly oriented, has no evident counterpart in *A. gossypii*. Especially in terms of movement, such cables were not observed. Yet, there seem to be two distinct classes of Abp140p-GFP cables in *A. gossypii*: the linear, tip-associated, dim Abp140p-GFP cables and the spiraling, strongly fluorescent cables away from the tip.

Tip-associated cables are seen less frequently in fixed rhodamine-phalloidin stainings than in live recordings of the Abp140p-GFP strain. This may be due to the fact that they are usually weakly stained and especially in the apical zone outshone by the intense fluorescent brightness of actin patches. With actin patches being less bright and numerous in the Abp140p-GFP strain, this may account for an unmasking effect. Another possibility is that these short-lived cables are delicate and rarely withstand fixation procedures. It is a plausible assumption that the tip-associated cables are responsible for delivering exocytotic vesicles. In contrast, the bright variant of cables back in the hypha usually showing a spiral, cortical arrangement and found only in older hypha of 20h age, its main function may be of structural nature.

The question whether different patches exist in *A. gossypii* cannot be answered by this study. What in budding yeast was previously thought to indicate different classes of actin patches, for example by the finding that Abp1p and Sla1p patches can exist separately (Warren et al., 2002), has now been shown to be actin patches differing in their protein composition

depending on their stage in the life cycle (their 'age'), which also determines their movement pattern (Kaksonen et al., 2003).

References

- Adams AE, Pringle JR., 1984. Relationship of actin and tubulin distribution to bud growth in wild-type and morphogenetic-mutant *Saccharomyces cerevisiae*. *J Cell Biol.* 1984 Mar;98(3):934-45.
- Aebi U, Smith PR, Isenberg G, Pollard TD., 1980. Structure of crystalline actin sheets. *Nature.* 288(5788):296-8.
- Amberg DC. 1998. Three-dimensional imaging of the yeast actin cytoskeleton through the budding cell cycle. *Mol Biol Cell.* 9(12):3259-62.
- Asakura T, Sasaki T, Nagano F, Satoh A, Obaishi H, Nishioka H, Imamura H, Hotta K, Tanaka K, Nakanishi H, Takai Y., 1998. Isolation and characterization of a novel actin filament-binding protein from *Saccharomyces cerevisiae*. *Oncogene.* 16(1):121-30.
- Atkinson HA, Daniels A, Read ND., 2002. Live-cell imaging of endocytosis during conidial germination in the rice blast fungus, *Magnaporthe grisea*. *Fungal Genet Biol.* 37(3):233-44.
- Ayad-Durieux Y, Knechtle P, Goff S, Dietrich F, Philippsen P. 2000. A PAK-like protein kinase is required for maturation of young hyphae and septation in the filamentous ascomycete *Ashbya gossypii*. *J Cell Sci.* 113 Pt 24:4563-75.
- Bagnat M, Simons K. 2002. Lipid rafts in protein sorting and cell polarity in budding yeast *Saccharomyces cerevisiae*. *Biol Chem.* 383(10):1475-80.
- Bagnat M, Simons K. 2002. Cell surface polarization during yeast mating. *Proc Natl Acad Sci U S A.* 99(22):14183-8.
- Bauer Y, Knechtle P, Wendland J, Helfer H, Philippsen P., 2004. A Ras-like GTPase Is Involved in Hyphal Growth Guidance in the Filamentous Fungus *Ashbya gossypii*. *Mol Biol Cell.*
- Bobola, N., Jansen, R.P., Shin, T.H., and Nasmyth, K. (1996). Asymmetric accumulation of Ash1p in postanaphase nuclei depends on a myosin and restricts yeast mating-type switching to mother cells. *Cell* 84, 699-709.
- Bolte S, Talbot C, Boutte Y, Catrice O, Read ND, Satiat-Jeunemaitre B., 2004. FM-dyes as experimental probes for dissecting vesicle trafficking in living plant cells. *J Microsc.* 214(Pt 2):159-73. Review.
- Bretscher A., 2003. Polarized growth and organelle segregation in yeast: the tracks, motors, and receptors. *J Cell Biol.* 160(6):811-6. Review.
- Carlile M.J., Watkinson S.C., Gooday G.W., 2001. *The fungi* (second edition). Academic Press.
- Cheney RE, O'Shea MK, Heuser JE, Coelho MV, Wolenski JS, Espreafico EM, Forscher P, Larson RE, Mooseker MS., 1993. Brain myosin-V is a two-headed unconventional myosin with motor activity. *Cell.* 75(1):13-23.
- Cooper JA, Schafer DA., 2000. Control of actin assembly and disassembly at filament ends.

Curr Opin Cell Biol. 12(1):97-103. Review.

Dietrich FS, Voegeli S, Brachat S, Lerch A, Gates K, Steiner S, Mohr C, Pohlmann R, Luedi P, Choi S, Wing RA, Flavier A, Gaffney TD, Philippsen P., 2004. The *Ashbya gossypii* genome as a tool for mapping the ancient *Saccharomyces cerevisiae* genome. *Science*. 304(5668):304-7.

dos Remedios CG, Dickens MJ., 1978. Actin microcrystals and tubes formed in the presence of gadolinium ions. *Nature*. 1978 Dec 14;276(5689):731-3.

Doyle T, Botstein D. 1996. Movement of yeast cortical actin cytoskeleton visualized in vivo. *Proc Natl Acad Sci U S A*. 93(9):3886-91.

Fischer-Parton S, Parton RM, Hickey PC, Dijksterhuis J, Atkinson HA, Read ND. 2000. Confocal microscopy of FM4-64 as a tool for analysing endocytosis and vesicle trafficking in living fungal hyphae. *J Microsc*. 198 (Pt 3):246-59.

Fowler WE, Aebi U., 1983. A consistent picture of the actin filament related to the orientation of the actin molecule. *J Cell Biol*. 97(1):264-9.

Gietz RD, Schiestl RH. 1991. Applications of high efficiency lithium acetate transformation of intact yeast cells using single-stranded nucleic acids as carrier. *Yeast*. 7(3):253-63.

Gow N.A.R., Gadd G.M., 1995. *The growing fungus*. Chapman & Hall, London.

Griffin D.H., 1994. *Fungal Physiology* (second edition). Wiley-Liss, New York.

Grove SN, Bracker CE. 1970. Protoplasmic organization of hyphal tips among fungi: vesicles and Spitzenkorper. *J Bacteriol*. 104(2):989-1009.

Guex N., and M.C. Peitsch. 1997. SWISS-MODEL and the Swiss-PdbViewer: An environment for comparative protein modeling. *Electrophoresis*. 18:2714-2723.

Guild GM, Connelly PS, Ruggiero L, Vranich KA, Tilney LG., 2003. Long continuous actin bundles in *Drosophila* bristles are constructed by overlapping short filaments. *J Cell Biol*. 162(6):1069-77.

Gumbiner BM., 1996. Cell adhesion: the molecular basis of tissue architecture and morphogenesis. *Cell*. 84(3):345-57. Review.

Hill KL, Catlett NL, Weisman LS., 1996. Actin and myosin function in directed vacuole movement during cell division in *Saccharomyces cerevisiae*. *J Cell Biol*. 135(6 Pt 1):1535-49.

Hoepfner, D., van den Berg, M., Philippsen, P., Tabak, H.F., and Hetteema, E.H. (2001). A role for Vps1p, actin, and the Myo2p motor in peroxisome abundance and inheritance in *Saccharomyces cerevisiae*. *J Cell Biol* 155, 979-990.

Hoepfner D, Brachat A, Philippsen P. 2000. Time-lapse video microscopy analysis reveals astral microtubule detachment in the yeast spindle pole mutant *cnm67*. *Mol Biol Cell*. 11(4):1197-211.

Johnston, G.C., Prendergast, J.A., and Singer, R.A. (1991). The *Saccharomyces cerevisiae* MYO2 gene encodes an essential myosin for vectorial transport of vesicles. *J Cell Biol* 113, 539-551.

Kim K, Yamashita A, Wear MA, Maeda Y, Cooper JA. 2004. Capping protein binding to actin in yeast: biochemical

- mechanism and physiological relevance. *J Cell Biol.* 164(4):567-80.
- Kammerer RA, Schulthess T, Landwehr R, Lustig A, Engel J, Aebi U, Steinmetz MO., 1998. An autonomous folding unit mediates the assembly of two-stranded coiled coils. *Proc Natl Acad Sci U S A.* 95(23):13419-24.
- Knechtle P, Dietrich F, Philippsen P., 2003. Maximal polar growth potential depends on the polarisome component AgSpa2 in the filamentous fungus *Ashbya gossypii*. *Mol Biol Cell.* 14(10):4140-54.
- Kopp J, Schwede T., 2004. The SWISS-MODEL Repository of annotated three-dimensional protein structure homology models. *Nucleic Acids Res.* 1;32 Database issue:D230-4.
- Lauffenburger DA, Horwitz AF., 1996. Cell migration: a physically integrated molecular process. *Cell.* 84(3):359-69.
Review
- Loisel TP, Boujemaa R, Pantaloni D, Carlier MF., 1999. Reconstitution of actin-based motility of *Listeria* and *Shigella* using pure proteins. *Nature.* 401(6753):613-6.
- Mellman, I., 1996. Molecular sorting of membrane proteins in polarized and non-polarized cells. *Cold Spring Harb. Symp. Quant. Biol.* 60, 745-752.
- Meyer RK, Aebi U., 1990. Bundling of actin filaments by alpha-actinin depends on its molecular length. *J Cell Biol.* 110(6):2013-24.
- Millonig R, Salvo H, Aebi U., 1988. Probing actin polymerization by intermolecular cross-linking. *J Cell Biol.* 106(3):785-96.
- Mukhopadhyay K, Kohli A, Prasad R. 2002. Drug susceptibilities of yeast cells are affected by membrane lipid composition. *Antimicrob Agents Chemother.* 46(12):3695-705.
- Pelham RJ Jr, Chang F., 2001. Role of actin polymerization and actin cables in actin-patch movement in *Schizosaccharomyces pombe*. *Nat Cell Biol.* 3(3):235-44.
- Pruyne DW, Schott DH, Bretscher A. 1998. Tropomyosin-containing actin cables direct the Myo2p-dependent polarized delivery of secretory vesicles in budding yeast. *J Cell Biol.* 143(7):1931-45.
- Pruyne D, Bretscher A., 2000. Polarization of cell growth in yeast. *J Cell Sci.* 113 (Pt 4):571-85. Review.
- Pruyne D, Evangelista M, Yang C, Bi E, Zigmund S, Bretscher A, Boone C., 2002. Role of formins in actin assembly: nucleation and barbed-end association. *Science.* 297(5581):612-5.
- Read ND, Kalkman ER., 2003. Does endocytosis occur in fungal hyphae? *Fungal Genet Biol.* 39(3):199-203.
- Rossanese, O.W., Reinke, C.A., Bevis, B.J., Hammond, A.T., Sears, I.B., O'Connor, J., and Glick, B.S. (2001). A role for actin, Cdc1p, and Myo2p in the inheritance of late Golgi elements in *Saccharomyces cerevisiae*. *J Cell Biol* 153, 47-62.
- Sagot, I., Klee, S.K., and Pellman, D. (2002a). Yeast formins regulate cell polarity by controlling the assembly of actin cables. *Nat Cell Biol* 4, 42-50.

- Sagot, I., Rodal, A.A., Moseley, J., Goode, B.L., and Pellman, D. (2002b). An actin nucleation mechanism mediated by Bni1 and profilin. *Nat Cell Biol* 4, 626-631.
- Schmidt H, Brown EB, Schwaller B, Eilers J., 2003. Diffusional mobility of parvalbumin in spiny dendrites of cerebellar Purkinje neurons quantified by fluorescence recovery after photobleaching. *Biophys J.* 84(4):2599-608.
- Schott D, Huffaker T, Bretscher A., 2002. Microfilaments and microtubules: the news from yeast. *Curr Opin Microbiol.* 2002 Dec;5(6):564-74. Review.
- Shah AA, Giddings MC, Parvaz JB, Gesteland RF, Atkins JF, Ivanov IP, 2002. Computational identification of putative programmed translational frameshift sites. *Bioinformatics* 18(8):1046-53.
- Simon, V.R., Swayne, T.C., and Pon, L.A. (1995). Actin-dependent mitochondrial motility in mitotic yeast and cell-free systems: identification of a motor activity on the mitochondrial surface. *J Cell Biol* 130, 345-354.
- Sinicrope, F. A., P. K. Dudeja, B. M. Bissonnette, A. R. Safa, and T. A. Brasitus. 1992. Modulation of P-glycoprotein-mediated drug transport by alterations in lipid fluidity of rat liver canalicular membrane vesicles. *J. Biol. Chem.* 267:24995-25002.
- Sil, A., and Herskowitz, I. (1996). Identification of asymmetrically localized determinant, Ash1p, required for lineage-specific transcription of the yeast HO gene. *Cell* 84, 711-722.
- Sizonenko GI, Karpova TS, Gattermeir DJ, Cooper JA., 1996. Mutational analysis of capping protein function in *Saccharomyces cerevisiae*. *Mol Biol Cell.* 7(1):1-15.
- Smith MG, Swamy SR, Pon LA. 2001. The life cycle of actin patches in mating yeast. *J Cell Sci.* 114(Pt 8):1505-13.
- Steinmetz MO, Hoenger A, Tittmann P, Fuchs KH, Gross H, Aebi U., 1998. An atomic model of crystalline actin tubes: combining electron microscopy with X-ray crystallography. *J Mol Biol.* 1998 May 15;278(4):703-11.
- Takagi T, Ishijima SA, Ochi H, Osumi M., 2003. Ultrastructure and behavior of actin cytoskeleton during cell wall formation in the fission yeast *Schizosaccharomyces pombe*. *J Electron Microsc (Tokyo)* 52(2):161-74.
- Takizawa, P.A., DeRisi, J.L., Wilhelm, J.E., and Vale, R.D. (2000). Plasma membrane compartmentalization in yeast by messenger RNA transport and a septin diffusion barrier. *Science* 290, 341-344.
- Valdez-Taubas J, Pelham HR. 2003. Slow diffusion of proteins in the yeast plasma membrane allows polarity to be maintained by endocytic cycling. *Curr Biol.* 13(18):1636-40.
- Vida TA, Emr SD., 1995. A new vital stain for visualizing vacuolar membrane dynamics and endocytosis in yeast. *J Cell Biol.* 128(5):779-92.
- Wach A, Brachat A, Pohlmann R, Philippsen P., 1994. New heterologous modules for classical or PCR-based gene disruptions in *Saccharomyces cerevisiae*. *Yeast.* 10(13):1793-808.
- Waddle JA, Karpova TS, Waterston RH, Cooper JA. 1996. Movement of cortical actin patches in yeast. *J Cell Biol.* 132(5):861-70.
- Waddle JA, Cooper JA, Waterston RH., 1993. The alpha and beta subunits of nematode actin capping protein function in yeast. *Mol Biol Cell.* 4(9):907-17.

- Wedlich-Soeldner R, Bolker M, Kahmann R, Steinberg G, 2000. A putative endosomal t-SNARE links exo- and endocytosis in the phytopathogenic fungus *Ustilago maydis*. *EMBO J.* 19(9):1974-86.
- Wendland J, Philippsen P., 2002. An IQGAP-related protein, encoded by *AgCYK1*, is required for septation in the filamentous fungus *Ashbya gossypii*. *Fungal Genet Biol.* 37(1):81-8.
- Wendland J, Philippsen P., 2001. Cell polarity and hyphal morphogenesis are controlled by multiple rho-protein modules in the filamentous ascomycete *Ashbya gossypii*. *Genetics.* 157(2):601-10.
- Wendland J, Philippsen P., 2000. Determination of cell polarity in germinated spores and hyphal tips of the filamentous ascomycete *Ashbya gossypii* requires a rhoGAP homolog. *J Cell Sci.* 113 (Pt 9):1611-21.
- Winckler B, Forscher P, Mellman I., 1999. A diffusion barrier maintains distribution of membrane proteins in polarized neurons. *Nature.* 397(6721):698-701.
- Wright MC, Philippsen P., 1991. Replicative transformation of the filamentous fungus *Ashbya gossypii* with plasmids containing *Saccharomyces cerevisiae* ARS elements. *Gene.* 109(1):99-105.
- Yamashita A, Maeda K, Maeda Y. 2003. Crystal structure of CapZ: structural basis for actin filament barbed end capping. *EMBO J.* 22(7):1529-38.
- Yang HC, Pon LA., 2002. Actin cable dynamics in budding yeast. *Proc Natl Acad Sci U S A.* 99(2):751-6.
- Young ME, Cooper JA, Bridgman PC., 2004. Yeast actin patches are networks of branched actin filaments. *J Cell Biol.* 166(5):629-35.

Figures and Tables

Ag ORF name	Sc homolog(s)	Sc standard name for homolog(s)	% identity to Sc homolog(s)
Patches			
AGL237C	YCR088W	ABP1	55
ABR222W	YFL039C	ACT1	99
ABL043W	YMR092C	AIP1	54
ADR316W	YDL029W	ARP2	89
AFR419C	YJR065C	ARP3	90
ADL061W	YIL062C	ARC15	61
AFR584C	YLR370C	ARC18	75
ACL092C	YKL013C	ARC19	85
AGL221W	YNR035C	ARC35	62
AFL022W	YBR234C	ARC40	70
ABR007C	YKL007W	CAP1	47
ADL101C	YIL034C	CAP2	59
ADL337W	YBR109C	CMD1	96
ADR235W	YLL050C	COF1	86
AER114W	YLR429W	CRN1	64
AER416C	YNL084C	END3	49
ACL157C	YLR206W	ENT1	58
	YDL161W	ENT2	60
AER155C	YJR125C	ENT3	58
ACL061C	YLL038C	ENT4	40
AGR048C	YLR113W	HOG1	84
AGR285W	YOR181W	LAS17 / BEE1	53
AEL306C	YMR109W	MYO3	74
	YKL129C	MYO5	70
ADR018C	YIR006C	PAN1 / DIM2	42
ADL217W	YIL095W	PRK1	45
	YNL020C	ARK1	46
AER193W	YCR009C	RVS161 / END6	85
AGR069C	YDR129C	SAC6	80
AGR170C	YBL007C	SLA1	55
-	YNL243W	SLA2 (END4)	-
AFR061W	YNL138W	SRV2	57

Ag ORF name	Sc homolog(s)	Sc standard name for homolog(s)	% identity to Sc homolog(s)
ABR105C	YGR080W	TWF1	41
ABR038C	YLR337C	VRP1 / END5	50
AEL209W	YHR161C	YAP1801	44
	YGR241C	YAP1802	46
Cables			
ACR130W	YOR239W	ABP140	49
ABR222W	YFL039C	ACT1	99
AGR069C	YDR129C	SAC6	80
AER424C	YNL079C	TPM1	70
	YIL138C	TPM2	61
ADR354W	YOR326W	MYO2	66
	YAL029C	MYO4	51
Rings			
ABL200W	YNL233W	BNI4	38
AFR301C	YIL159W	BNR1	31
AAL016C	YCL014W	BUD3	51
AGL306C	YJR092W	BUD4	31
AFR111C	YLR314C	CDC3	58
AAR001C	YCR002C	CDC10	75
AER445C	YJR076C	CDC11	74
AER238C	YHR107C	CDC12	78
ABL159W	YDL225W	SHS1	60
AEL190W	YBR038W	CHS2	68
AEL189W	YBR023C	CHS3	66
ACR227W	YBL061C	CHS4/SKT5	48
	YER096W	SHC1	37
ABL034W	YKL101W	HSL1	43
AFR696C	YDR507C	GIN4	56
	YCL024W	KCC4	53
ABR082W	YMR032W	HOF1	35
AFL150C	YPL242C	IQG1	35
ACL168C	YOR122C	PFY1	83
ACR068W	YHR023W	MYO1	48

Table 0 Comparison of actin cytoskeleton components in *Ashbya gossypii* (Ag) and *Saccharomyces cerevisiae* (Sc) (based on Pruyné and Bretscher, 2000).

The first column shows the systematic names of the homologous genes in *Ashbya gossypii*, the second those of *Saccharomyces cerevisiae* (with some duplicated). The third row features the standard names for respective homologs in *S. cerevisiae*. The last column indicates the percentage of homology between the different homologs.

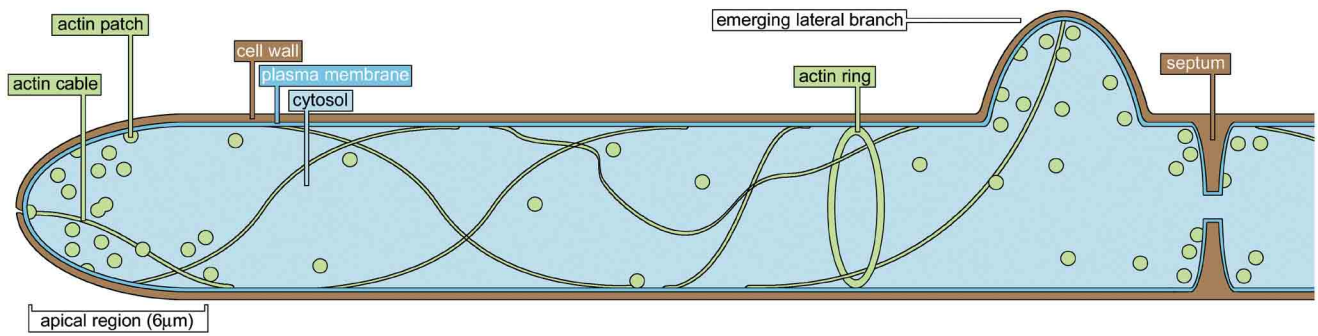


Figure 0 Schematic overview of the actin structures in *Ashbya gossypii*

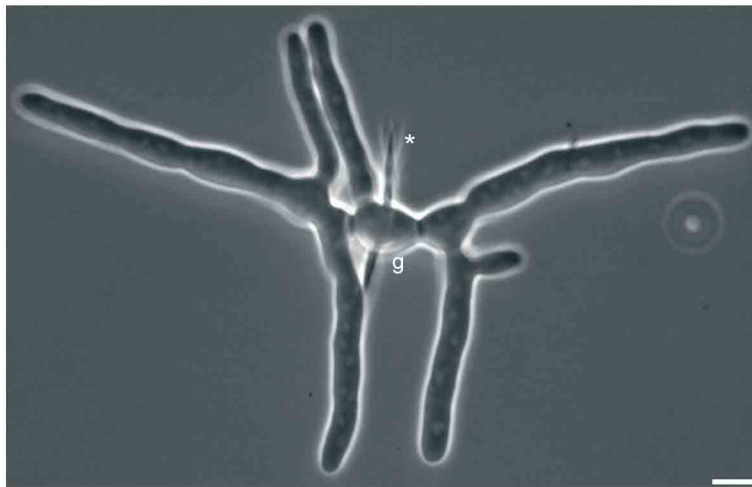


Figure 1 **Wildtype appearance of the filamentous growth of *Ashbya gossypii***
 Brightfield image of a young wild-type mycelium of *A.gossypii* of twelve hours age. Germination from a needle-shaped spore, marked by an asterisk (*), resulted in the spherical structure below it, the germ bubble (g). This germ bubble gave rise to three germ tubes - the hyphae which are directly attached to the germ bubble. Two connection sites (of the horizontal hyphae to the left and to the right) now have a septum, a crosswall for compartmentalizing the mycelium. The tips of the hyphae will continue to extend, while the diameter of the hypha does not increase.
 Scalebar=5µm

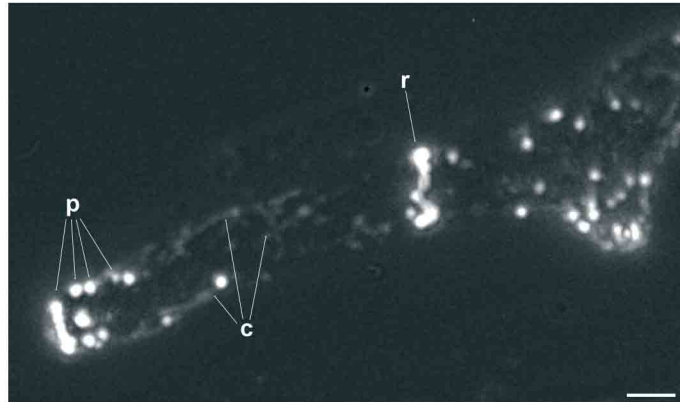


Figure 2 The three main components of the actin cytoskeleton in a rhodamine-phalloidin staining of a hypha of *Ashbya gossypii*

The hyphal tip, left, is populated by bright dots, the actin patches (p). Further back in the hypha, weak linear structures can be discerned, the actin cables. The third element is the actin ring, visible as a bright band crossing the hypha. At the right end of the image, a lateral branch is emerging, growing downwards. The tip of the branch has many actin patches as well. Scalebar=5 μ m

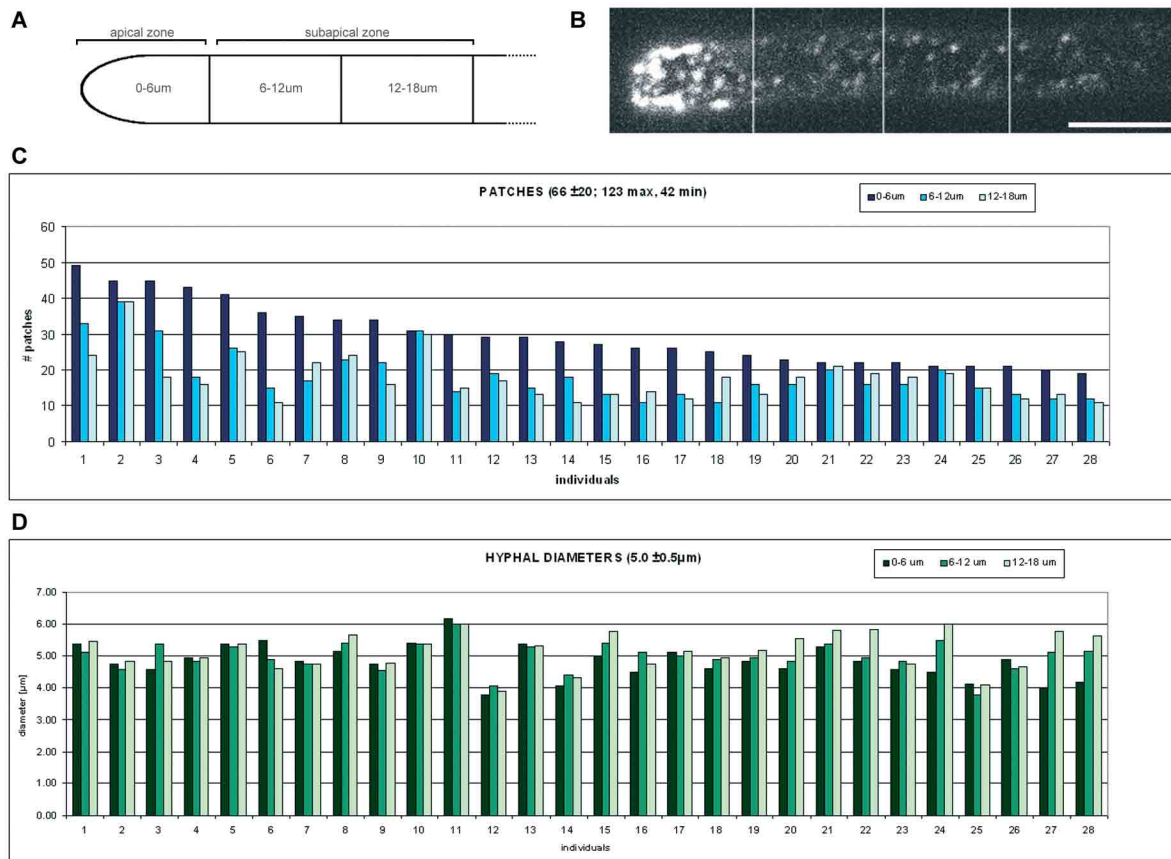


Table 1 Actin patch number and hyphal diameters in Rhodamine-Phalloidin stainings of *Ashbya gossypii* tips

A) To assess polarization of actin patches, the first 18 μ m behind the tip were divided into three equally long parts. The first six micrometers away from the tip form the apical region (0-6 μ m). The two following parts, 6-12 μ m and 12-18 μ m, are the subapical regions. B) Example of a Rhodamine-Phalloidin staining with the three compartments of six micrometers each indicated. C) Actin patches were recorded in hyphal tip stainings in large Z-series at the highest magnification and counted in each plane. The majority features a clear concentration of actin patches in the apical zone. There is no distribution pattern visible in the subapical regions, though. D) To assure that the number of actin patches is not dependent on the size of the hypha, diameters of the respective hyphae from C) were measured, resulting in no obvious correlation. Scalebar=5 μ m

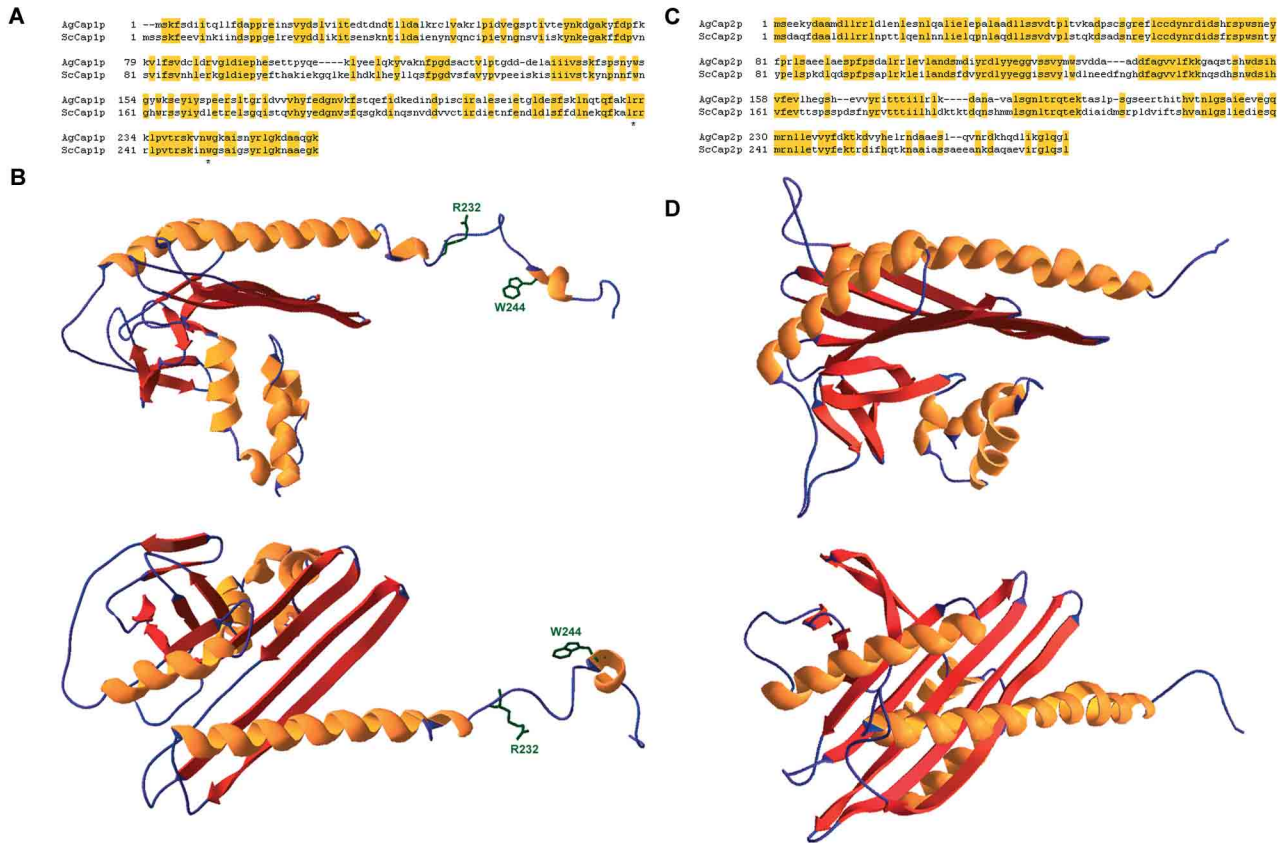


Figure 3 Structure of the Ag Cap1p and Cap2p, the subunits of capping protein

A) Comparison of the AgCap1p protein sequence to Cap1p of *Sc*. Overall identity lies at 45%. Pivotal amino acids essential for the 'tentacular' model of capping protein are indicated with asterisks. B) Model of Cap1p, made with the protein database SwissProt. The upper ribbon model is viewed from the side, the lower one from top. The mushroom structure is evident, with the stalk composed by alpha-helices (orange) at the bottom and the hat being formed by beta-sheet (red arrows). On top of the beta-sheet, an alpha-helix bears the putative tentacle. Amino acids which were shown to be crucial to the function of capping protein in budding yeast are found at the conserved location and are indicated in green. C) Comparison of AgCap2p to ScCap2p. They are 56% identical. D) Swissprot model of AgCap2p. Again, mushroom structure and tentacle can well be recognized (as described for Cap1p). In budding yeast, the subunits combine to form a heterodimer.

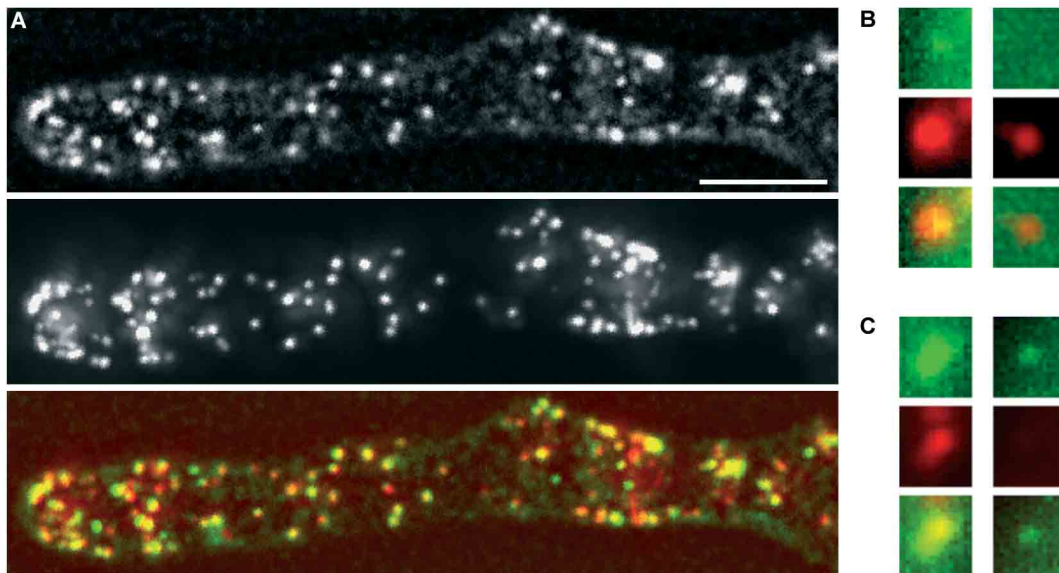


Figure 4 Cap-GFP patches colocalize fully with actin patches in Rhodamine-Phalloidin stainings

A) From top to bottom: Cap1-GFP, Rhodamine-Phalloidin staining and both combined (green and red, respectively). Note that the actin ring to the left of the hypha, visible in the Rhodamine-Phalloidin staining, is not labelled in the Cap1-GFP image. Fluorescent intensity of the patches was compared in both stainings. While the majority of Cap-GFP patches showed the same relative intensity as their corresponding patches in the Rhodamine-Phalloidin staining, exceptions were observed. B) shows two cases of patches where the Cap-GFP patch (upper row) is barely (left) or not at all visible (right), while the fluorescent signal is well defined. This may be explained by the fact that the weak Cap-GFP signal has dropped to the level of hyphal autofluorescence. Still, the difference is remarkable. C) Opposite cases of different signal intensity. Here, the Cap-GFP signal is stronger than the weak (left) or invisible (right) signal of the Rhodamine-Phalloidin patch. Scalebar=5um

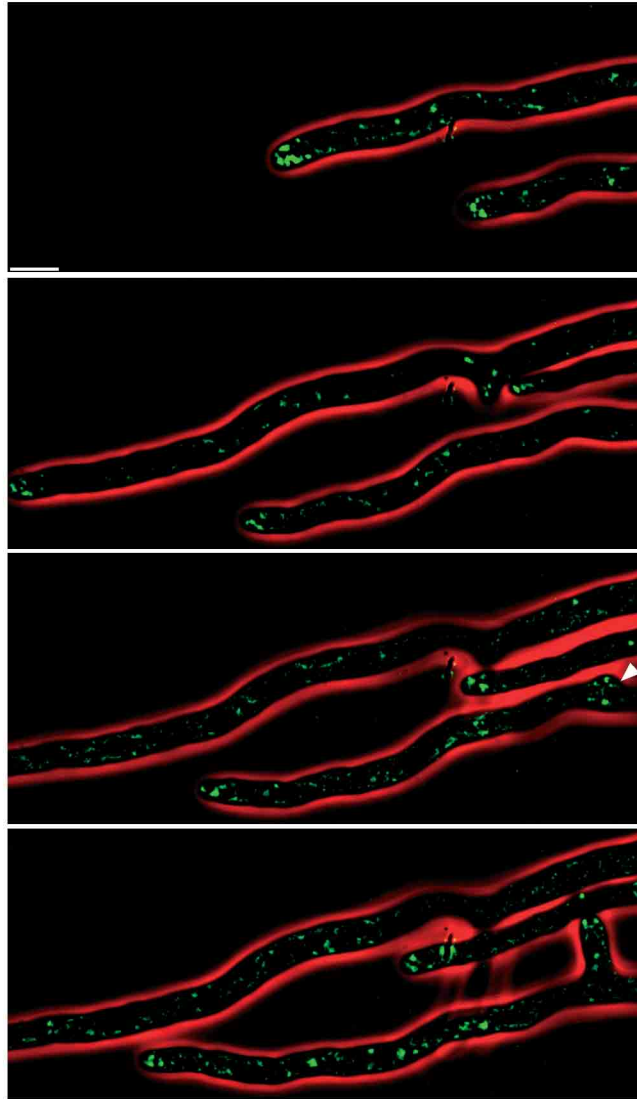


Figure 5 Cap-GFP patches are concentrated in the apical region

Still images of a time lapse movie of Cap-GFP patches in the hypha of *A.g.* An image was taken all two minutes for nearly three hours, during which Cap-GFP patches were constantly concentrated at the tip. The arrowhead to the right side in the penultimate picture indicates Cap-GFP patches accumulating at the site of an emerging lateral branch. Scalebar=5um

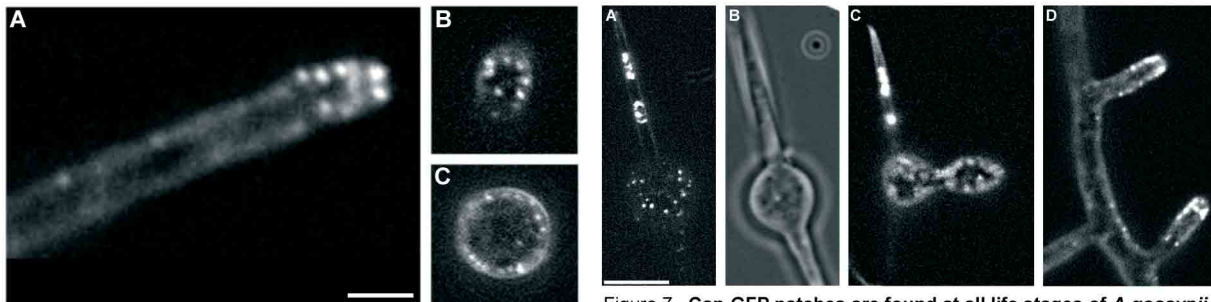


Figure 6 Distribution of Cap-GFP patches in the hypha
Still images of time-lapse movies of Cap-GFP patches in the hypha of *A.gossypii*. A) Distribution of patches in the hypha viewed from the side. While most patches are at the tip, there are also some further back in the hypha. B) A tip viewed from front. Actin patches show high activity at the tip. The apical calotte tends to be free, though. C) Distribution further back in a large hypha. Patches are mostly cortical, although some are well cytoplasmic. Scalebar=5um.

Figure 7 Cap-GFP patches are found at all life stages of *A.gossypii*
Still images of time-lapse movies of Cap-GFP patches in *A.g.* A) A germ bubble in the middle of a needle-shaped spore. This is the youngest stage of a developing mycelium. Here already, Cap-GFP patches can be seen moving. The bright bands in the needle stem from autofluorescence. B) Its corresponding brightfield picture. C) An emerging germ tube leads to the first hypha. Here as well, Cap-GFP patches are moving about, already showing polarization at the tip. D) Cap-GFP patches in lateral branches. While most patches are concentrated at the tip, there are also patches way back in the hypha. These findings are congruent with the developing actin cytoskeleton investigated in rhodamine-phalloidin stainings. Scalebar=5um

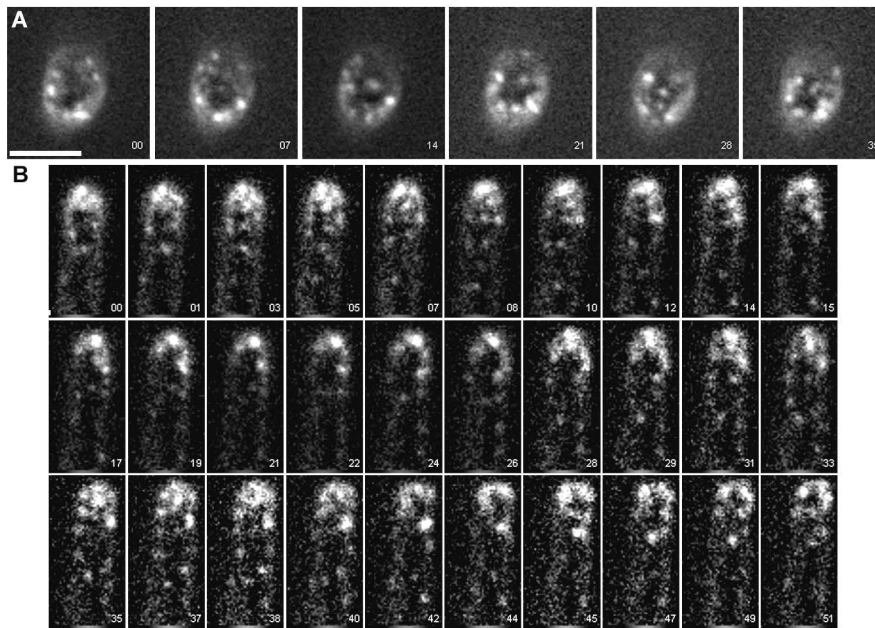


Figure 8 Movement of Cap-GFP patches in the apical region

Still images of time-lapse movies of Cap-GFP patches in the hypha of *A.g.* A) Cap-GFP patches in a tip viewed from a frontal position (i.e. along the main axis of growth). While activity seems rather frenzied in the tip, surprisingly few patches are seen at the very tip. Over a time of more than half a minute, the apical calotte of the tip is mostly free of Cap-GFP patches. This is in concordance with the analysis of the actin patches in rhodamine-phalloidin stainings of wildtype (Knechtle et al., 2003). Collision and fusion of Cap-GFP patches is often observed at the tip, most probably on account of the crowding conditions.

B) Rapid 4D analysis of Cap-GFP patch movement in the tip, viewed from the side. Any patch chosen in the subapical region can be seen moving away from the tip. All the while, the concentration of patches at the tip remains unchanged.

Scalebars=5um

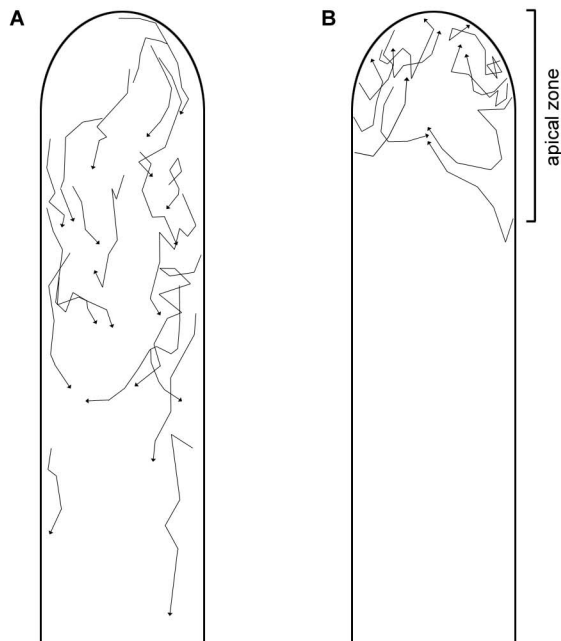


Figure 9 Motion analysis of Cap-GFP patches

Movement of directed Cap-GFP patches was analyzed in different tips and individual tracks combined in these two schemes. Two clear motion patterns could be observed: A) The bulk of Cap-GFP patches moves away from the tip, sometimes over distances as long as six micrometers. They may also split or fuse in the process, although this is not a rule.

B) Another motion pattern is redirection of retrograde Cap-GFP patches back towards the tip. This pattern is only observed in the apical region, i.e. the first six micrometers behind the tip. While many redirected patches move directly back to the very tip, some move towards the center of the apical region, where they disintegrate.

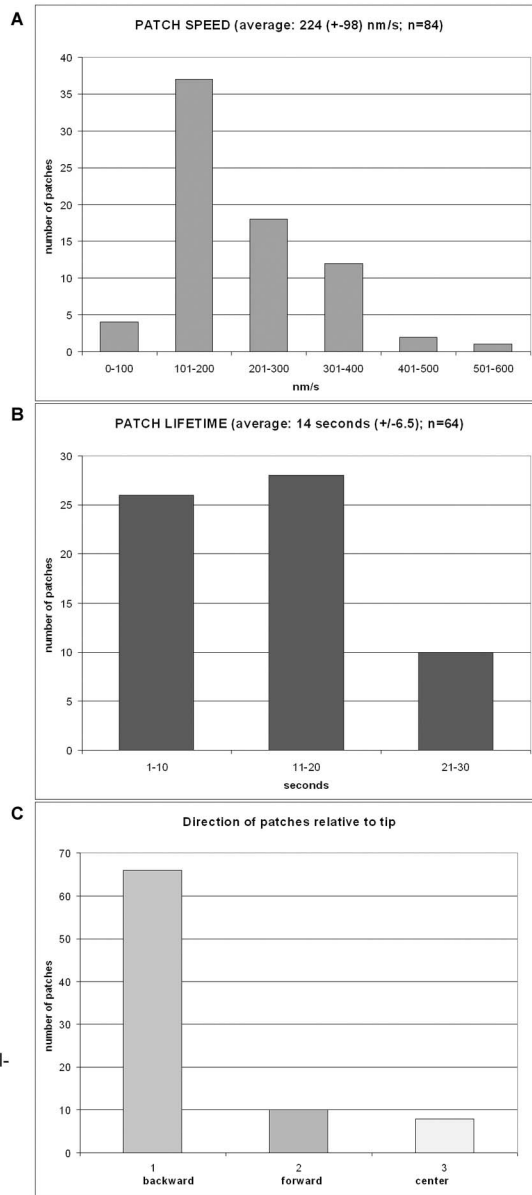


Table 2 Speed, lifetime and directionality of Cap-GFP patches in the hypha of *Ashbya gossypii*
 A) Patch speed as measured in several high-speed recordings of hyphal tips in Cap-GFP strains. With an average of 224 nm/s, the bulk of the patches is found in the 101-200 nm/s section, spreading into the upper range. The fastest patch reached 566nm/s. B) Patch lifetime observed in single and multiple plane time lapse recordings. C) Directionality of actin patches, relative to the tip. 'Backward' meaning retrograde movement away from the tip, while 'forward' patches move towards the tip. 'Center' direction is from the plasma membrane towards the main axis of growth. Redirected patches comprise both latter categories of movement.

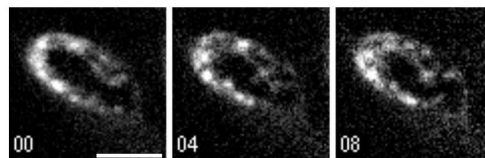


Figure 10 Actin patches form cables in the *Bnr1p-ΔDAD-Cap1-GFP* strain
 Still images of time-lapse movies of Cap-GFP patches in a strain with the constitutively active formin Bnr1. Filamentous structures, probably actin cables, are seen in association with the Cap-GFP patches. Filamentous structures are never seen in the normal Cap-GFP strains. Scalebar = 5μm, time format = ss

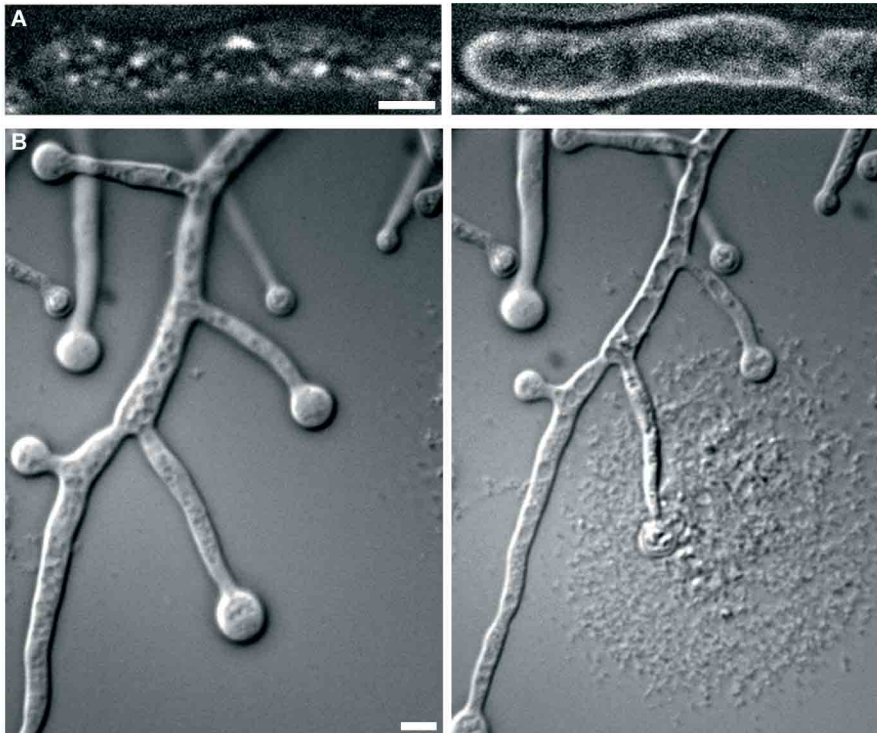


Figure 11 Latrunculin A desintegrates Cap-GFP patches and depolarizes hyphal tips

A) Left: A hyphal tip of a Cap-GFP strain shortly after administration of 200uM Latrunculin A, an actin depolymerizing drug. Cap-GFP actin patches are well visible, with the most found in the apical region. Right: Eight minutes later, patch structures have vanished. B) Left: Swelling of tips after prolonged exposure to Latrunculin A. After twenty minutes in an environment with 200uM Latrunculin A, hyphal tips show strong swelling, resulting in the characteristic 'frog fingers'. Right: The swelling continues until the spherical tip explodes, giving in to turgor pressure. Note considerable thinning of the entire hypha and appearance of large vacuoles after lysis of the tip. Scalebar=5um.



Figure 12 Staining with the endocytic marker FM4-64 in a Cap-GFP strain

Left image: Cap-GFP patches in the hyphal tip of a Cap-GFP strain. Middle image: FM4-64 stains the plasma membrane brightly. In addition, two distinguished punctate structures are visible. Right image: Color combination of the precedent images. Cap-GFP is green, while FM4-64 is red. Scalebar=5um.

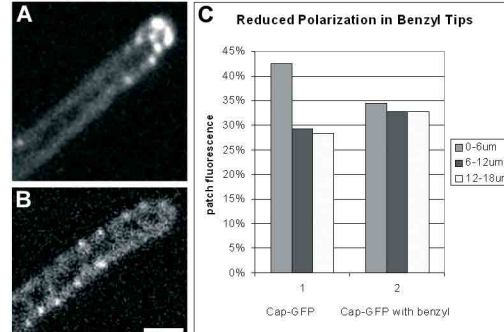


Figure 13 Polarization of Cap-GFP patches is lost by applying the membrane fluidizer benzyl alcohol

A) Distribution of Cap-GFP patches in a Cap-GFP strain. Concentration of patches is highest in the apical region. B) Hyphal tip after application of benzyl alcohol. There are no patches flocking in the apical region. C) Quantification of this loss of polarized patches. While in Rhodamine-Phalloidin stainings of WT and in Cap-GFP strains as well, almost half of all patches are found in the apical region six micrometers behind the tip, they are nearly equally distributed throughout the hypha after application of benzyl alcohol. Scalebar=5um.

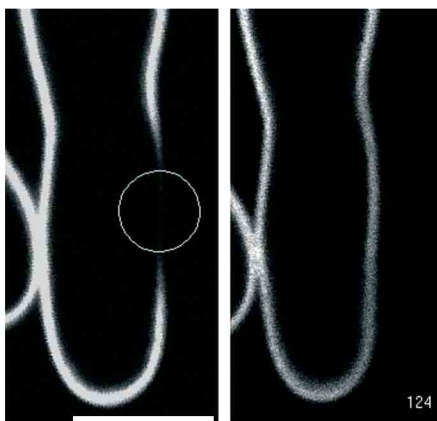


Figure 14 Lateral diffusion in the plasma membrane of *Ashbya gossypii*

Confocal images of a FRAP experiment. Left: In a plasma membrane brightly stained with FM4-64, an area of 3.2um was bleached. Right: Two minutes later, the gap in fluorescent membrane is entirely filled. Repeated experiments made for a diffusion coefficient of 0.0086um²/s (+/-0.0016), reflecting slow lateral mobility in the apical membrane of *A.gossypii*. Scalebar=5um.

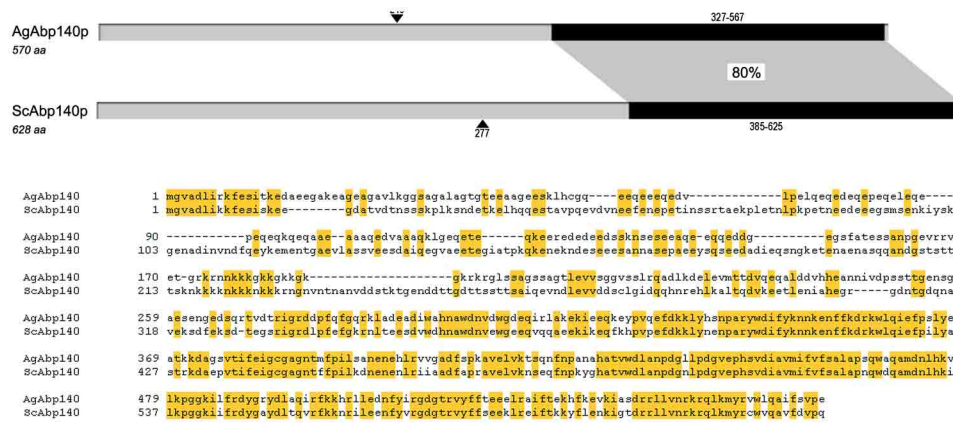


Figure 15 Comparison of the protein sequence of AgAbp140p and ScAbp140p
Identity lies at 49% and increases towards the C-terminus. AgAbp140p (ACR230W) does not show homology to any known actin binding protein and is expressed in cells by fusion of two ORFs by means of a +1 translational frameshift. ScAbp140p was characterized as a weak crosslinker (Asakura et al., 1998), but the molecular structure of the protein has not yet been identified.

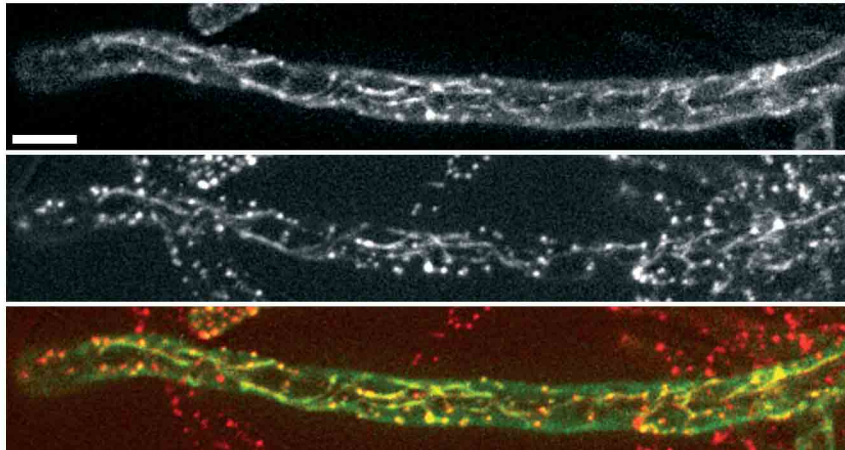


Figure 16 Abp140p-GFP cables and patches colocalize fully with actin cables and patches in Rhodamine-Phalloidin stainings
From top to bottom: Abp140p-GFP, Rhodamine-Phalloidin staining and both combined (green and red, respectively). The background in the merged image shows Rhodamine-Phalloidin structures not stained with Abp140p-GFP. As a plasmidic construct, Abp140p-GFP is expressed at different levels in individual hypha.
Scalebar=5um

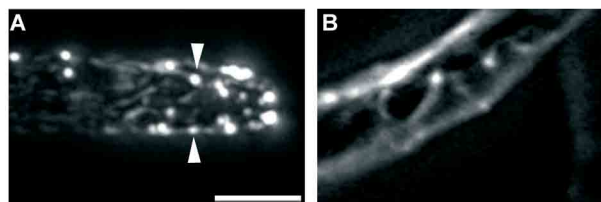


Figure 17 Actin patches in association with actin cables
A) Rhodamine-phalloidin staining of a hyphal tip. The arrowheads indicate an actin patch in the middle of a cable. B) Two Abp140p-GFP actin patches associated with actin cables.
Scalebar=5um

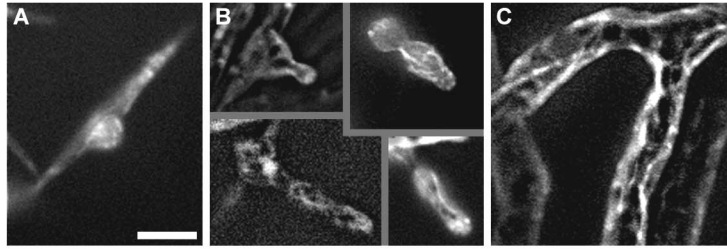


Figure 18 Abp140p-GFP cables are visible at all stages in *A.gossypii* 's life cycle

Still images of time-lapse movies of Abp140p-GFP patches in young developmental stages of Ag. A) Abp140p-GFP cables are already discernible in the germ bubble. B) As a unipolar germ tube emerges, Abp140p-GFP cables can be seen running the entire length of it. Note that in both left images of this composite, Abp140p-GFP patches can be seen at the very tip. C) As the mycelium develops, cables can be seen spanning the hypha cortically and often in a spiral fashion. They can be as long as 40um. Scalebar=5um.

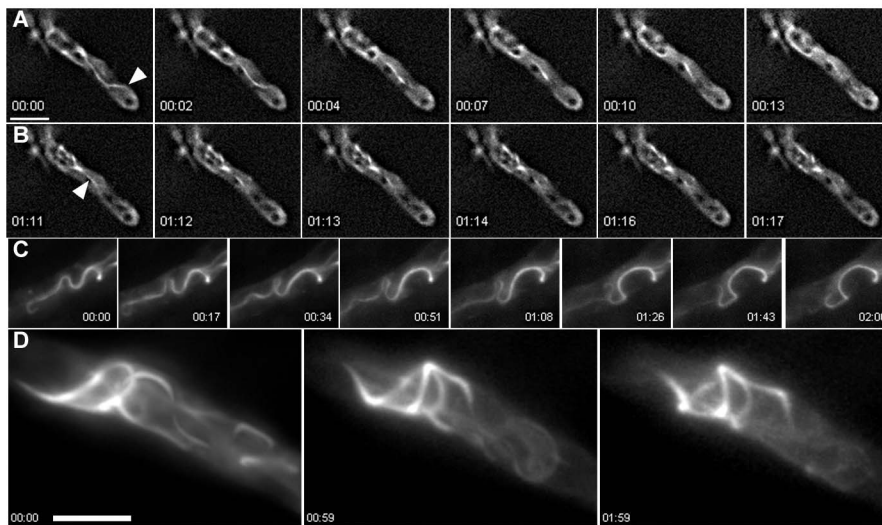


Figure 19 Dynamics of Abp140p-GFP in *Ashbya gossypii* reveal highly motile cables

Still images of time-lapse movies of Abp140p-GFP cables in hyphae of A.g. A) Movement of an Abp140p-GFP cable emanating from the tip of a unipolar germling. Events like this one allowed for determination of the elongation rate of extending Abp140p-GFP cables. B) A similar event in the same unipolar germling, but movement occurs in the other direction. C) Bright cables are often found back in the hypha. Their dynamic form is striking and changes considerably within two minutes. D) Another example of strong cables in the hypha. Looping and kinking is often observed. In terms of fluorescent intensity and stability over time, these cables are different compared to cables connecting to the tip. Scalebar = 5um, time format = mm:ss.

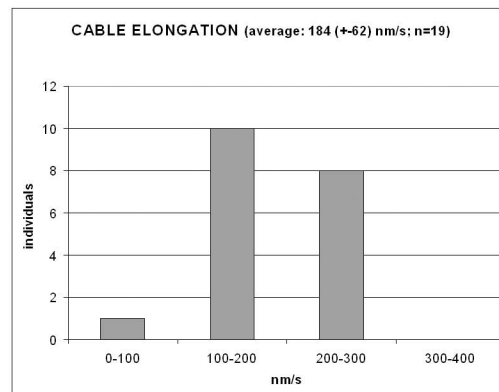


Table 3 Elongation rate of Abp140p-GFP cables

Interestingly, the bulk of elongating cable speed lies in the same section as the speed of Cap-GFP patches.

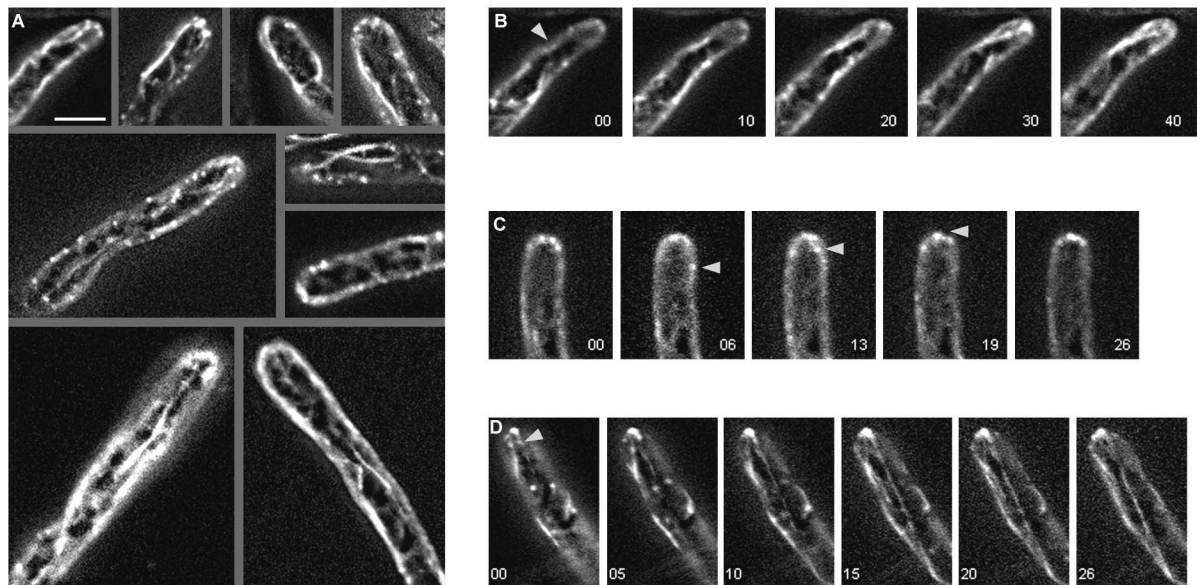


Figure 20 Abp140p-GFP cables are often connected to the tip and show events strongly suggesting secretion
 Still images of time-lapse movies of Abp140p-GFP cables in the hypha of *A.g.* A) Various examples of Abp-cables emanating from the tip. While some are seen in the middle of the hypha, others reach the tip in a purely cortical manner. Note that many are connected with punctate structures, the Abp140p-GFP patches. B) Event of an Abp140p-GFP patch moving towards the tip on a Abp140p-GFP cable. Once the patch reaches the tip, it dissolves. C) Similar event, but here, the Abp140p-GFP patch originating at 6 seconds is a distinct structure before the cable seen at 13 seconds is formed. C) Another example of strong Abp140p-GFP fluorescence at the very tip, concomitant with punctate structures moving on Abp140p-GFP cables. Note that the cable in the image of 26 seconds appears to be branched. Scalebar = 5µm, time format = s.

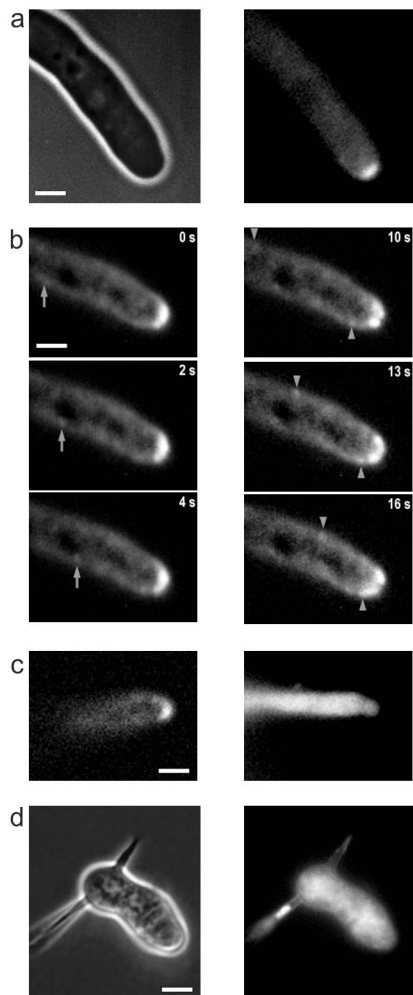


Figure 21 Distribution of GFP-Sec4p in wildtype and Δ Agbni1
 A) Brightfield (left) and GFP-fluorescence (right) micrographs of a single wild type hypha carrying a GFP-SEC4 fusion. The main fluorescence localizes to the tip. B) Sequential series of GFP-fluorescence pictures showing directed movements of GFP-Sec4p labeled vesicles towards the tip. The time is given in seconds in the top right corner. Three individual vesicles are marked by arrows. The first one is visible from timepoint 0 - 4 seconds. The second and the third one from 10 to 16 seconds. C) Localisation of GFP-Sec4p prior (left) and after (right) treatment with 200mmolar Latrunculin A for 1.5 minutes. D) Brightfield (left) and GFP-fluorescence (right) images of Δ Agbni1 carrying a GFP-SEC4 fusion gene (kindly provided by Hans-Peter Schmitz). The Sec4p-GFP fluorescence is visible throughout the formin deletion mutant and no longer localizes to the tip. Scalebars = 5µm.

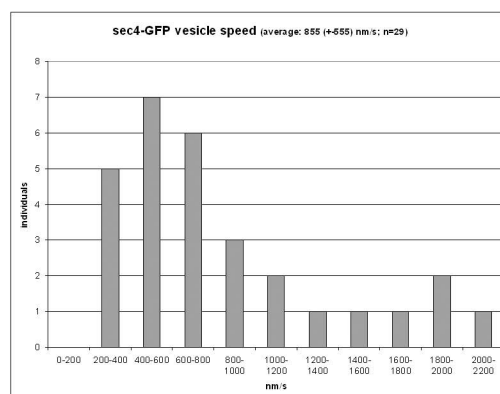


Table 4 Speed of Sec4p-GFP labelled exocytic vesicles
 Velocity of vesicles was measured in rapid single plane time lapse recordings. Sec4-GFP vesicles move mostly toward the tip. Apart from Cap-GFP patches, Abp140p-GFP patches and Sec4p-GFP vesicles, there are probably many more vesicular structures of different characteristics acting in the tip of *Ashbya gossypii*.

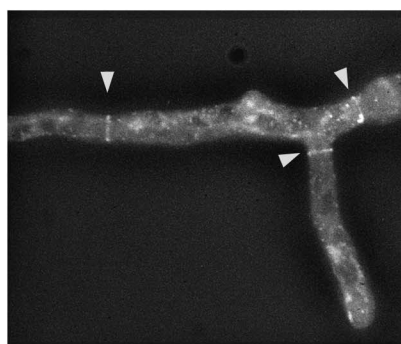
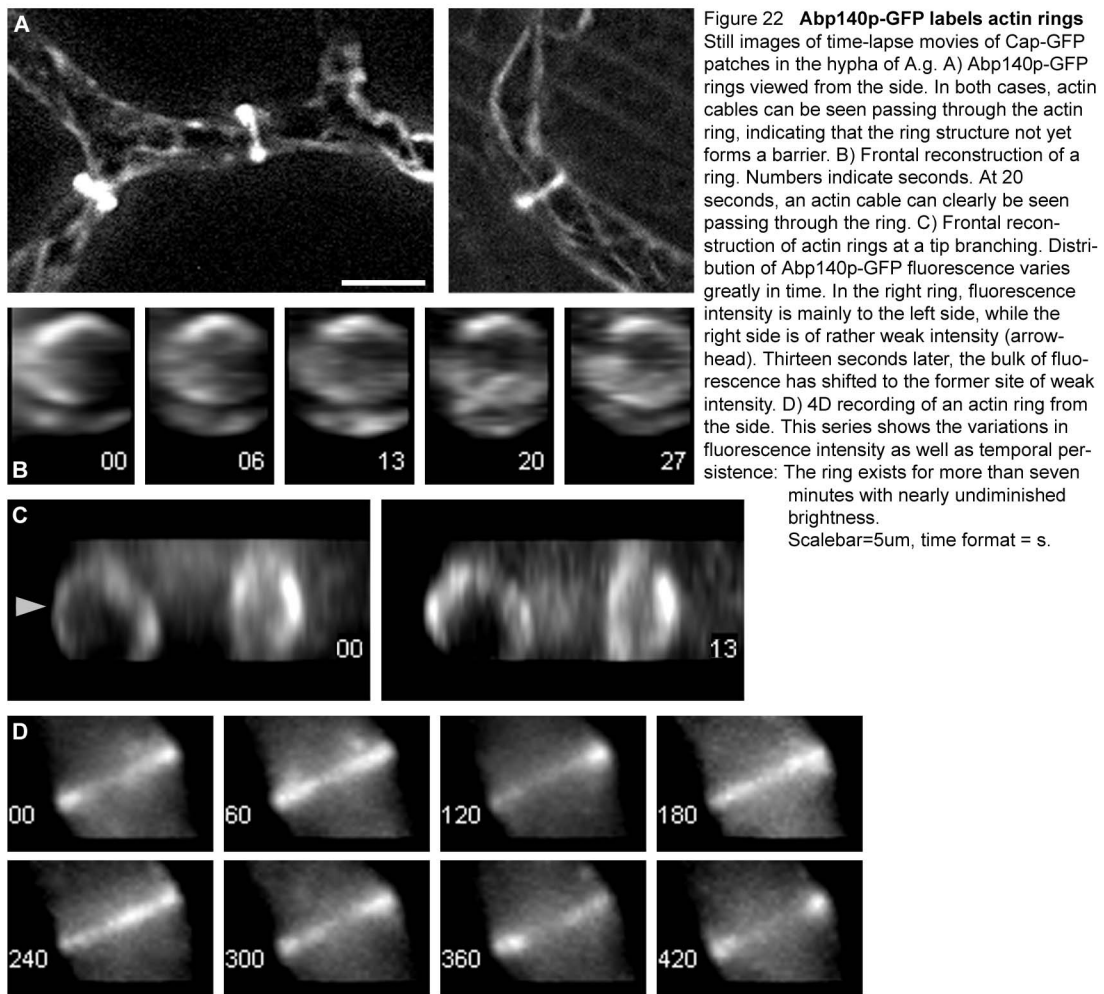


Figure 23 Actin rings of genomically integrated ABP140-GFP
 Fluorescent image of ABP140-GFP integrated in the genome. Three actin rings are marked by arrowheads. Here as well, the actin ring is the strongest structure visible, reflecting a high concentration of Abp140p-GFP.

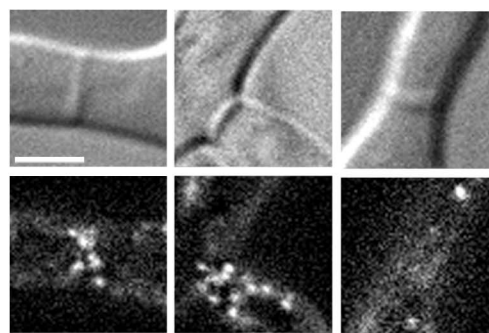
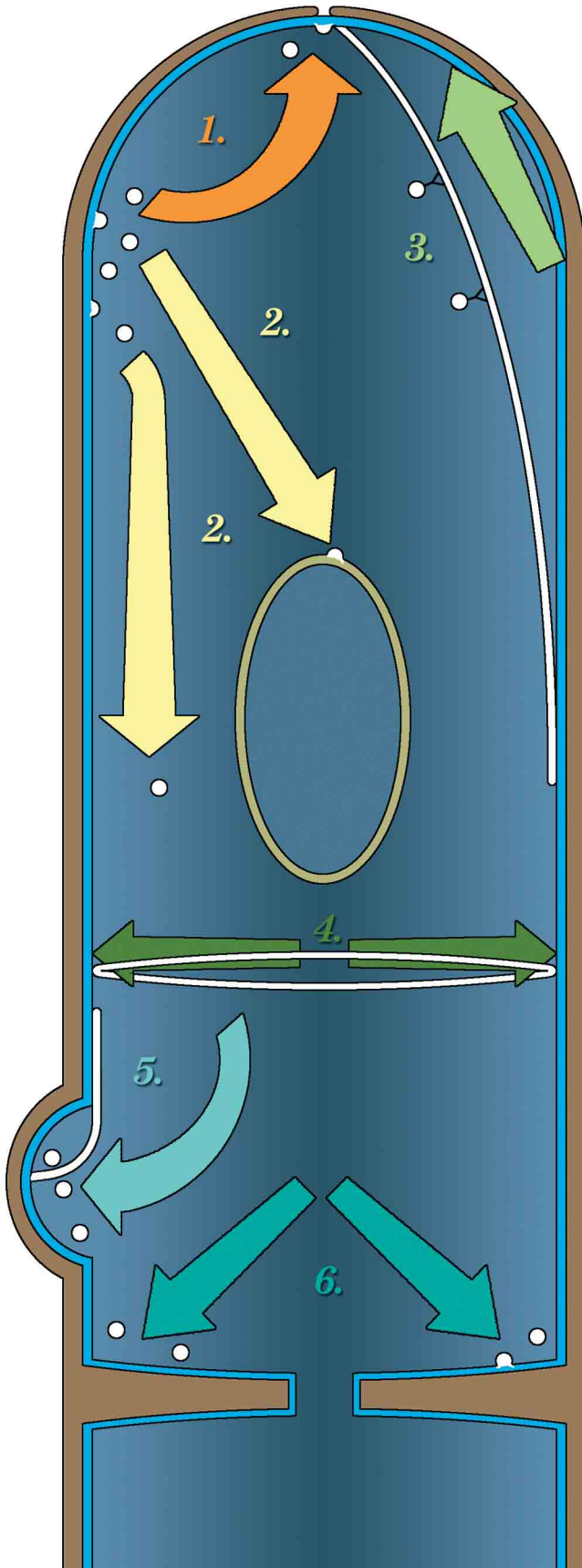


Figure 24 Cap-GFP patches appear at developing septa
 Still images of time-lapse movies of Cap-GFP patches at septa. Top row, from left to right: DIC images of the developing septal crosswall. While the left septum is thin and not strongly defined, the septum in the neighboring image is stronger. The right image shows a fully developed septum with characteristic width. Bottom row: The corresponding fluorescence images of Cap-GFP patches. With increasing width of the septum, more patches are visible. But in the last image of a finished septum, Cap-GFP patches are no longer visible, apart from the usual hyphal ones.
 Scalebar=5 μ m



1. Maintenance of polarization by endocytic recycling via redirected patches

2. Endocytosis via patches and delivery to endosomal structures (e.g. vacoules)

3. Cable-mediated exocytosis of secretory vesicles and actin patches

4. Actin ring formation via actin cables

5. Concentration of actin patches and cables at sites of branch emergence

6. Patch-mediated septation

Figure 25 Model of different tasks of the actin cytoskeleton in *A.gossypii*

Supplemental Material

Movies:

S01_Fig01: (Movie corresponds to Figure 1)

Phase contrast time-lapse movie.

Development of wild-type mycelium grown on agar, starting with a germ bubble.

Time format: Min : Sec

S02_Fig02: (Movie corresponds to Figure 2)

Three-dimensional reconstruction of a rhodamine-phalloidin stained hypha, 12 hours old.

The main structures of the actin cytoskeleton are visible: actin patches, actin cables and an actin ring.

S03_Fig05: (Movie corresponds to Figure 5)

Combination of phase contrast (red) and fluorescent (green) time-lapse recording of nearly four hours growth of hyphae of the Cap1-GFP strain.

Cap1-GFP patches (green) are constantly at the tip of all hyphae, of which the cell wall contours are shown in red.

S04_Fig06_A: (Movie corresponds to Figure 6 A)

Rapid fluorescent recording ('streaming movie') (green) of a hyphal tip of a Cap-GFP strain.

Cap-GFP patches are concentrated at the tip, but also visible at the cell wall throughout the rear part of the hypha.

Time format: Sec

S05_Fig06_B: (Movie corresponds to Figure 6 B)

Streaming movie of a frontal tip of a Cap-GFP hypha.

Cap-GFP patches are seen moving at the tip. While a directionality is hard to determine, the very tip is often devoid of patches.

Time format: Sec

S06_Fig06_C: (Movie corresponds to Figure 6 C)

Streaming movie of a frontal hypha of the Cap-GFP strain.

Cap-GFP patches are seen moving cortically at the cell wall, although some are shortly in the cytoplasm.

Time format: Sec

S07_Fig07_ABC: (Movie corresponds to Figure 7 A, B and C)

Brightfield images followed by time-lapse recording of a germ bubble (bottom) and a unipolar germling (top right, with germ tube pointing to the right) of the Cap-GFP strain.

Cap-GFP patches are seen moving in both young structures.

S08_Fig07_D: (Movie corresponds to Figure 7 D)

Brightfield image followed by streaming movie of lateral branches in 12h old mycelium of the Cap-GFP strain.

Cap-GFP patches are concentrated at all three tips, but also visible at the cell wall throughout the main part of the hypha.

Time format: Sec

S09_Fig08_A: (Movie corresponds to Figure 8 A)

Brightfield image followed by streaming movie of a hyphal tip viewed from front, of 12h old mycelium of the Cap-GFP strain.

Cap-GFP patches are seen moving in the apical region, while the very tip is mostly devoid of patches. Patches fusing during their itinerary can also be seen.

Time format: Sec

S10_Fig08_B: (Movie corresponds to Figure 8 B)

Rapid sequential z-series ('four-dimensional' or 4D recording) of the entire tip region of a 12h old hypha of the Cap-GFP strain.

Cap-GFP patches are seen concentrated at the tip in the apical region. In the subapical region, all patches are seen moving away from the tip. This illustrates the movement depicted in Figure 9 A.

Time format: Sec

S11_Fig09_B: (Movie example of motion depicted in Figure 9 B)

4D recording of the tip of a 12h old hypha of the Cap-GFP strain.

Cap-GFP patches are seen concentrated at the tip in the apical region. One patch originates on the left side, shortly behind the tip, and moves towards the tip. This is a typical example of a 'redirected' patch, which may be involved in endocytic cycling.

Time format: Sec

S12_Fig10: (Movie corresponds to Figure 10)

4D recording of the tip region of a 12h old hypha of the Bnr1 Δ DAD-Cap1GFP strain.

In this strain with the constitutively active formin Bnr1p, Cap-GFP patches are associated with filamentous structures.

Time format: Sec

S13_Fig18_B: (Movie corresponds to Figure 18 B)

4D recording of a unipolar germling of the Abp140p-GFP strain.

Here, Abp140p-GFP cables are seen moving in the hypha and are often connected to the tip, where Abp140p-GFP patches are concentrated. The lower part of the image is shaded because of the overpowering autofluorescence present in the needle-shaped spore.

Time format: Min : Sec

S14_Fig18_C: (Movie corresponds to Figure 18 C)

4D recording of branches of 15h old mycelium of the Abp140p-GFP strain.

Abp140p-GFP cables are seen moving in the hypha, often spanning a considerable length.

Time format: Min : Sec

S15_Fig19_AB: (Movie corresponds to Figure 19 A and B)

4D recording of a unipolar germling of the Abp140p-GFP strain.

Abp140p-GFP cables move in the hypha of this unipolar germling, extending towards and away from the tip. Abp140p-GFP patches are concentrated at the tip.

Time format: Min : Sec

S16_Fig19_C: (Movie corresponds to Figure 19 C)

4D recording of a 15h old hypha of the Abp140p-GFP strain.

A strongly fluorescent Abp140p-GFP cable is highly motile, showing undulating movements and changing its appearance completely within nine minutes.

Time format: Min : Sec

S17_Fig19_D: (Movie corresponds to Figure 19 D)

4D recording of a 15h old hypha of the Abp140p-GFP strain.

Strongly fluorescent Abp140p-GFP cables, arranged in a spiral manner back in the hypha, show undulating movements and change appearance completely within six minutes.

Time format: Min : Sec

S18_Fig20_A1: (Movie supporting events depicted in Figure 20)

4D recording of an evolving lateral branch of 15h old mycelium of the Abp140p-GFP strain.

A secretion event is shown: From second 11 to second 38, an Abp140p patch, originating at the upper side in the region just behind the tip, moves on an Abp140p-GFP cable towards the very tip, where it desintegrates. A new patch forms at the site where the desintegrated Abp140p-GFP patch emerged. Actin cables behind the tip reach into the main hyphal part.

Time format: Sec

S19_Fig20_A2: (Movie supporting events depicted in Figure 20)

4D recording of a hyphal tip of 15h old mycelium of the Abp140p-GFP strain.

Two secretion events are visible. At the very beginning of the movie, an Abp140p patch moves towards the very tip and desintegrates there, while at second 52, an Abp140p patch moves from the upper part behind the tip towards the tip and again is disassembled.

Time format: Sec

S20_Fig20_B: (Movie corresponding to Figure 20 B)

4D recording of a hyphal tip of 15h old mycelium of the Abp140p-GFP strain.

The secretion event depicted in Figure 20 B is shown with the extended hypha behind the tip.

It starts at 59 seconds.

Time format: Min : Sec

S21_Fig21_A: (Movie corresponding to Figure 21 A)

Streaming movie of a hyphal tip of 15h old mycelium of the Sec4p-GFP strain.

The apical localization of the Sec4p-GFP signal is evident, and movement of punctate structures towards the tip can be observed.

Time format: Sec : Millisec

S22_Fig21_B: (Movie corresponding to Figure 21 B)

Streaming movie of a hyphal tip of 15h old mycelium of the Sec4p-GFP strain.

The tip-directed movement of Sec4p-GFP vesicles indicated in Figure 21 B is visible.

Time format: Sec : Millisec

S23_Fig21: (Further example of events depicted in Figure 21 A and B)

Streaming movie of a hyphal tip of 15h old mycelium of the Sec4p-GFP strain.

At second 4, a Sec4p-GFP vesicle originates from the left side directly behind the tip, moves towards the very tip and fuses with the brightly fluorescing Sec4p-GFP 'cap' at the very tip.

Time format: Sec : Millisec

S24_Fig22_A: (Movie corresponds to Figure 22 A, left side)

4D recording of a 15h old hypha of the Abp140p-GFP strain.

Strongly fluorescent actin rings are visible in the Abp140p-GFP strain, and Abp140p-GFP cables can be seen moving through the actin rings.

Time format: Sec

S25_Fig22_A: (Movie corresponds to Figure 22 A, right side)

4D recording of a 15h old hypha of the Abp140p-GFP strain.

An actin ring is visible in the upper part of the hypha, and Abp140p-GFP cables can be seen moving through it.

Time format: Min : Sec

S26_Fig22_D: (Movie corresponds to Figure 22 D)

4D recording of a 15h old hypha of the Abp140p-GFP strain.

The varying fluorescent brightness of an Abp140p-GFP actin ring is shown, which persists for 24 minutes.

Time format: Min : Sec

S27_Fig24: (Movie corresponds to Figure 24, images to the left)

DIC brightfield image followed by a streaming movie of a 12h old hypha of the Cap-GFP strain.

The septum is visible in the brightfield picture, and the activity of Cap-GFP patches at the septum is subsequently shown.

Time format: Sec

S27_Fig24: (Movie corresponds to Figure 24, images in the middle)

DIC brightfield image followed by a streaming movie of a 15h old hypha of the Cap-GFP strain.

The septum is visible in the brightfield picture, and the frenzied activity of Cap-GFP patches at the septum is subsequently shown.

Time format: Sec

**Part II – Far11p is required to prevent premature hyphal abscission in
the filamentous fungus *Ashbya gossypii***

Abstract

AgFar11p belongs to the Far proteins which have diverse functions. In the budding yeast *Saccharomyces cerevisiae*, the syntenic homolog ScFar11p links pheromone response to the cell cycle. In the filamentous fungus *Neurospora crassa*, the Far11p homolog (NcHAM-2) is required for hyphal fusion. While this process is important for communication and homeostasis in filamentous fungi, it has not been observed in *A.gossypii*. We investigated the structure and role of AgFar11p. It is a putative transmembrane protein and bears conserved domains found in the homologs of *S.cerevisiae* and *N.crassa*. Deletion of the FAR11 gene in *Ashbya gossypii* leads to premature hyphal abscission at septa and lysis of hyphal compartments. This chain of events occurs in wild type only at the end of the life cycle, when spores are released from hyphal compartments. We conclude that hyphal abscission in *far11Δ* strains is premature and suggest that in *A.gossypii*, Far11p is involved in the timing of sporangium formation.

Index descriptors: *Ashbya gossypii*, FAR11, HAM-2, filamentous fungus, hyphal abscission, hyphal lysis, sporangium formation.

Introduction

Far proteins are found in many fungi, but also in fly, man and worm. Detailed studies have been done in the budding yeast *Saccharomyces cerevisiae*, with Far1 being the best researched family member. ScFar1p was shown to function as a pheromone-dedicated cyclin-dependent kinase inhibitor for Cdc28 (Peter and Herskowitz, 1994). Its deletion mutant fails to arrest in G1 after stimulation with alpha-factor, thus linking pheromone response to the cell cycle. Interestingly, it also plays a role in cell polarity (Nern and Arkowitz, 2000, O'Shea and Herskowitz, 2000, Shimada et al., 2000). Far3 and Far7 to Far11, on the contrary, have been shown to prevent premature recovery from pheromone arrest. They work by a different pathway and as a complex (Kemp and Sprague Jr, 2003).

But the role of Far11 seems to be a quite different one in filamentous fungi. The homolog of ScFar11p, NcHam-2p, was investigated in the filamentous fungus *Neurospora crassa*. It accounts for somatic cell fusion during vegetative growth: Deletion mutants of NcHAM-2 are incapable of hyphal fusion (anastomosis). In hyphal anastomosis, two compartments of different hyphae fuse completely, allowing nearly unrestricted flow of protoplasm. This process forms hyphal grids and is responsible for augmenting the level of communication and providing homeostasis in the organism. Hyphal fusion in filamentous fungi may share features with both mating cell fusion in *Saccharomyces cerevisiae* (Glass et al., 2000; Hickey et al., 2002) and somatic cell fusion events resulting in syncytia, such as muscles, bones, and placenta formation in animals, as proposed in Xiang et al. (2002).

In *A.gossypii*, hyphal fusion has not been observed (Louise Glass, personal communication). And pheromone response, a process in which Far11 plays a role in *Saccharomyces cerevisiae*, is absent as well. We thus wanted to elucidate the role of this protein in *A.gossypii*.

Materials and Methods

***Ashbya gossypii* strains and growth conditions**

Agfar11 Δ was produced as an Agfar11 Δ ::GEN3, leu2 Δ , thr4 Δ genotype for this study, using the Agleu2 Δ thr4 Δ genotype as background strain (Altmann-Jöhl and Philippsen, 1996). Wild-type strain Agleu2 Δ thr4 Δ was used as reference. All strains were grown under the same conditions. *A. gossypii* media preparation and culture conditions were performed as described in Wendland et al., 2000. For macroscopical growth analysis and microscopical time-lapse recordings, Ashbya Full Medium was used. In each case, 1.0 M sorbitol was added to osmotically stabilize the medium to exclude osmosis as a factor for hyphal abscission and lysis. AFM and 1.0 M sorbitol were also used for cultures grown in liquid medium.

Generation of the Agfar11 Δ strain

We used a polymerase chain reaction (PCR)-based approach (Wendland et al., 2000) to construct the Agfar11 Δ gene deletion. The dominant drug resistance marker GEN3 was amplified in a preparative PCR reaction from the *E. coli* plasmid pGEN3 by using the oligonucleotides 5'-CGAAGAATTCACGAACGTGGATGAGATTGACGGGCCGATCTCGCCGCTAGGGATAACAGGGTAAT-3' and 5'-GTACCAATGCCTAGGGGCAACTCTTTTAATCTATAAGTTTTCTTGCAGGCATGCAAGCTTAGATCT-3'. The oligonucleotides carried 45 base pair extensions at their 3' site with homology to the AgFAR11 locus. Ten micrograms of PCR product were transformed into Agleu2 Δ thr4 Δ , deleting the complete coding region of the AgFAR11 gene between the start and the stop codon. Correct integration of the cassette was verified by analytical PCR using the oligonucleotides 5'-GAAGAAGCAACAGAACAAGAAG-3' and 5'-GCAATTTTCATGTCCATAGGCATCATG-3' binding to the promoter and terminator region of AgFAR11, in combination with the standard oligonucleotides binding to the GEN3 sequence. Three independent homokaryotic Agfar11 Δ transformants were obtained. All three showed the same growth phenotype.

Cell wall staining

For staining the cell wall, Calcofluor White M2R was used (Sigma-Aldrich Chemie GmbH, Germany). *A. gossypii* mycelium was grown in liquid Ashbya Full Medium (AFM) in selective

conditions and with shaking, spun down at 2000 x *g* and incubated for 5-10 min in a 0.17 mg/ml Calcofluor White solution (Stock solution 1 mg/ml Calcofluor white in sterile H₂O, stored at -20 °C). The cells were washed twice with Ashbya Minimal Medium (AMM, with a pH of 7.0) for minimal background fluorescence, and five microliters were used for microscopy. Since Calcofluor is harmless in low doses for at least three hours, the images were taken of live specimens.

Cytoskeletal staining

The actin cytoskeleton was visualized using phalloidin coupled fluorophores (according to Amberg, 1998, modified). *A. gossypii* was cultured in AFM and 1.0 M sorbitol for 15-20h in selective conditions. After letting mycelia settle to the ground, 200 µl of the culture were mixed with 1.5 ml of 4% paraformaldehyde and fixed for 1 h. Mycelia were centrifuged at 2000 x *g*, washed twice with phosphate-buffered saline (PBS), and 100 µl thereof resuspended in PBST (PBS containing 0.03% Triton X-100). Ten microliters of rhodamine-phalloidin (6.6 µM in MeOH; Molecular Probes, Eugene, OR) were added, and mycelia incubated for 1 h in the dark. After three washing procedures in PBST, mycelia were resuspended in 50 µl of Vectashield mounting medium (Vector Laboratories, Burlingame, CA). Five microliter thereof were put on a slide, covered with a coverslip and sealed with rubber cement ("Fixogum," Marabuwerke GmbH & Co., D-71732 Tamm). Images were taken during the next five hours to ensure that any possibility of biological changes induced by old age in the organism was avoided.

Microscope setup

The microscopy unit used (as described in Hoepfner *et al.*, 2000, modified) consisted of an Axioplan 2 imaging microscope (Carl Zeiss, Feldbach, Switzerland) and images made with the objectives Plan Apochromat 100 x Ph3 numerical aperture (N.A.) 1.4 and Plan Apochromat 63 x N.A. 1.4. It was equipped with a 75 W XBO illumination source controlled by a MAC2000 shutter and filter wheel system (Ludl Electronics, Hawthorne, NY). The camera was a TE/CCD-1000PB back-illuminated cooled charge-coupled device camera (Princeton Instruments, Trenton, NJ). The following filter sets for different fluorophores were used: #15 for rhodamine (Carl Zeiss) and 31044v2 for Calcofluor (Chroma Technology Corp, Rockingham, VT). Phase contrast was used according to the manufacturer (Carl Zeiss). The excitation intensity was controlled with different neutral density filters (Chroma Technology). The setup, including microscope, camera, and Ludl controller, was controlled by MetaMorph 4.1.7 software (Universal Imaging Corporation, Downingtown, PA).

Image acquisition and processing

Brightfield and fluorescence images were taken with exposure times ensuring maximum

contrast. For time-lapse movies, single images were taken at three minute intervals. In the other cases, Z-series were made to assure the complete three-dimensional information – 1.0 μm for brightfield Z-series and 0.4 μm for fluorescence images. For time-lapse acquisition, the fungus was grown on a slide with a cavity (time-lapse slide) that was filled with agar-solidified AFM (AMM for fluorescent images) and 1.0 M sorbitol for osmotic stability. Spores were preincubated in a humid chamber without coverslip until they reached the required developmental stage. A coverslip was then applied.

Brightfield and fluorescent images and stacks were scaled using the "scaling" drop-in in MetaMorph. Z-series were projected on a single plane with the "Best Focus" for brightfield or "Maximum" algorithm for fluorescent images. In some cases, the "Flatten Background" command was used for equalizing gradients caused by non-uniform illumination. For three-dimensional reconstructions, stacks were assembled with MetaMorph's "3D reconstruction" drop-in. Fluorescent picture sets were processed as mentioned above and overlaid using Meta-Morph's "overlay" drop-in. The time-lapse image series were transformed into movies (QuickTime format (Apple Computer, Cupertino, CA)) using MetaMorph. Adobe Photoshop 6.0 (Adobe Systems, Mountain View, CA) was used for still pictures.

Analysis of the AgFar11p protein sequence

The sequence of AGR339C, the *A.gossypii* homolog of ScFar11p, was retrieved from the Ashbya genome database generated from the complete genome sequencing approach by Dietrich et al., 2004. The resulting amino acid sequence was used for analyzing the homologous genes in *S. cerevisiae*, ScFar11p (YNL127W), and *N. crassa*, NcHam-2p (NCU03727.1). The program of the Centre for Bioinformatics and Biocomputing of the Karolinska Institute in Sweden (Persson and Argos, 1996; Persson and Argos, 1994; <http://130.237.130.31/tmap/>) was used for predicting transmembrane domains in all three proteins. The PSORT II program, developed by Nakai and Horton (1999), was used to predict the subcellular localization of proteins derived from translated ORFs. Regions of identity were defined using the Align Plus 5.03 module of the CloneManager 7.03 suite (Scientific & Educational Software, Cary, NC). "Compare multiple sequences" was used in Multi-Way mode for multiple alignment without reference. "Align two sequences" in the global alignment mode was used to determine the percentage of identity in similar regions. For all analyses, the BLOSUM 62 scoring matrix for amino acids was chosen.

Results

Analysis of the AgFar11p protein sequence

AgFar11p is a putative transmembrane protein. Three transmembrane (TM) domains were predicted and three conserved regions found by multiple sequence alignment, as shown in Figure 1. AgFar11p was compared to the Far11p homologs of *Neurospora crassa* and *Saccharomyces cerevisiae*. It shares an identity of 44% percent with ScFar11p, but only 19% compared to NcHam-2p. The Domains 1 and 2, as described in Kemp and Sprague (2003), were also found in *A.gossypii*, with an identity of 61% for both domains compared to budding yeast. The comparison with those domains in *N.crassa* yielded an identity of only 31% for Domain 1 and 21% for Domain 2. A third conserved region was detected in the middle of the three putative proteins. We dubbed it the 'proline repeat'. Although it is only 13 amino acids (aa) long, identity was 92% percent in the case of both comparisons, with *S.cerevisiae* and *N.crassa*. The consensus sequence is HIATPAPSPPXSP (with X being any aa). This sequence is, like Domain 1 and 2, a motif of hitherto unknown function. The main theme is a four-fold repetition of Proline preceded by an amino acid with a hydroxyl group (or Alanine, in one case).

Multiple aligned sequences of the three proteins were used to predict TM domains. These follow a similar arrangement in all proteins, with one TM domain being closer to the N-terminus and two neighboring TMs towards the C-terminus. This is in agreement with the previous studies of TM domains in *N.crassa* (Xiang et al, 2002; Kemp and Sprague, 2003).

Agfar11Δ mutants commit hyphal abscission

The *far11Δ* phenotype shows complete abscission of hyphal compartments. Figure 2 compares wild type (left half) with the FAR11 deletion mutant (right half). The large phase contrast image of 14h old wild-type mycelium reflects normal development: In the middle of a needle-shaped spore, a germ bubble forms (black arrow) and gives rise to a germ tube, the primary hypha. Two to three hours later, a second hypha emerges at the other end. As these main hyphae grow in opposite directions, they start forming lateral branches, a process which is repeated with every branch, resulting in a ramification pattern. This dendritic stage is called the mycelium. All the while, crosswalls called septa are formed to compartmentalize the hyphae (white arrowheads). A septum contains a pore and is formed at the base of a hypha or behind its tip. Figure 2 B shows a septum behind the tip at higher magnification. With radial expansion of the mycelium originating from a single spore, a dense, circular layer will be formed (Figure 2 C). Figure 2 D demonstrates the defect of the FAR11 deletion mutant. Though the germ bubble (black arrow) has a hypha attached at its lower end, it is completely detached from the upper part. Since the upper mycelial part contains no needle-shaped spore, its origin can only be the now dissociated germ bubble, so the two structures must have been connected at an earlier stage. The site of former attachment is indicated by an asterisk (*). Hyphae of the upper mycelial part are less streamlined than in wild type, and the main, vertical hypha is enlarged. Correlated with the number of lateral hyphae, it is far shorter

than the main hyphae of wild type. Weak septa can be discerned at the bases of lateral hyphae. But in three cases, the hyphal base is severely constricted. The same aspect is depicted in Figure 2 E in a hyphal tip of 18h old mycelium. Disturbed growth is also seen when the FAR11 deletion mutant is grown on osmotically stabilized agar (Figure 2 F): It is irregularly shaped and covers less than one sixth of the area of wild-type mycelium (Figure 2 C). To assure that this is not a consequence of slower growth, expansion speed of hyphal tips was measured, resulting in the same average value of 6-10 $\mu\text{m}/\text{h}$ observed in young wild-type mycelium (Knechtle et al. 2003). With hyphae maintaining a stable, linear axis, curved growth may also be excluded as a cause for impaired mycelial expansion.

Hyphal abscission occurs at septa of the *Agfar11* Δ mutant

The only possible structure capable of hyphal constriction is the septum. This notion was supported by the finding that constrictions are always visible in places where septa usually form. To verify this, development of septa in the mutant phenotype was investigated in time lapse recordings. Figure 3 (Movie S1) shows a main hypha (A), of which a lateral branch emerges (B). The base of a lateral hypha is a site predestined for septum formation. Indeed, about five hours after emergence, a septal crosswall is visible at the base (C), rising to wild-type appearance in (D). But constriction of the cell wall rapidly continues at the septum (E,F,G) and ultimately leads to abscission of the hypha (H). Abscission seems complete in highly magnified images of the constricted septa. We proceed to demonstrate this by a different means.

Hyphal abscission leads to complete separation

FAR11 deletion mutants grown on osmotically stabilized agar often show hyphal parts which are translocated from their part of origin (Figure 2 D, 3 H, 6 C and 7 C). Our hypothesis was that, if abscission is complete, the lack of a solid substrate would produce hyphal parts lacking a germ bubble with its typical needle-shaped spore. This is shown in Figure 4. (A) is the phase contrast image of such a mycelial piece, (B) its cell wall stained by Calcofluor White, a fluorescent probe that interacts with polysaccharides of the fungal cell wall. (C) is the combination of (A) and (B). The cell wall staining shows that one end of the hyphal bit is strongly fluorescent. Since septa are rich in cell wall material and thus very bright in Calcofluor stainings of wild type and the *far11* Δ mutant, this bright end must be the site of abscission. The completely separated mycelial parts are still capable of growth. This means that the septa, which in their wild-type form are perforated by a septal pore, are plugged in *far11* Δ mutants, thus preventing loss of cytoplasm and turgor pressure.

A prerequisite for septum formation is the actin ring. We thus investigated the structure of the actin cytoskeleton in *far11* Δ mutants. Figure 5 shows actin stained with rhodamine-coupled phalloidin. The central germ bubble, pointed out by the white arrow, is surrounded and

isolated by large gaps. These gaps, which are not stainable with rhodamine-phalloidin, are even bigger than in mature septa (Knechtle et al., 2003) and show that mature septa no longer contain actin. Actin rings (demarcated by a small 'r') are also visible and of normal, wild-type appearance. The bright dots are actin patches, seen throughout the hypha and concentrated at the three emerging hyphal tips pointing to the top of the image. These findings suggest that organisation and therefore polarization of the actin cytoskeleton are undisturbed in *far11Δ* mutants with respect to these aspects. Actin patches also gather at septa (Figure 4B and C). This is observed in wild type, where actin patches are believed to deposit cell wall material required for septum formation. But the difference here is that the gaps which demarcate the septum in *far11Δ* mutants are considerably wider, and that they appear early in *Agfar11Δ* young mycelium. In wild type, septal localization of actin patches stops once the septum is visible as a thin gap. The still visible concentration of actin patches at already broad septal gaps is another feature in *Agfar11Δ*.

Hyphal abscission is often followed by displacement and lysis

After hyphal abscission, two distinct events may ensue. One occurrence is that the abscised hyphal compartment is bent, resulting in a turning movement with one end of the septum forming the pivotal center. Figure 6 (Movie S2) demonstrates such an incident, in which the hyphal compartment in the process of abscission is bent backwards by 125 degrees. The origin or mechanism of this movement is not known, but must reflect tension stemming either from an unequal constriction or unsymmetrical cell wall deposition. It is in any case reminiscent of the vigorous action which cytokinesis can exhibit.

The other, graver occurrence often following hyphal abscission is hyphal lysis. Lysis of hyphal compartments may be preceded by displacement, but the two events are not inevitably coupled. Figure 7 (Movie S3) explores a case which led to annihilation of the entire mycelium. While the chain of events is described in detail in the figure legend, one observation needs to be pointed out separately: Lysis of one hyphal compartment does not necessarily affect the adjacent compartment. This is best illustrated in Figure 7 E, where the proximal compartment of the hypha at eight o'clock lyses, while the distal part keeps on growing. This is a clear indication that hyphal abscission leads to plugged septa.

Figure 7 demonstrates another characteristic of *FAR11* deletion mutants: Hyphal abscission is often follows a temporal order, first occurring at older septa. Although the germ bubble is the mycelial point of origin, it is the last mycelial structure to lyse in Figure 7. In order to prevent lysis, it must be completely sealed by hyphal abscission from the rest of the mycelium. This temporal order of hyphal abscission was observed in many other cases and may also be concluded from the segregation of the germ bubble in Figure 2 D.

Hyphal abscission and lysis showed different grades of severeness. While in some specimens abscission of hyphal parts was visible only 20 hours after formation of the first hypha, extreme cases started making total cytokinesis as the first septum near the germ

bubble appeared. In these, lysis occurred soon after emergence of the primary hypha and often continued until the entire mycelium was lysed. Less severe cases did not have lysing compartments and were able to construe an entire mycelium. These cases showed increased invasive growth, though. However, the majority features early abscission and lysis: Of 233 specimens, 172 were severe cases with hyphal abscission.

To understand why FAR11 deletion mutants commit hyphal abscission and lysis, we wanted to see where these processes may occur in wild type.

Sporangium formation in wild type features hyphal abscission and lysis as well

Constriction at septa, hyphal abscission and lysis are processes which cannot be detected in young mycelium of wild type. They are observed in mycelium of three days age, though. The end of the life cycle in *A.gossypii* is initiated by building special compartments for spore formation. In these so called sporangia, eight needle-shaped spores are formed. They are subsequently released by rupture of the encasing cell wall. Septation followed by cytokinesis is found at the ends of sporangia, which are often detached from the old mycelium (Wendland and Philippsen, 2002). Figure 8 shows images of a developing sporangium (A), its constricted and abscided ends (B, C) and rupture of the cell wall with the end of a spore exiting (D).

Discussion

This study shows that the lack of FAR11 in Ag leads to hyphal abscission at septa and lysis of hyphal compartments. Normally, these events observed at the end of Ag's wild-type life cycle. Hence, the simplest explanation is that Far11p is responsible for scheduling these processes required for spore formation and release. This would mean that after septation, AgFAR11 deletion mutants continue directly to the program for sporangium formation, where abscission of hyphal parts and rupture of the cell wall is needed for releasing the spores. This could also explain lysis. Since all AgFAR11 deletion mutants were grown on osmotically stabilized medium, a defect in osmotic regulation can be excluded as reason for lysis. Thus, AgFAR11 deletion mutants would suffer from an event early their life which for wild-type cells only occurs at the end of the individual life cycle.

Septa are used as crosswalls for making hyphal compartments in filamentous fungi. In *A.gossypii*, although septa restrict cytoplasmic flow between compartments, septal pores ensure that even nuclei can traverse septal crosswalls (Alberti-Segui et al., 2001). Since in FAR11 deletion mutants, detached hyphal parts can be found where one end has lysed and the other keeps growing (Figure 4), the septal pore must be closed. Septation is a complex process involving many different proteins (Wendland, 2003; Ayad-Durieux et al., 2000; see also Walther and Wendland, 2003) and is essential for sporangium formation (Wendland and Philippsen, 2002). Hyphal abscission at septa, as shown in Figure 8, is required to line out the spore-bearing compartment, the sporangium. Spores are then released by hyphal lysis.

The function of the Far11 protein in Ag cannot be the same as that of the Far11 protein homologs in *Neurospora crassa* or *Saccharomyces cerevisiae*. In the latter two, it participates in processes (hyphal fusion and pheromone response, respectively) which are absent in Ag. Yet, compartmentalization, septal plugging and cell lysis are events observed during heterokaryon incompatibility in *N.crassa* (Marek et al., 2003). This filamentous fungus is capable of hyphal fusion, in contrast to *Ashbya gossypii*. If the fusion partner is a genetically different individual, then a heterokaryon can be formed. But the viability of such heterokaryons is governed by specific genetic loci. These are the so-called het-loci and responsible for heterokaryon incompatibility (Glass and Kulda, 1992). In the case of het-locus incompatibility, the fusion cell auto-destructs, a process which was likened to programmed cell death. Whether hyphal anastomosis nor het-loci are known to exist in *A.gossypii*. Hence, Far11 must play a different role in this organism. And there is no evident link between hyphal fusion and septation. Although it was observed that a septum formed at the site of hyphal fusion in the nematode-trapping fungus *Arthrobotrys oligospora* (Nordbring-Hertz et al., 1989), no other findings yet support a connection between those two diverse processes.

AgFar11p might also just ensure correct septum formation. This connection has been shown for other proteins already. BIMG phosphatase for example is directly involved in septum formation, distinct from its role in mitosis (Fox et al., 2002). And in budding yeast, it was proposed that Far3 and Far7 to Far11 are part of a checkpoint that monitors cell fusion (Kemp and Sprague, 2003): They might be required to prevent premature re-entry into mitosis, thus ensuring that mating cells have enough time to fuse. So Far11 could be responsible for ending septum formation in *A.gossypii*. In a hypha, once the septum is formed, the older compartment does not require further cell wall deposition, whereas the younger one needs it at the growing tip. AgFar11p would be the checkpoint calling for a stop of cell wall deposition. The continuous cell wall deposition at already thick septa in *A.gossypii* (Figure 5) could be explained by Far11 deletion mutants missing out on the stop signal for septum construction. In this scenario, hyphal abscission and lysis would be consequences of relentless cell wall deposition at septa, but not an implemented part of the program for septation.

A possibility which cannot be excluded is that the phenotype of the Far11 deletion is due to a biochemical defect. Specifically, the deposited cell wall material would not be fully functional. Many events of lysis have been recorded, and in some specimens older than 20h, ruptures in the cell wall were observed. In this scenario, *A.gossypii* would try to compensate a weak cell wall with additional deposition of material, resulting in the thicker cell wall visible in Calcofluor stainings. But the fact that cells also lyse on osmotically stabilized medium is not in favor of this hypothesis, nor does it explain hyphal abscission at septa.

The reason for the varying degrees of severeness in Far11 deletion mutants is unknown. Less severe cases, which didn't show lysis of hyphal compartments, had more invasive growth. The surrounding medium in invasive growth stabilizes a weak cell wall, as

demonstrated by spheroblasts embedded in agar (Solingen and Haas, 1970). Hyphal lysis could be prevented this way.

Apart from the comparison to *N.crassa* and *S.cerevisiae*, AgFar11p was aligned with the homologs in the human fungal pathogen *Candida albicans*, the fruitfly *Drosophila melanogaster* (CG11526 (AE003477)) and us, *Homo sapiens* (KIAA1170 (AB093 2996)) (data not shown). Conservation of Domain 1 and 2 was found in all these hypothetical proteins as well. The third domain in the middle of AgFar11p, the proline repeat, was only conserved in *Candida albicans* (besides *S.cerevisiae* and *N.crassa*), but could not be detected in the homologs of the other compared species. This suggests that the 4x(T,A,S)P motif may be specific to fungi. A thorough search yielded no immediate corresponding motif. But the consensus sequence HIATPAPSPPXSP may be broken down into two motifs, PXPpP followed by PxxP. These motifs were found in a recent study concerning the acetylation of the transcription factor p53 (Dornan et al., 2003). The tumor suppressor protein p53 is one of the most well-studied stress-responsive eukaryotic transcription factors that function in a damage-induced cell cycle checkpoint pathway, and the study shows that its acetylation depends on the transcriptional coactivator p300. p300 binds in vitro to PXXP-containing peptides derived from the proline repeat domain, and PXXP-containing peptides inhibit sequence-specific DNA-dependent acetylation of p53, indicating that p300 docking to a contiguous PXXP motif in p53 is required for p53 acetylation. If this binding to a transcription factor is a role for the proline repeat in the Far11 protein, remains to be seen. This goes for the transmembrane domains and Domain 1 and 2 as well, since none of these regions is confirmed on a biochemical or ultrastructural level for any of the above species.

No detailed model of the mode of action of Far proteins exists so far, with exception of the well investigated ScFar1p. There, it has been shown that a Cdc24p-Far1p complex is exported from the nucleus as a reaction to pheromone exposure. This mode of action is also a possibility for Far3 and Far7 to Far11 proteins, as they might play a general role in RNA metabolism (Kemp and Sprague, 2003).

AgFAR11 deletion mutants have a disturbed septation process. It is of paramount interest to investigate a FAR11 deletion in a septum mutant. The best candidate for such a double deletion is the CYK1 deletion strain, in which no septa at all are formed. If Far11p governs septation, the hyphal abscission/lysis phenotype of Agfar11 Δ would be invisible in a Agfar11/cyk1 double deletion.

References

Alberti-Segui C., Dietrich F., Altmann-Johl R., Hoepfner D., Philippsen P., 2001. Cytoplasmic dynein is required to oppose the force that moves nuclei towards the hyphal tip in the filamentous ascomycete *Ashbya gossypii*. J Cell Sci. 114(Pt 5):975-86.

- Ayad-Durieux, Y., Knechtle P., Goff S., Dietrich F., Philippsen P., 2000. A PAK-like protein kinase is required for maturation of young hyphae and septation in the filamentous ascomycete *Ashbya gossypii*. *J. Cell Sci.* 113, 4563–4575.
- Dietrich F.S., Voegeli S., Brachat S., Lerch A., Gates K., Steiner S., Mohr C., Pohlmann R., Luedi P., Choi S., Wing R.A., Flavier A., Gaffney T.D., Philippsen P., 2004. The *Ashbya gossypii* genome as a tool for mapping the ancient *Saccharomyces cerevisiae* genome. *Science*. 304(5668):304-7.
- Dornan D, Shimizu H, Burch L, Smith AJ, Hupp TR., 2003. The proline repeat domain of p53 binds directly to the transcriptional coactivator p300 and allosterically controls DNA-dependent acetylation of p53. *Mol Cell Biol.* 23(23):8846-61.
- Fox H., Hickey P.C., Fernandez-Abalos J.M., Lunness P., Read N.D., Doonan J.H., 2002. Dynamic distribution of BIMG(PP1) in living hyphae of *Aspergillus* indicates a novel role in septum formation. *Mol Microbiol.* 45(5):1219-30.
- Glass N.L., Kuldau G.A., 1992. Mating type and vegetative incompatibility in filamentous ascomycetes. *Annu. Rev. Phytopathol.* 30:201-224.
- Glass N.L., Jacobson D.J., Shiu P.K., 2000. The genetics of hyphal fusion and vegetative incompatibility in filamentous ascomycete fungi. *Annu Rev Genet.* 34:165-186. Review.
- Hickey P.C., Jacobson D., Read N.D., Glass N.L., 2002. Live-cell imaging of vegetative hyphal fusion in *Neurospora crassa*. *Fungal Genet Biol.* 37(1):109-19.
- Kemp H.A., Sprague G.F. Jr., 2003. Far3 and five interacting proteins prevent premature recovery from pheromone arrest in the budding yeast *Saccharomyces cerevisiae*. *Mol Cell Biol.* 23(5):1750-63.
- Marek S.M., Wu J., Glass L.N., Gilchrist D.G., Bostock R.M., 2003. Nuclear DNA degradation during heterokaryon incompatibility in *Neurospora crassa*. *Fungal Genet Biol.* 40(2):126-37.
- Nakai K, Horton P., 1999. PSORT: a program for detecting sorting signals in proteins and predicting their subcellular localization. *Trends Biochem Sci.* 1999 Jan;24(1):34-6.
- Nern, A., and R. A. Arkowitz. 2000. Nucleocytoplasmic shuttling of the Cdc42p exchange factor Cdc24p. *J. Cell Biol.* 148:1115-1122.
- Nordbring-Hertz B., Friman E., Veenhuis M., 1989. Hyphal fusion during initial stages of trap formation in *Arthrotrichum oligospora*. *Antonie Van Leeuwenhoek.* 55(3):237-44.
- O'Shea E. K., Herskowitz I., 2000. The ins and outs of cell-polarity decisions. *Nat. Cell Biol.* 2:E39-E41.
- Persson, B., Argos, P., 1996. Topology prediction of membrane proteins. *Protein Sci.* 5(2), 363-371.
- Persson, B., Argos, P., 1994. Prediction of transmembrane segments in proteins utilising multiple sequence alignments. *J. Mol. Biol.* 237(2):182-92.
- Peter, M., Herskowitz I., 1994. Direct inhibition of the yeast cyclin-dependent kinase Cdc28-Cln by Far1. *Science* 265:1228-1231.

Reinhardt A., Hubbard T., 1998. Using neural networks for prediction of the subcellular location of proteins. *Nucleic Acids Res.* 26(9):2230-6.

Shimada, Y., Gulli M. P., Peter M., 2000. Nuclear sequestration of the exchange factor Cdc24 by Far1 regulates cell polarity during yeast mating. *Nat. Cell Biol.* 2:117-124.

Walther A., Wendland J., 2003. Septation and cytokinesis in fungi. *Fungal Genet Biol.* 40(3):187-96. Review.

Wendland J., 2003. Analysis of the landmark protein Bud3 of *Ashbya gossypii* reveals a novel role in septum construction. *EMBO Rep.* 4(2):200-4.

Wendland J., Philippsen P., 2002. An IQGAP-related protein, encoded by AgCYK1, is required for septation in the filamentous fungus *Ashbya gossypii*. *Fungal Genet Biol.* 37(1):81-8.

Wendland J., Ayad-Durieux Y., Knechtle P., Rebischung C., Philippsen P., 2000. PCR-based gene targeting in the filamentous fungus *Ashbya gossypii*. *Gene.* 242(1-2):381-91.

Xiang Q., Rasmussen C., Glass N. L., 2002. The *ham-2* locus, encoding a putative transmembrane protein, is required for hyphal fusion in *Neurospora crassa*. *Genetics* 160:169-180.

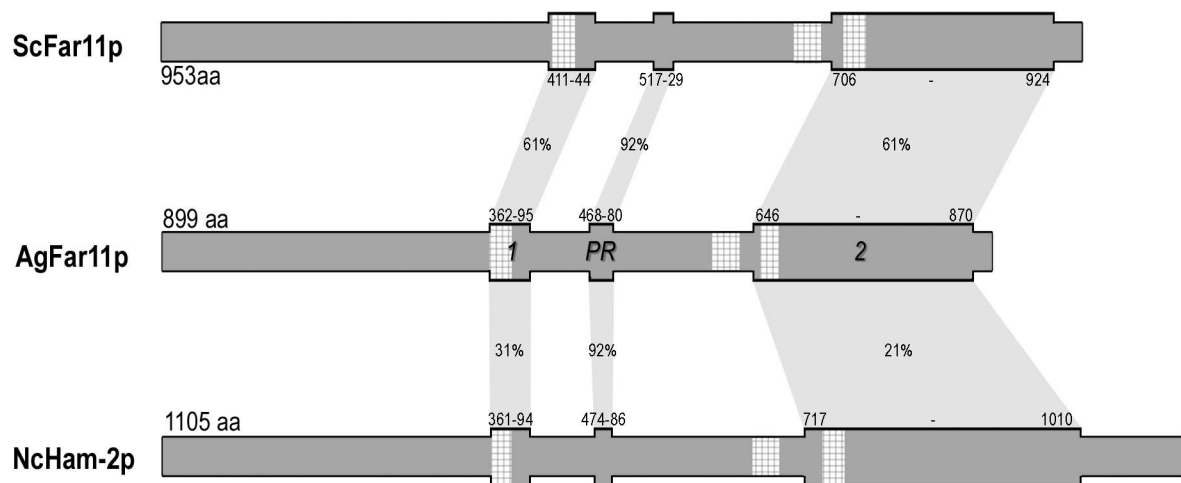


Figure 1 Comparison of Far11p homologs

From top to bottom, the putative transmembrane protein Far11p of *Saccharomyces cerevisiae*, its homolog in *Ashbya gossypii* and the Far11p homolog Ham-2p of *Neurospora crassa* are shown. Compared to AgFar11p, ScFar11p is 44% identical, while NcHam-2p shares only 19% identical amino acids. Grid boxes display the putative transmembrane domains of each protein as predicted by TMAP (multiple sequence alignment, <http://www.mbb.ki.se/tmap/>). Crossbands indicate the percentage of homology between similar domains, with elevated positions demarcated by small numbers indicating amino acids. From left to right: Domain 1 ('1') as described in Kemp and Sprague (2003), the proline-repeat domain ('PR') and Domain 2 ('2', Kemp and Sprague, 2003).

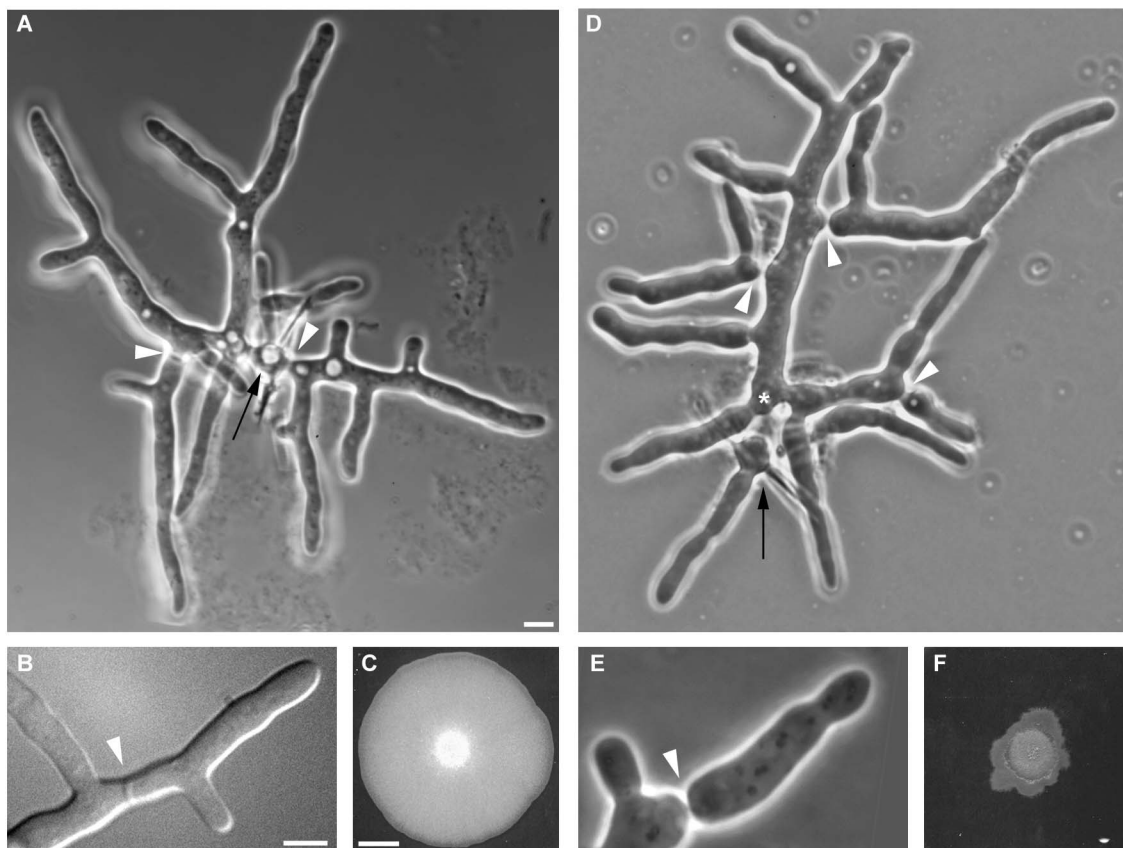


Figure 2 Comparison of wildtype and mutant phenotype of the FAR11 deletion strain

A) Phase contrast image of a 14h old wildtype mycelium, originating from a single germ bubble (black arrow). The arrowheads indicate two septa. The one at the germ bubble is normally the first septum formed. B) DIC image of a hyphal tip of young wildtype mycelium. The arrowhead points to the septal crosswall formed behind the tip. Scalebar = 5µm. C) Wildtype mycelium grown on full medium for three days. D) Phase contrast image of mycelium of the FAR11 deletion mutant grown on osmotically stabilized medium for 14h. The germ bubble is pointed out by a black arrow. The hyphal part above the germ bubble was originally attached to the germ bubble. It is now completely separated by hyphal abscission. The site of abscission is marked by a black asterisk (*). Further sites of abscission at lateral branches are indicated by white arrowheads. E) Phase contrast image of a hyphal tip of young mutant mycelium. The arrowhead indicates the site where septum formation led to hyphal abscission. F) Mutant mycelium grown on osmotically stabilized medium for three days. Growth is severely diminished and no isometrical expansion achieved. Scalebar = 5µm (A,B,D and E), 1cm (C and F)

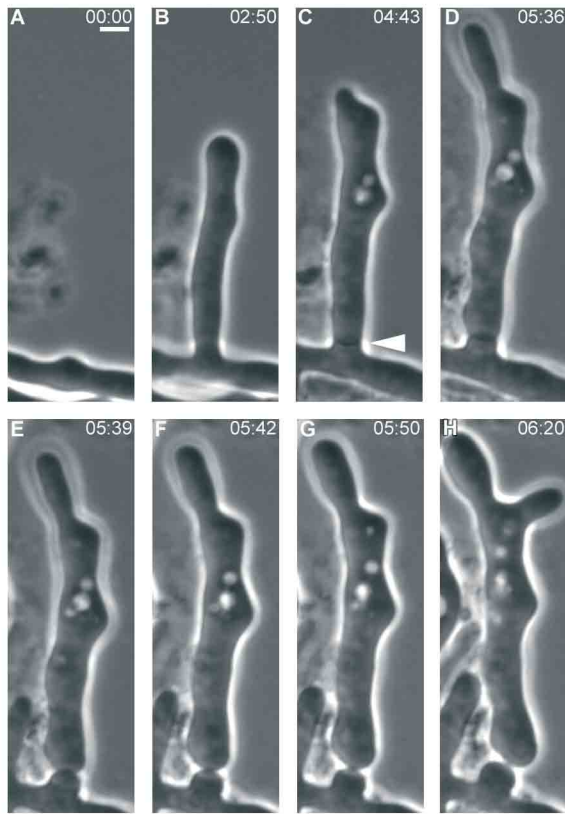


Figure 3 Phase contrast images of a hyphal abscission in a FAR11 deletion mutant

Still images from a time-lapse recording of an eight hours old mutant individual grown on osmotically stabilized medium. A) The main hypha (germ tube) is shown at the bottom of the image. B) Nearly three hours later, a lateral branch has developed. C) After another two hours, a dark crossband (arrowhead) can be discerned at the base of the lateral branch, which is a site predestined for septum formation. D) The septum is now clearly visible. In wild type, septum formation is complete at this stage. E) Only three minutes later, the cell wall indentation at the septum suggests constriction, which is increasingly visible in F) and G). H) Two hours after septum formation started, the lateral hypha is detached from the main one. Scalebar=5um

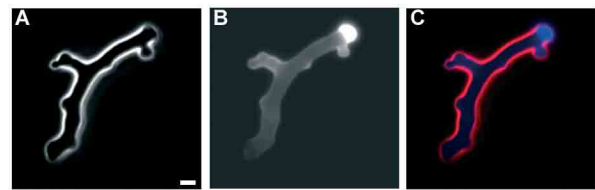


Figure 4 Abscised hypha of a FAR11 deletion mutant grown in liquid, osmostabilized medium

A) Brightfield image of a detached hyphal compartment. There is no needle shaped spore or spherical germ bubble visible. Shaking of the liquid culture has detached this mycelial compartment entirely from its site of origin. B) Calcofluor staining of the hyphal compartment, the bright blue stain in the upper right corner indicating the site of abscission. C) Merged images of the brightfield image (red) and the Calcofluor staining (blue). Scalebar = 5um

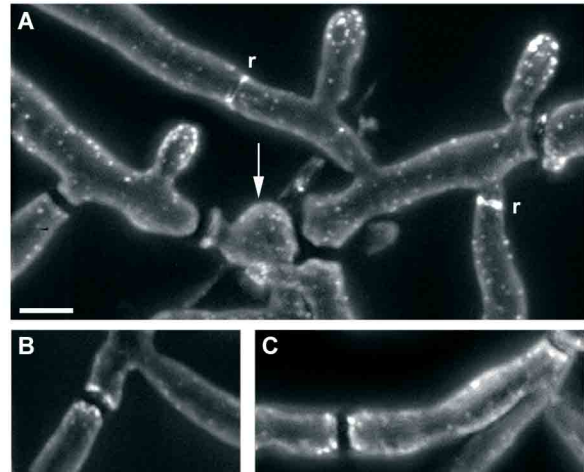


Figure 5 Rhodamine-Phalloidin stainings of FAR11 deletion mutants

A) Fluorescent image of a Rhodamine-Phalloidin staining of 24h old mutant mycelium. The germ bubble, indicated by a white arrow, is surrounded by large black bands. These bands are the places of septal crosswalls, which completely isolate the germ bubble. Two other features though are similar to wild type: Actin rings (r) are well visible, and polarization of actin patches at hyphal tips is undisturbed. B) and C) are examples of large septa, where actin patches are surprisingly still accumulated. Scalebar=5um

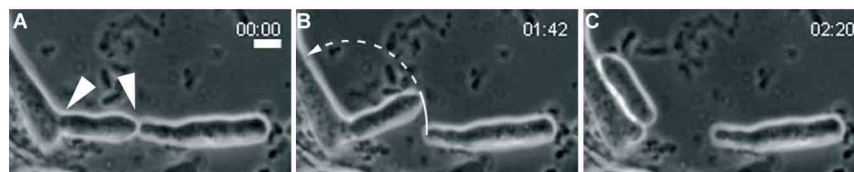


Figure 6 Hyphal abscission and bending in FAR11 deletion mutants

Still images of a phase contrast recording of violent hyphal abscission at the septum. A) The two arrowheads indicate septa. B) Almost two hours later, the middle part of the hypha is completely separated from the distal part and starts to bend backwards. C) Forty minutes later, the middle hyphal part is bent backwards by 125 degrees. Scalebar = 5um

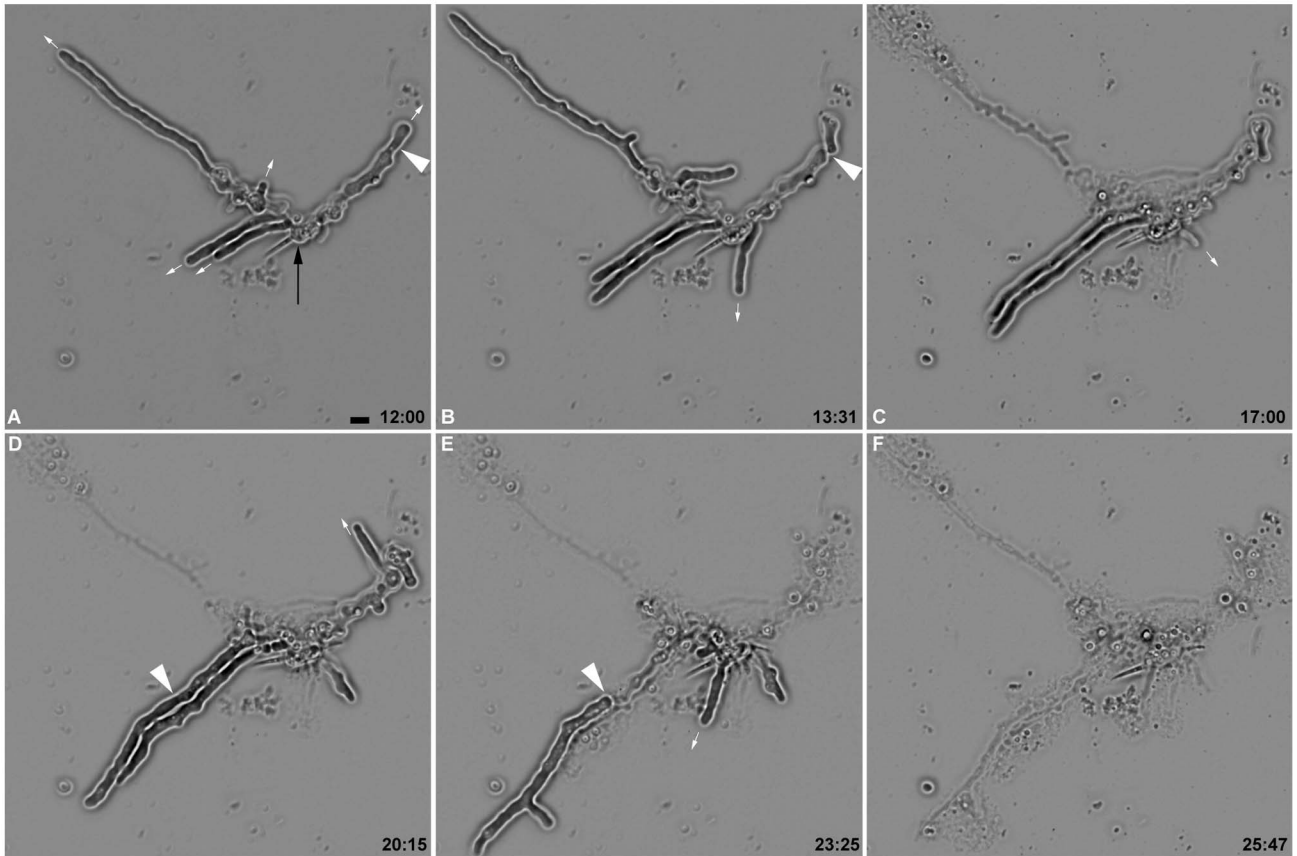


Figure 7 Phase contrast images of a FAR11 deletion mutant with total lysis

Still images from a time-lapse recording of a FAR11 deletion mutant grown on osmotically stabilized medium. A) A germ bubble (black arrow, forming the center of the descriptive 'clock') gives rise to a primary hypha (at ten o'clock) and a secondary hypha (at two o'clock). The primary hypha has developed two adjacent lateral branches, while a septum has formed in the distal part of the secondary hypha (white arrowhead). Hyphal growth is indicated by small white vectorial arrows. B) One and a half hours later, the distal part of the hypha at two o'clock has undergone abscission (arrowhead). A lateral branch of the same hypha is emerging at six o'clock. C) After seventeen hours, the longest hypha at ten o'clock and the short lateral one at six o'clock have entirely lysed, leaving the remnant cell wall visible, while the cytoplasmic content erupted primarily at the tip of the hypha. The main hypha (at two o'clock) is producing another lateral hypha (small white arrow). Note how the segregated hyphal tip at two o'clock is sliding away from the lower hyphal part. D) The distal part of the hypha with the segregated tip is producing another lateral branch, while the two hyphae at eight o'clock continue to grow. The arrowhead indicates the site on the upper hypha where a septum is built. E) The branch at two o'clock has lysed, while its lower lateral branch is still growing. Of the two adjacent hyphae at eight o'clock, the lower one has lysed, while of the upper one only the proximal part has exploded. This proves that the septum which was formed in D must be completely closed. Meanwhile, the germ bubble is producing a third main hypha. F) This severe case led to total annihilation: After nearly 26 hours, the mycelium has lysed entirely. Only the the needle shaped sides of the former germ bubble and the traces of the lysed hyphae can be seen.

Scale bar = 5um

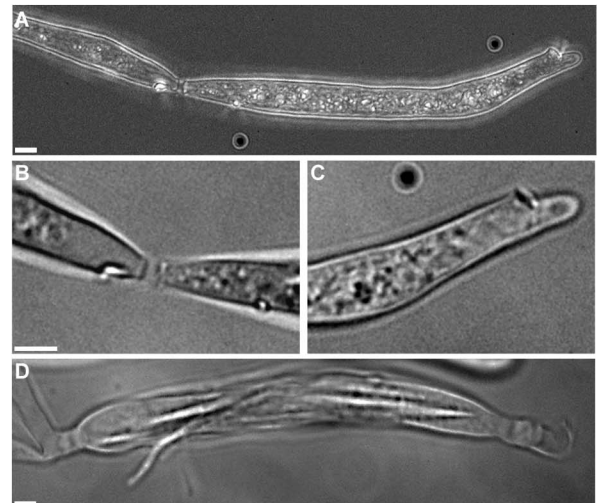


Figure 8 Sporangium formation in wild type

A) A hyphal compartment becomes a sporangium. Here, a part of the hypha is isolated by septal abscission. The left end has undergone cytokinesis but is still attached to the mycelium. The right end shows complete abscission. B) Single plane showing that the abscission of the left end of the sporangium shown in A is complete. C) Single plane of the right end showing the site of cytokinesis. D) Mature sporangium containing eight needle-shaped spores. The cell wall is breached at its lower left end and the emerging end of a spore can be seen. Note restriction and detachment at the right end of the sporangium.

Scalebar=5um

Supplemental Material

Movie S1: Phase contrast recording of a hypha of 15h age.

Hyphal abscission forming at a septum in a FAR11 deletion mutant.

Movie corresponds to Figure 3 of this publication.

Time format: Min : Sec

Movie S2: Phase contrast recording of a hypha of 15h age.

Violent abscission with bending in a FAR11 deletion mutant.

Movie corresponds to Figure 6 of this publication.

Time format: Min : Sec

Movie S3: Phase contrast of a 12h old mycelium.

FAR11 deletion mutant with complete mycelial lysis.

Movie corresponds to Figure 7 of this publication.

Time format: Min : Sec

Appendix

This appendix deals with important aspects of electronic fluorescence microscopy. Because GFP strains with generally weak signal intensity were used for this study, the limits of this fluorescence video microscopy setup were explored and determining factors evaluated and optimized.

For general information on human vision with respect to science, John C. Russ has posted a script on his website ('Seeing the scientific image', <http://www.drjohnruss.com/archives/000013.html>). Providing an enthralling read, it informs on general principles of visual perception like adaptation, pattern recognition, color/grayscale differentiation, and their use in science. It might also help to avoid some common mistakes, for example going from the bright laboratory space to the dark microscope room to 'quickly check a GFP signal'.

Resolution for video microscopy of live organisms is not solely determined by the optics of the microscope. Two other factors are equally important: Illumination time, which is the main factor in recording speed, and sensitivity. Here, sensitivity describes the signal intensity, which depends on the local concentration of the fluorophore. These three factors, optical resolution, recording speed and sensitivity, determine how much information about dynamics or structural arrangement may be gained from an observed specimen (not regarding the fact that the observed organism should, colloquially put, behave itself).

With the microscopes used in this study, optical resolution is state of the art. While lateral resolution is 100nm in x and y direction, resolution along the z-axis is limited to 300 nm. Hence, it rarely makes sense, in the case of z-series, to choose a z-step below 0.3 μm .

These limitations are given by the wavelength of light and cannot be improved. But other factors can be heavily improved. By improving signal-to-noise ratio and camera sensitivity, exposure time of the weak Cap-GFP signals has been decreased from an initial five seconds to 80 ms, improving resolution more than sixty-fold.

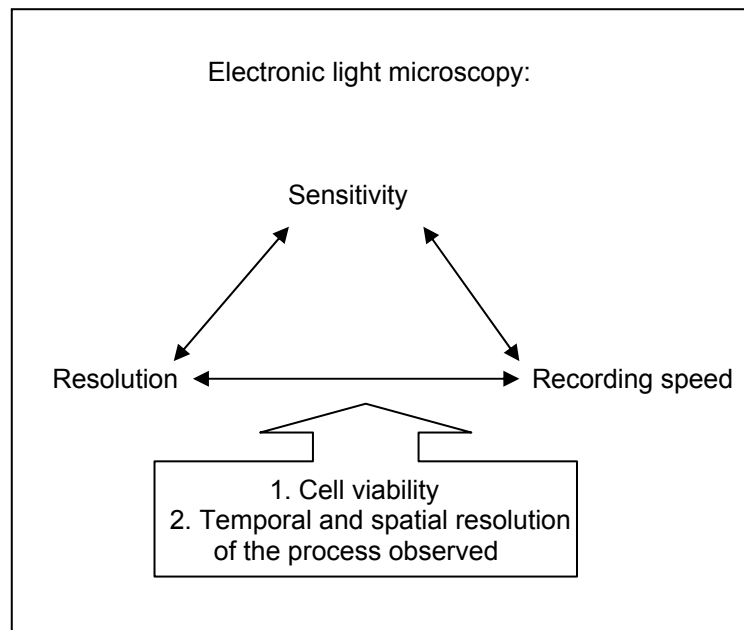


Figure 1 Factors responsible for resolution in electronic light microscopy. As the optical resolution cannot be maximized, it is important to push recording speed and sensitivity. These factors are, in turn, both dependent on the strength of the fluorescent signal.

(adapted from SD Kohlwein, 'The beauty of the yeast: live cell microscopy at the limits of optical resolution', published in Microscopy Research Technique, 2000)

The basis for excellent images in fluorescence microscopy is a good specimen. Your best images will be obtained from specimens of highest quality. This includes a number of factors:

General tissue quality

In *A.gossypii*, this is mostly determined by the age of the mycelium. Not only does hyphal autofluorescence increase with age, but also enlargement of vacuoles often makes for a porous overall appearance of the hypha. This must be balanced by the need for the strongest possible signal, though. In some cases, a good GFP signal appears only after proper folding, which may take as much as twelve hours. Temperature may contribute to the folding process: Chromophore formation of the wild-type GFP is strongly temperature dependent, favoring expression at lower temperatures of 20-25°C. Yet, improved GFP variants (Kimata et al., 1997; Siemering et al., 1996) impose no limitations for applications in the physiological temperature range of *Ashbya*. Hence, only the hottest summer days, where temperature in the microscope room may rise well above 30°C, should be excluded for long-term observations of GFP signals.

Special care must be applied in cases of double staining in a GFP strain (see below, 'Double labelling'). Many observations concerning fixation in a GFP strain, namely exclusion of centrifugation and fixation/staining on ice, have also yielded good results for visualizing the

delicate structure of actin cables in standard rhodamine-phalloidin stainings of the actin cytoskeleton.

Highest possible signal to noise ratio

The labelled process should be readily distinguished from the background. High background fluorescence is a general problem of this kind of microscopy. In budding yeast, it is often circumnavigated by overexpressing the protein of interest, which in turn poses other significant questions to answer. In the case of *A.gossypii*, this point needs to be elaborated.

In a CCD camera, the chip accumulates a charge proportional to the intensity of the incident light. As the amount of light declines, the camera produces a more grainy, noisy image. With progressively lower light levels, the camera fails to detect a sufficient number of incident photons to provide a useful image. This problem cannot be eliminated by averaging multiple weak images or integrating them via software. In colloid-based photography (like, old cameras with argentine rolls of film, that is), the photographer has a number of options:

- A) Increase the exposure time (=illumination time)
- B) Increase the aperture or light collecting ability of the optics
- C) Increase the 'speed' of the film (i.e. its sensitivity)

Interestingly, the natural reflex seems to be that exposure time is increased. This may have to do with the habit of common photography. But longer exposure to UV bleaches the signal faster, increases the chance of creating radiation artifacts and the longevity of the organism is reduced altogether. Luckily, video microscopy offers a myriad of other possibilities to counter this problem.

Increasing the diameter of the pinhole is an option for conventional photography and confocal microscopy, but in the normal fluorescence microscope, all incident light is collected anyway. So point B can not be altered in the setup of our microscopes. If you need to observe rapidly changing events, one possibility though is to increase the speed of the film (the ASA number; the higher, the more light sensitive, the quicker). In the case of fluorescent video microscopy, this means decreasing the energy used by a photon for triggering a charge release. This is done by elevating the base charge of the chip. The disadvantage of this technique is that signals resulting from thermic or non-specific signals (i.e. noise) also trigger a charge release more rapidly, resulting in noisier images altogether. But if the signal is sufficiently strong, this is a good way to get rapid sequential recordings, since exposure time can thusly be reduced.

There are other possibilities which may be exploited in digital fluorescent microscopy:

- D) Increasing the amount of illumination.
- E) Increasing signal intensity.

With the setup of a conventional fluorescence microscope, the amount of illumination is usually a constant value. But the LUDL controller allows to select a discrete amount of fluorescent excitation intensity. So exposure time may be reduced by using 100% fluorescent illumination instead of a lower amount calling for longer exposure. This should be considered

for rapid processes. While the exposure to more intense UV light again reduces the lifetime of the observed organism (or part thereof) and bleaches the signal faster, this is often the only resort for recording events happening in fractions of seconds.

Increasing signal intensity may be done in two ways. A first choice often is to tag the protein of interest with more than one GFP copy. This is often done in cases where a protein with low abundance is tagged. But this process should be considered only if all other parameters have been perfected for the process (protein) observed, as the complete viability of a protein with two GFPs attached may be more easily questioned. The other method of choice is to reduce the background of the medium in which the hypha is observed. A vast reduction of illumination time was achieved in this study by approaching the problem of signal strength this way.

This was done by replacing Ashbya Full Medium (AFM) with Ashbya Minimal Medium (AMM, also known as Ashbya Synthetic Dropout, ASD). This resulted in a fifth of the exposure time used for Cap-GFP in one third AFM and was further reduced by exploiting the possibilities of the rapid camera (the 'Meta' microscope).

After this improvement, the first time-lapse movies were done in the following way:

With a fluorescent image taken every 2 minutes, growing hyphae could be observed for 2 hours and 40 minutes without harm. While recording such a length of time is possible, bleaching of the signal makes it increasingly hard to discern from the background of hyphal autofluorescence, which overmore increases with the amount of UV illumination. Bleaching, however, is strongest in the first images taken, while the bleaching curve in latter images becomes asymptotic. This is due to relaxation of the fluorescing molecule, which is exponential.

This is of advantage when it comes to recording rapid processes. The alternative to long-time observation of a single focal plane is called 'streaming'. In this case, recorded images are kept in the working memory (Random Access Memory, RAM) of the computer, thereby not forfeiting valuable time for saving an image to harddisk. The speed with which images are taken is then solely determined by the size of the image and its exposure time. By focusing on the restricted apical zone, images could be taken in intervals as short as 63 milliseconds. Combining this kind of rapid time-lapse imaging with the three spatial axes x,y,z, multiple plains can be taken along the Z-axis at successive, short time intervals. With exposure time being limited to 80ms, successive image acquisition was brought down to 300ms for a single image of the apical zone. A hypha being covered by 6-10 images in 0.5 μm steps, the entire fluorescent action in a tip can be recorded in 2 to 3 seconds for one timepoint. Since many focal planes make up one single time point, the entire three-dimensional information for that time point is preserved. Adding multiple time points, this results in complete three-dimensional data over time, hence also dubbed 4D microscopy. The disadvantage of this technique is quick bleaching of the specimen. 4D recordings could be extended to 5 minutes, but usually, the best information was found in the first 2 minutes.

Double labelling. In cases of double labelling, good separation of fluorophores is required (considering e.g. that CCD video cameras are quite sensitive in the red to infra-red range). This is of less importance if your two (or more) proteins of interest are in different locations. If one is in the nucleus and the other in the cytoplasm, then the problem of bleed-through in two different spectra (i.e. one signal partly visible in the filter determined for visualization of the other protein) is of less concern.

Double stainings with one component being GFP are the most widespread application. Usually, the affiliation of a protein tagged with GFP and a cellular structure visualized by a known dye (Hoechst for nuclei, rhodamine-phalloidin for the actin cytoskeleton etc.) needs to be confirmed. In any case, the fluorescent excitation and emission spectra determined by the filters need to be considered. They are listed in Table 1 and 2 of this appendix. For example, when GFP is one component and rhodamine-phalloidin the other, then a bandpass filter has to be considered for GFP in order to avoid bleed-through in the upper nanometer range. Since the Endow GFP filter is a longpass, all signal above 500 nm is passed on to the camera, which would interfere with the rhodamine signal. This can be avoided by choosing the Piston filter for the GFP. Its emission being limited to 500-530 nm, rhodamine may then be recorded without any crosstalk of the fluorophores.

In the case of fixation in a GFP strain, structural preservation is an important factor. Cells are usually concentrated in a tube by centrifugation. It should be noted, however, that high centrifugal force may alter vacuolar morphology as well as the cytoskeleton. While double stainings of GFP and, for example, rhodamine-phalloidin, need to be adjusted to the specific GFP strain investigated (mainly regarding the fixation protocol), it is revealing that the colocalization images of Cap-GFP (see Part I, Figure 4) and Abp140p-GFP (Figure 16), both combined with rhodamine-phalloidin, were only achieved by letting the mycelia settle to the ground prio to fixation. After fixation, centrifugation steps were avoided as well.

Tissue preservation is also increased by low temperatures. Especially in double stainings with GFP, fixation and subsequent staining on ice may greatly increase conservation of the GFP signal. This was again the case with the Cap-GFP and Abp140p-GFP fusion constructs.

FILTERS	units: [nm]	Manufacturer:
Microscope: Meta2		
#1 YFP Excitation 490 - 510	Emission 520 – 550	Chroma
#2 RHODAMIN Excitation 527.5 - 552.5	Emission 577.5 – 627.5	Chroma
#3 PISTON GFP (BANDPASS) Excitation 450 - 490	Emission 500-530	Chroma
#4 DIC		Chroma
#3 ENDOW GFP (LONGPASS) Excitation 450 - 490	Emission 500+	Chroma
#6 FITC Excitation 450 - 490	Emission 515 – 565	Zeiss
#7 CFP Excitation 426 - 446	Emission 460 – 500	Chroma
#8 DAPI Excitation 365	Emission 420+	Zeiss

Table 1: Filter spectra and specifications on microscope Meta2

FILTERS	units: [nm]	Manufacturer:
Microscope: PicMic		
#1 FITC Excitation 450 - 490	Emission 520+	Zeiss
#2 DAPI Excitation 365	Emission 420+	Zeiss
#3 DIC		Chroma
#4 EGFP Excitation 450 - 490	Emission 500+	Chroma
#5 FRET Excitation 426 – 446	Emission 520 - 550	Chroma
#6 CFP Excitation 426 - 446	Emission 460 – 500	Chroma
#7 YFP Excitation 490 - 510	Emission 520 – 550	Chroma
#8 RHODAMIN Excitation 540 - 552	Emission 590+	Zeiss

Table 2: Filter spectra and specifications on microscope PicMic

Acknowledgements

I would like to thank Prof. Philippsen for giving me the opportunity to work in his group, for supervising this study and for good advice in the science of publishing. His concern for the well-being of all members of his lab is outstanding and I am very grateful for having been able to experience it.

It was a great honor to have Prof. Ueli Aebi in my thesis committee, and I would also like to thank Prof. Martin Spiess for presiding it.

A 'Thank you' the size of Alaska goes to Dr. Hans-Peter Schmitz for showing me the ropes in molecular biology, at the bench and at the computer, providing me with the Sec4p-GFP strain and ultimately constructing the Abp140p-GFP strain. In the end, however, I will most fondly remember his good humour and his admirable capability of interrupting no matter what he was doing to help someone – always with utter competence and a smile.

I am very grateful to Dr. Philipp Knechtle for letting me work with the Cap1p-GFP and Cap2p-GFP strains, and as an interesting partner for discussions about fungi and the scientific environment.

Dr. Amy Gladfelter and Hanspeter Helfer (a.k.a. 'Pesche', *fr.* 'Piicha') have been dear friends and important moral support in hard times. Thank you two for all the help and the falafels and beers that went with it! And I won't even start mentioning scientific advice and imaging wizardry...

All other lab members have often been very helpful and supportive as well, but due to the impossibility of singling out people, I would like to thank 'em all in one go: Riccarda Rischatsch, Andreas Kaufmann, Michael Köhli, Katrin Hungerbühler, Dr. Kamila Boudier, Daniele 'Michele' Cavicchioli, Ivan Schlatter, Sylvia Voegeli, Claudia Birrer, Virginie Galati, Nicoleta Sustreanu and the members of the 'old league' Dr. Sophie Lemire-Brachat, Dr. Dominic Hoepfner, Dr. Florian Schaerer, Dr. Christine Alberti-Segui and Dr. Yasmina Bauer.

Thank you, Markus Duerrenberger, for assistance at the confocal microscope, and Jean Pieters, for letting me use the Zeiss Meta.

I would also like to acknowledge the summer students, Claire Seguela for integrating the Abp140p-GFP into the genome and the 'Two Isabelles' for the construction of both Cap-GFP strains.

Brigitte Berglas was of priceless assistance during the ESBS courses. It is her merit, in combination with Roger Sauder, Daniel Oeschger, the experience of Philipp Knechtle and the friendly people at Unser Bier, that made an amazingly good brew possible.

Kudos also go to the invaluable help of Bettina Hersberger, Sandra Götz, Doris Rossi, Esther Graf and, for the odd emergency, Werner Metzger.

As for the production of this thesis itself, I would like to thank Ingrid Singh and Annette Roulier of the Digital Imaging Facility for much patience and deadline assistance, and Esther Thalmann for friendly advice.

Finally, I would like to thank Ashbya itself for enduring all the manipulation. An amazing creature and a fungus with its own free will (and a concomitant potential to drive a scientist mad), I wish her a good place in the Hall of Fame of Model Organisms.

Curriculum vitae

PARTICULARS

Family name	Laissue
Christian names	Pierre Philippe
Work address	Department of Applied Microbiology Klingelbergstrasse 50/70, 4056 Basel
Work number	061 267 1489
email address	philippe.laissue@unibas.ch
Home address	Elsässerstrasse 111, 4056 Basel
Home number	061 321 6373
Date of birth	01/03/1971
Nationality	Swiss
Civil status	unmarried

EDUCATION

University of Basel, Biozentrum August 2001 - November 2004: Ph.D. *cum laude*; Certificate in Microbiology. Currently research assistant to Prof. Peter Philippsen.

University of Fribourg December 1999. Diploma in Biology *magna cum laude*.

PUBLICATIONS

Laissue PP, Brogli K and Philippsen P.

Far11p is required to prevent premature hyphal abscission in the filamentous fungus *Ashbya gossypii*. (Submitted).

Laissue PP, Schmitz HP, Knechtle P and Philippsen P.

The dynamic actin cytoskeleton of the filamentous fungus *Ashbya gossypii*. (Submitted).

Schmitz HP, Kaufmann A, Köhli M, **Laissue PP**, Philippsen P.

From Function to Shape: A Novel Role of a Formin in Morphogenesis of the Fungus *Ashbya gossypii*. Mol Biol Cell. 2006 Jan;17(1):130-45.

Laissue PP, Reiter C, Hiesinger PR, Halter S, Fischbach KF, Stocker RF.

Three-dimensional reconstruction of the antennal lobe in *Drosophila melanogaster*. J Comp Neurol 1999 Mar 22; 405(4):543-52.

RESEARCH EXPERIENCE

Biozentrum, University of Basel Doctoral Thesis (2001-2004) Advisor: Prof. Dr. Peter Philippsen. Department for Applied Microbiology.

- Studied the dynamics of the actin cytoskeleton and vesicular traffic in the filamentous fungus *Ashbya gossypii* using GFP constructs, extensive fluorescence microscopy, image processing and quantitative image analysis
- In collaboration with Dr. Hans-Peter Schmitz maintained, updated and expanded software and hardware for the microscope unit

Albert Einstein College of Medicine Internship (Summer, 2000) Advisor: Prof. Dr. John Condeelis, Analytical Imaging Facility.

- Developed methods and programs for the visualization of four-dimensional data from fluorescence microscopy, which I set up in a website for users of the facility

University of Fribourg Diploma Thesis (1996-1999) Advisor: Prof. Dr. Reinhard F. Stocker, Department of Neurobiology, in co-operation with the **Albert-Ludwigs-Universität Freiburg**, Germany (Advisor: Prof. Dr. Karl-Friedrich Fischbach, Department of Neurobiology).

- Extensively analyzed the antennal lobe of *Drosophila melanogaster* with immunocytochemical methods and confocal microscopy, discovering several new glomeruli
- Condensed the findings into a three-dimensional, web-based model, making a user-friendly, interactive map for the research community of *Drosophila* olfaction

University of Bern, Department of Pathology Internship (Summer, 1986) Advisor: Prof. Dr. Thomas Schaffner.

- Made a three-dimensional reconstruction of the rat brain using an Amiga computer and serial sections

MEETINGS AND SEMINARS

XXII International Conference on Yeast Genetics and Molecular Biology. Selected for talk on Cytoskeleton and Morphogenesis. XXII International Conference on Yeast Genetics and Molecular Biology, August 7-12, 2005, Bratislava, Slovak Republic.

Frontiers in Bio-Imaging. Poster presentation: The dynamic actin cytoskeleton of a filamentous fungus. June 6-7, 2005, Basel.

XXIII Fungal Genetics Conference. Talk: The Actin and Microtubule Cytoskeleton in *Ashbya gossypii*, held by Prof. Peter Philippsen, and Poster presentation. March 15-20, 2005, Asilomar, USA.

Gordon Research Conference. Accepted for Poster presentation: Dynamics of the actin cytoskeleton in the filamentous fungus *Ashbya gossypii*. August 15-20, 2004, New Hampshire, USA.

EMBO Young Investigator Programme. Mini-Symposium on Fluorescence Microscopy. May 12-13, 2003, EMBL Heidelberg, Germany.

Live Cell Imaging Workshop, Swiss Federal Institute of Technology, October 9-10, 2002, Lausanne.

Swiss Yeast Meeting. Poster presentation: Live imaging of capping protein in the filamentous fungus *Ashbya gossypii*. September 20, 2002, Zurich.

European Conference on Fungal Genetics, Poster presentation: The kinesin motor AgKip2p participates in the oscillatory motion of nuclei in the filamentous fungus *Ashbya gossypii*.
April 6-9, 2002, Pisa, Italy.

MetaMorph Imaging Seminar, October 25, 2001, Puchheim, Germany.

Workshop for Confocal Microscopy, Image Processing and 3-D reconstruction,
February 2-9, 1998, Freiburg, Germany.

25th and 26th Göttingen Neurobiology Conferences, Poster presentations: 3D
Reconstruction of the antennal lobe of *Drosophila melanogaster*. May 1997 and March 1998.

Erklärung

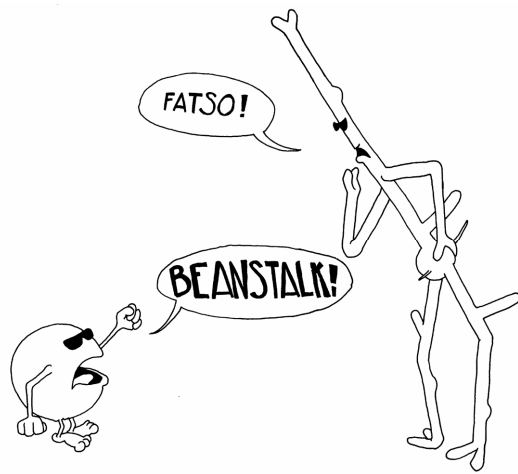
Ich erkläre, dass ich die Dissertation

“Morphogenesis of a filamentous fungus: Dynamics of the actin cytoskeleton and control of hyphal integrity in Ashbya gossypii”

nur mit der darin angegebenen Hilfe verfasst und bei keiner anderen Fakultät eingereicht habe.

Basel, Dezember 2005

Philippe Laissue



Budding yeast, *Ashbya* and the old controversy of morphology